学位論文

The merger processes of multiple stellar-mass black holes

（多重恒星質量ブラックホールの合体過程）

平成２８年１２月博士（理学）申請

東京大学大学院理学系研究科

天文学専攻

田川　寛通

Abstract

Exploring the merger processes of stellar-mass black holes (BHs) is important since the mergers of stellar-mass BHs are related to the various unsolved problems such as formation processes of supermassive BHs (SMBH), an evolutional channel of the gravitational wave (GW) event, GW150914, and the origin of r-process elements. So far, the merger of stellar-mass BHs has been thought to result from the evolution of binary stars. In our study, we newly propose the merger processes evolved from a multiple of non-binary isolated BHs under gas rich environments.

In this thesis, we first explore the merger processes of multiple BHs under gas rich environments. For the purpose, we perform post-Newtonian N-body simulations, incorporating the effects of the gas dynamical friction, gas accretion, and GW emission. The attention is concentrated on the effects of the dynamical friction and the Hoyle-Lyttleton mass accretion by ambient gas. Our simulations solve the merger of more than three BHs with effects of gas for the first time. Such merger processes are important because a third BH, which decays due to the gas dynamical friction, effectively transports the angular momentum of binary BHs by the three-body interaction. As a result, our simulations suggest that multiple BHs are able to merge into one BH within 100 Myr in a wide range of BH number density. We also show that mergers of accreting stellar-mass BHs are classified into four types: a gas drag-driven merger (type A), an interplay-driven merger (type B), a three body-driven (type C), or an accretion-driven merger (type D). We find the relation between the merger mechanism and the gas density ($n_{\rm gas}$), the BH density ($\rho_{\rm BH}$), and the initial typical extention of BH spatial distribution ($r_{\rm typ}$). Type A or B merger occurs if $n_{\rm gas}\rho_{\rm BH}^{-1}r_{\rm typ}^{-1}$ is higher or lower than 8×10^4 cm^{-3}pc$^2/M_\odot$, respectively. Furthermore, we derive a critical accretion rate ($\dot{m}_{\rm c}$), below which the BH growth is promoted faster by mergers. Also, it is found that the effect of the recoil by the GW emission can reduce $\dot{m}_{\rm c}$ especially in gas number density higher than 10^8 cm^{-3}, and enhance the escape probability of merged BHs.

Furthermore, we consider an evolutional channel of GW event, GW150914. Recently, the Laser Interferometer Gravitational-Wave Observatory (LIGO) has detected the GW event, GW150914, as a result of the merger of a $\sim 30\ M_\odot$ BH pair. So far, the merger of stellar-mass BHs has been thought to result from the evolution of binary stars. Here, we propose a novel path of the merger stemming from non-binary isolated stars. In our studies, we have found that multiple non-binary stellar-mass BHs whose separations are larger than 1000 AU can merge with each other under gas-rich environments through the gas dynamical friction and three-body interaction. In this case, a considerable amount of gas can accrete onto BHs before the merger, that is, the initial mass of BHs

can be lower than 30 $M_\odot$. Based on our simulations, we find that the BH merger in GW150914 can be accounted for by the merger in galactic nuclear regions or dense interstellar cloud cores if the initial BH mass is higher than 25 $M_\odot$. Furthermore, we roughly estimate event rates to be ~ 0.4 yr^{-1} in galactic nuclear regions and ~ 8 yr^{-1} in dense interstellar cloud cores, and find that this estimated event rate is almost consistent with the event rate implied from hitherto detected GW events.

Next, we apply the merger processes to the several issues. First, we study the origin of r-process elements. Recently, it has been argued that r-process elements in galaxies primarily originate from the mergers of double neutron stars (NSs) and BH-NS. However, it has been pointed out that the estimated merger timescale (0.1-1 Gyr) is much longer than the timescale inferred from the abundance of r-process elements of metal poor stars in the Galactic halo (1-10 Myr). To solve this problem, we propose the rapid merger processes in gas-rich first-generation objects in a high redshift epoch. To explore the possibility of mergers in a system composed of multiple NSs as well as BHs, we perform post Newtonian N-body simulations. As a result, we find that NS-NS or NS-BH can merge within 10 Myr in first-generation objects. These results imply that the mergers in early cosmic epochs may reconcile the conflict on the timescale of NS mergers.

Also, we roughly estimate the event rates of short gamma-ray bursts (GRBs) by the NS-NS mergers evolved from non-binary stars. As a result, the NS-NS merger rates are ~ 0.6 yr^{-1}Gpc^{-3} in galactic nuclear regions and ~ 2 yr^{-1}Gpc^{-3} in dense interstellar cloud cores. We find that the non-binary star merger is likely to be a minor path of short GRBs.

Finally, to consider the formation processes of SMBHs at $z \sim 6$, we discuss the possibility of the efficient growth of BHs via BH-BH mergers at high-redshift epochs. As a result, we suppose that the center regions of primordial galaxies can provide promising environments for the efficient growth of BHs via BH-BH mergers.

Acknowledgements

I deeply thank Prof. Masayuki Umemura for continuously teaching me and for discussions despite of his busyness. During my Ph.D. course, he taught me a lot of things such as how to proceed research, how to write papers, and how to advertise results of research. Without help from him, I couldn't write this Ph.D. thesis.

I deeply thank Prof. Naoteru Gouda for supervising me for 5 years. He has given me a lot of advice about research, life, future, and so on. Especially, he taught me how to write documents and papers effectively taking his time. He always provides my consultation and answer my questions although he is busy. Besides, he kindly introduce me to Prof. Masayuki Umemura, because I am interested in the research about the merger of BHs using numerical simulations. He gave me numerous support so that my research proceeds well.

I am grateful to Dr. Taihei Yano for helping me for 5 years. He always responses to my questions kindly, and discuss various things with me.

I am also grateful to all staff members, postdocs, students in JASMINE project office for warm supports during daily life and writing Ph.D. thesis. Because of the supports, I could pursue the research in this 5 years without feeling a strong stress.

Finally, I am most grateful to my family for always supporting me.

Contents

Abstract 1

Acknowledgements 3

Chapter 1 General introduction 6
1.1 Black holes 6
1.2 Merger of massive black holes 7
1.3 Merger of stellar-mass black holes 10

Chapter 2 Numerical model 25
2.1 Equation of motion 25
2.2 Key parameters 33
2.3 Conditions for simulations 35

Chapter 3 Merger processes of multiple black holes 38
3.1 Merger mechanisms of multiple black holes 38
3.2 Merger time of multiple black holes 48
3.3 Critical accretion rate for the black hole growth 56
3.4 Effect of Recoil Kick 60

Chapter 4 Non-binary black hole merger in GW150914 64
4.1 Mergers at GW150914 from smaller mass BHs 64
4.2 Event rates 68

Chapter 5 Application to several issues 70
5.1 Origin of r-process elements by neutron star mergers 70
5.2 Event rates for short gamma-ray bursts 73
5.3 Formation processes of supermassive black holes 74

Chapter 6 Summary and conclusions 75
6.1 Merger processes of multiple black holes 75
6.2 Non-binary black hole merger in GW150914 77

6.3 Application to several issues 78

AppendixA 80
A.1 Merger mechanisms without gas accretion 80

References 85

Chapter 1

General introduction

1.1 Black holes

A BH is a structure of spacetime, which exhibits strong gravitational effects. Everything such as particles and electromagnetic radiation cannot escape from inside the BH due to its strong gravity. According to the mass, BHs are often classified into several classes: supermassive BHs (SMBH, $\gtrsim 10^5\ M_\odot$), intermediate-mass BHs (IMBH, $\sim 10^2 - 10^4\ M_\odot$), and stellar-mass BHs ($\sim 10\ M_\odot$).

SMBHs are found in the centers of most large galaxies, and are supposed to bring a significant effect on the evolution of their host galaxies. BHs onto which gas accretes can release considerable amounts of energy into their surroundings, and so star formation and BH growth are possibly quenched (e.g. Silk & Rees, 1998). Hence, the growth of SMBHs plays a key role in the formation of galaxies.

As for IMBHs, no unambiguous detection has been reported. However, there are indirect implications such as the observation of ultra-luminous X ray sources (Maccarone et al., 2007) and stellar velocity dispersion of globular clusters (Lützgendorf et al., 2015). Whether IMBHs exist in the center of dwarf galaxies is thought to be important information for probing the origin of SMBHs (Volonteri et al., 2008).

In our study, we especially focus on stellar-mass BHs. There are supposed to be about 10^8 stellar-mass black holes (BHs) in Milky Way-sized galaxies (Remillard & McClintock, 2006). Basically, a stellar-mass BH is formed by the gravitational collapse of a massive star (Heger et al., 2003). Recently, the gravitational wave (GW) events, GW150914 (Figure 1.1) and GW151226, as results of BH mergers, have been reported (Abbott et al., 2016a,c). From these events, existence of stellar-mass BH binaries and its merger within the cosmic time are directly confirmed. It is expected that a lot of GW events will be detected in the near future (e.g. Nakamura et al., 2016). The GW events give distinguished information about merged objects such as the precise masses and spins of merged objects, a luminosity distance, and celestial coordinates

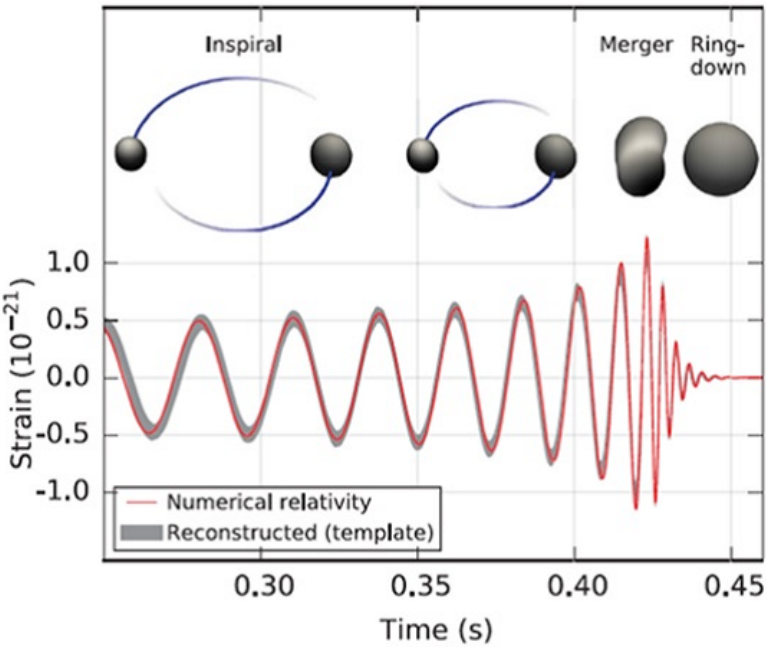

Fig. 1.1 Estimated gravitational wave strain amplitude from GW150914. The inset images show numerical relativity models of the black hole horizons as the black holes coalescence. Taken from figure 2 of Abbott et al. (2016a).

of a event source. Now, the era of great progress in the BH astrophysics using the GW observations is coming. Hence, the study about mergers of BHs is especially important in this era.

1.2 Merger of massive black holes

The merger processes of SMBHs are related to the several unsolved problems such as the final parsec problem (Merritt & Poon, 2004), the origin of the Maggorian relation (Kormendy & Ho, 2013), formation processes of high-z SMBHs, and galaxy formation and evolution. Hence, it is important to unveil the merger processes of SMBHs.

According to the hierarchical merger history of galaxies, multiple massive BHs (MBHs) are likely to form after galaxy mergers. However, most of galaxies harbor only one SMBH in their centers, with several exceptions like a triple AGN in the galaxy SDSS J1027+1749 at $z = 0.066$ (Liu et al., 2011), three MBHs of $10^6 - 10^7 M_\odot$ in a clumpy galaxy at $z = 1.35$ (Schawinski et al., 2011), a quasar triplet QQQJ1432–0106 at $z = 2.076$ (Djorgovski et al., 2007), and a second quasar triplet QQQJ1519+0627 at $z = 1.51$ (Farina et al., 2013). Thus, it is thought that the merger of BHs might occur in some redshift epoch, resultantly forming one central SMBH in each galaxy.

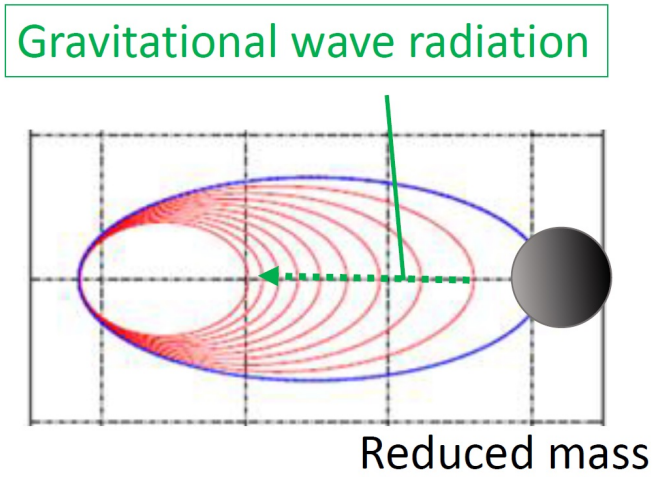

Fig. 1.2 Orbital decay due to the gravitational wave radiation.

To date, the merger of SMBHs in a galaxy has been studied extensively. If the separation of a SMBH-SMBH binary (SMBH binary) is reduced sufficiently, the merger of a SMBH binary is driven by the GW radiation within cosmic time (Figure 1.2). As for a binary of SMBHs formed after a galaxy merger, the orbit of a SMBH binary cannot shrink below one parsec due to the depletion of stars on orbits that intersect the binary SMBH (Begelman et al., 1980). Because of the lack of the transportation mechanisms of the angular momentum for a SMBH binary, the merger of a SMBH binary is theoretically difficult to expect in a simple situation. Whereas, because most of galaxies harbor one SMBH in the center of each bulge, the SMBH binary should merge into one SMBH within the cosmic time. This contradiction is often called the final parsec problem (e.g. Merritt & Poon, 2004). It is argued that if the host galaxy provides an aspherical potential, the final parsec problem can be solved (Khan et al., 2011, 2012, 2013). However, this solution of the problem is still under debate (Vasiliev et al., 2014). If there are more than two SMBHs in a galaxy, the angular momentum of a SMBH binary is significantly carried by a third SMBH when a third MBH intrudes into a binary SMBH (right panel of Figure 1.3). Then, the binary separation is reduced and eventually the merger of the binary is induced (Iwasawa et al., 2006). In the case of many SMBHs, the stellar dynamical friction allows a binary SMBH to interact frequently with other field SMBHs, and then the reduction of the binary separation leads to the merger (Tanikawa & Umemura, 2011, 2014).

For a binary of SMBHs formed after a merger of gas-rich galaxies, the gas dynamical friction and gas accretion (left panel of Figure 1.3) can also drive the merger. Hitherto, the merger processes by the gas dynamical friction and gas accretion have been investigated in the case of two massive BHs (e.g. Escala et al., 2004, 2005; Fi-

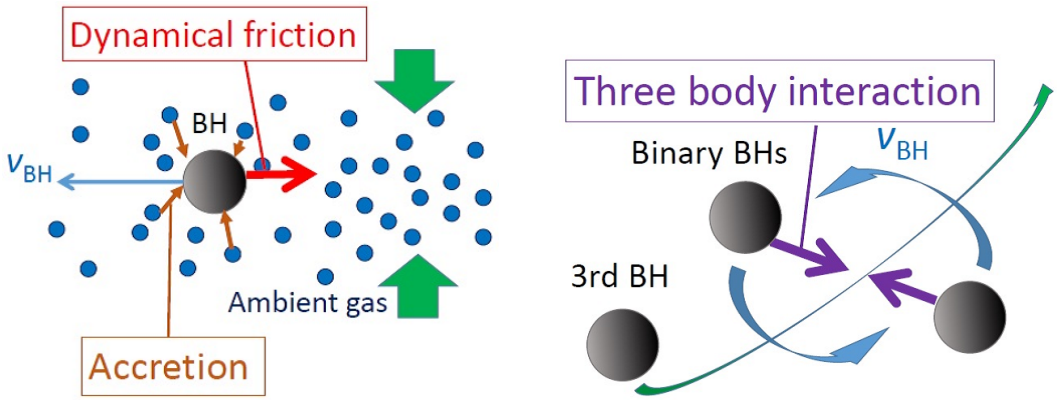

Fig. 1.3 The mechanisms that prompt the BH merger. Left: The decay of BH motion due to the dynamical friction and accretion by ambient gas. In the gas dynamical friction, the BH gravity creates density increase within ambient gas, which act as a drag force. Gas accretion changes the velocities of BHs and increases the Schwarzschild radius and mass of BHs. Right: The transportation of binary angular momentum due to the three-body interaction.

BH number	Background matter	
	Star	Gas
two	e.g. Khan et al. (2012, 2013)	e.g. Escala et al. (2004, 2005)
three	Iwasawa et al. (2006)	**Tagawa et al. (2015)**
multiple	Tanikawa & Umemura (2014)	**Tagawa et al. (2015, 2016)**

Fig. 1.4 Previous studies about BH merger through the interaction with background matter.

acconi et al., 2013). Escala et al. (2004, 2005) have shown that the major merger of two MBHs with the effects of gas is roughly predicted by the analytical fomulae if the gap is not opened in binary's surroundings. If a gap is opened, strong binary torques induce the gas accretion whose rates are comparable to the accretion rate in the single BH case (MacFadyen & Milosavljevic, 2008; Roedig et al., 2011, 2012; Shi et al., 2012; Noble et al., 2012; D'Orazio et al., 2013; Farris et al., 2015). The merger processes in the cases of two BHs are roughly predicted by the analytic fomulae.

On the other hand, the merger processes of three MBHs with effects of gas have not been investigated (Figure 1.4). Investigating such merger processes requires solving wide dynamic ranges (~ 7 digits) of orbital evolution, and so the computational cost becomes so high. However, such merger processes are important because a third BH, which decays due to the gas effects, effectively transports the angular momentum of binary BHs by the three body interaction (right panel of Figure 1.3). In our study, the merger processes of more than three MBHs with effects of gas are investigated for the first time in Section 3.2.1 (Tagawa et al., 2015). To reduce the computational cost, we employ the analytic formulae for the gas effects.

1.3 Merger of stellar-mass black holes

Investigating the merger processes of stellar-mass BHs is important since the merger of stellar-mass BHs are related to various unsolved problems such as formation processes of high-z SMBHs, an evolutional path of the GW event, GW150914, and the origin of r-process elements. Furthermore, the era of the GW astronomy has started recently. Hence, the merger of stellar-mass BHs is a hot field in astronomy.

So far, the mergers of stellar-mass BHs have been thought to result from the evolution of binary stars (Belczynski et al., 2010; Kinugawa et al., 2014; Dominik et al., 2015). On the other hand, in this thesis, we newly propose the mergers from non-binary stars. The non-binary BHs are expected to form during the first star formation and the galactic evolution, including galactic mergers and dynamical interaction. In Section 3, we investigate the merger processes of multiple BHs. In Section 4, we propose the merger processes of multiple BHs as an evolutional channel of GW150914. Furthermore, in Section 5, we apply the merger processes to several issues described in Section 1.3.1, 1.3.3 and 1.3.4.

1.3.1 Formation process of supermassive black holes in $z > 6$

Recent observations have found quasars that posses SMBHs with masses $\gtrsim 10^9\ M_\odot$ at redshifts higher than 6 (Figure 1.5, Fan et al., 2001; Kurk et al., 2007; Jiang et al., 2007; Wang et al., 2010; Mortlock et al., 2011; Venemans et al., 2013, 2015; Wu et al., 2015). It remains poorly understood how these early massive BHs formed and grew. For the growth of SMBHs, there are two major competitive scenarios, that is, the mass accretion and the merger of BHs (or stars) (Volonteri & Bellovary, 2012; Haiman, 2013). Possible building blocks for the high-redshift SMBHs are the remnants of first stars. The initial mass function of first stars is considered to be more or less top-heavy (Figure 1.6, Abel et al., 2000; Nakamura & Umemura, 2001; Bromm et al., 2002; Yoshida et al., 2006; Greif et al., 2011; Susa et al., 2014; Hirano

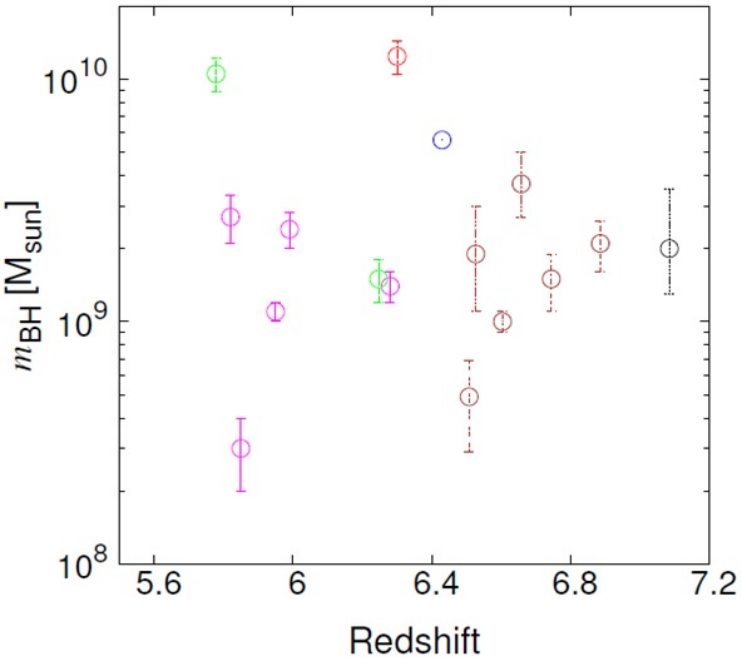

Fig. 1.5 The masses of discovered high-redshift SMBHs as a function of the redshift. Pink, green, blue, black, brown, and red plots represent the SMBHs discovered by Kurk et al. (2007), Jiang et al. (2007), Wang et al. (2010), Mortlock et al. (2011), Venemans et al. (2013, 2015), and Wu et al. (2015), respectively.

et al., 2014). First stars of several tens $M_\odot$ can leave BHs of few tens $M_\odot$ as results of stellar evolution (Figure 1.7, Heger & Woosley, 2002). If recently discovered high-redshift quasars, ULASJ112010+641 with the mass of $m_{\rm BH} = 2 \times 10^9\ M_\odot$ at redshift $z = 7.085$ (Mortlock et al., 2011) and SDSS J01001+2802 with $m_{\rm BH} = 1.2 \times 10^{10}\ M_\odot$ at $z = 6.30$ (Wu et al., 2015), grow only by mass accretion from such stellar-mass BHs, the Eddington ratio is required to be 1.4 for ULASJ112010+641, and 1.3 for SDSS J01001+2802. However, the average mass accretion rates should be lower than the Eddington rate due to feedback (Alvarez et al., 2009; Milosavljevic et al., 2009), although it is pointed out that the super-Eddington accretion may be possible in metal free systems (Volonteri & Rees, 2005). It is thought that the maximum rate of the super-Eddington accretion is given by Hoyle-Lyttleton accretion (Hoyle & Lyttleton, 1939; Bondi & Hoyle, 1944). However, it is not clear how such high accretion rate is realized in an early universe.

On the other hand, seed BHs may stem from supermassive stars of $10^{4-6}\ M_\odot$ due to the direct collapse of primordial density fluctuations (Umemura et al., 1993; Bromm & Loeb, 2003; Inayoshi & Omukai, 2012). These BHs are thought to be born in a

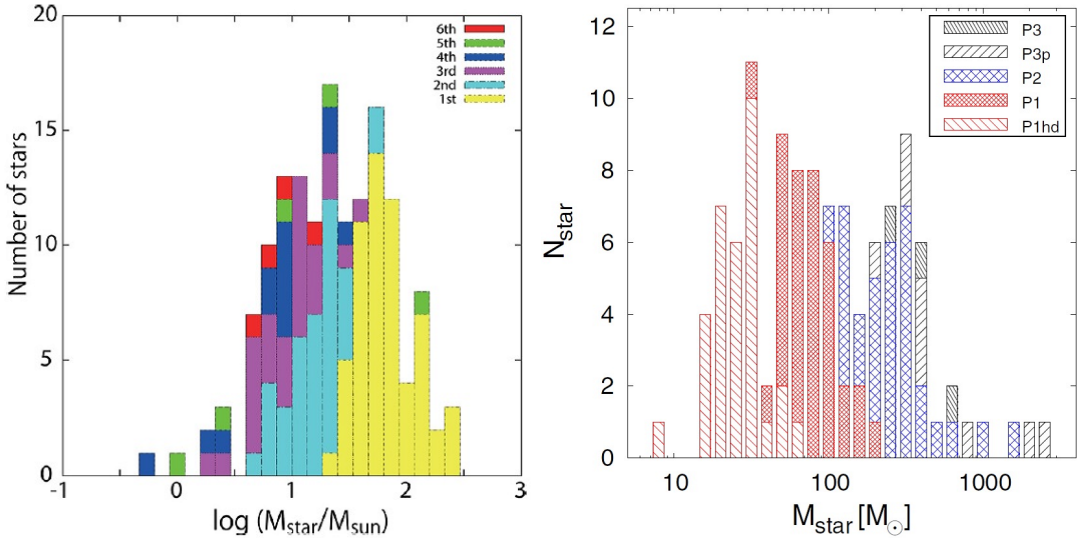

Fig. 1.6 Mass spectrums of 59 (Susa et al., 2014, left) and 110 (Hirano et al., 2014, right) first stars reproduced by numerical simulations. Left: The colors in the histogram correspond to the order of birth of these stars. Taken from figure 9 of Susa et al. (2014). Right: The red, blue, and black histograms represent the different paths of protostellar evolution: P1: Kelvin-Helmholtz contracting protostar (red), P2: oscillating protostar (blue), and P3: supergiant protostar (black). P1hd refers to the cases in which the gas clouds are formed by HD cooling and evolve on low-temperature tracks. P3p indicates the same cases as P3, except that the final masses are calculated from a correlation between the properties of the cloud and the resulting stellar mass (Equation (13) in Hirano et al. (2014)). Taken from figure 5 of Hirano et al. (2014).

primordial galaxy of $\sim 10^8 - 10^9\ M_\odot$ (Greene, 2012). If SMBHs grow via gas accretion from such massive BHs, the constraint on the accretion rate is alleviated.

Another possible pathway for SMBH formation is the merger of BHs. If the merger of multiple BHs proceeds in a high redshift universe, the constraint on the accretion rate can be alleviated.

Recent radiation hydrodynamic simulations on the first star formation show that multiple massive stars form in a primordial gas cloud of $\sim 10^4 - 10^5\ M_\odot$ with the number density of around 10^7 cm^{-3} and the extension of $\sim$0.01pc (Figure 1.8), where the gas fraction is 99% (Greif et al., 2011; Umemura et al., 2012; Susa, 2013; Susa et al., 2014). Here, since these multiple massive stars mainly receive the gravity from gas, these stars can be non-binary stars. According to the mass function of first stars, multiple non-binary BHs of several tens $M_\odot$ may be formed as first star remnants (Figure 1.7), in such a primordial could.

In this circumstance, BHs are decelerated and BH mergers are prompted by the gas

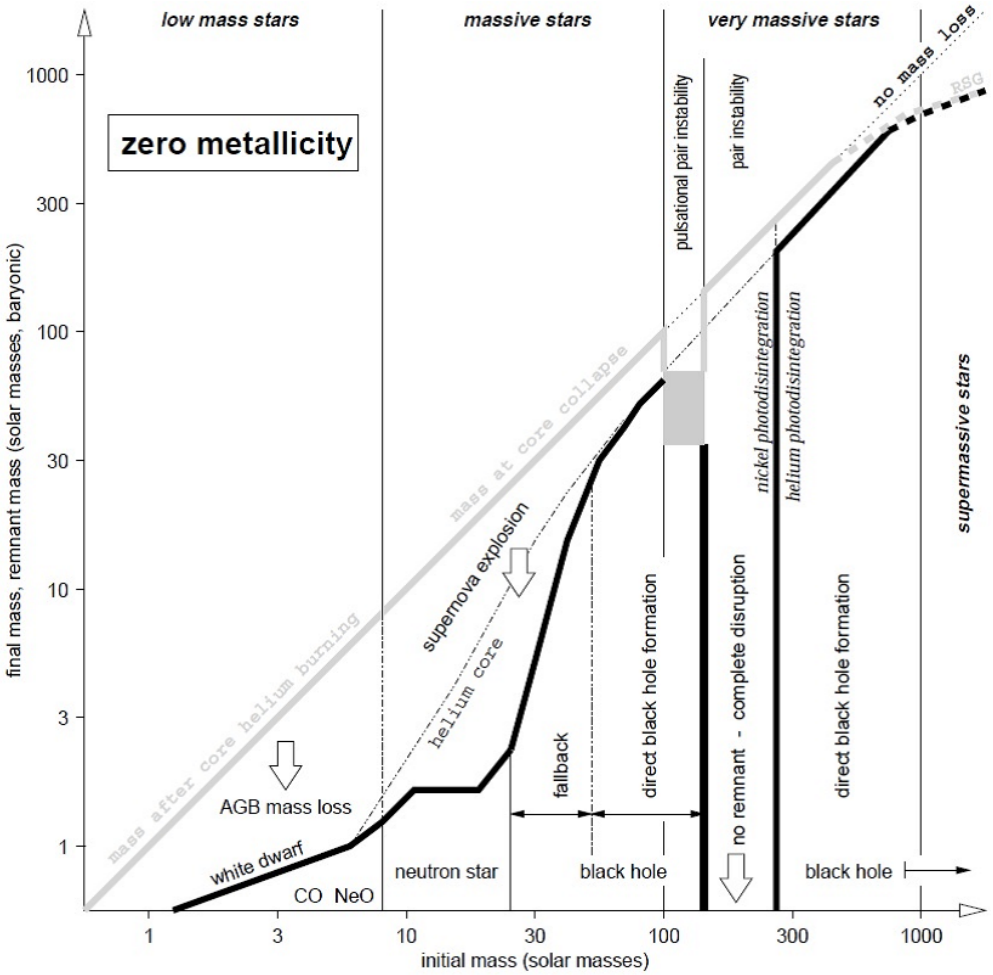

Fig. 1.7 The relation between initial and final mass for non-rotating metal-free stars. Thick black, thick gray, and dashed-double-dotted curves represent the final mass of the collapsed remnant, the mass of the star when the event begins that produces that remnant, and the hydrogen-rich envelope and parts of the helium core, respectively. Taken from figure 2 of Heger & Woosley (2002).

dynamical friction (Ostriker, 1999; Tanaka & Haiman, 2009, left panel of Figure 1.3). Hitherto, the merger processes by the gas dynamical friction have been investigated in the case of two BHs (e.g. Escala et al., 2004, 2005). However, the merger processes of three or more BHs with effects of gas has not been investigated. As also mentioned in Section 1.2, such merger processes are important because a third BH, which decay due to the gas dynamical friction, effectively transports the angular momentum of a binary BH by the three body interaction (right panel of Figure 1.3). In Section 3, we explore the merger of multiple non-binary BHs. For the settings of parameter regions in Section 3, we consider a first-generation object of $\sim 10^5 - 10^6\ M_\odot$ or a gas-rich

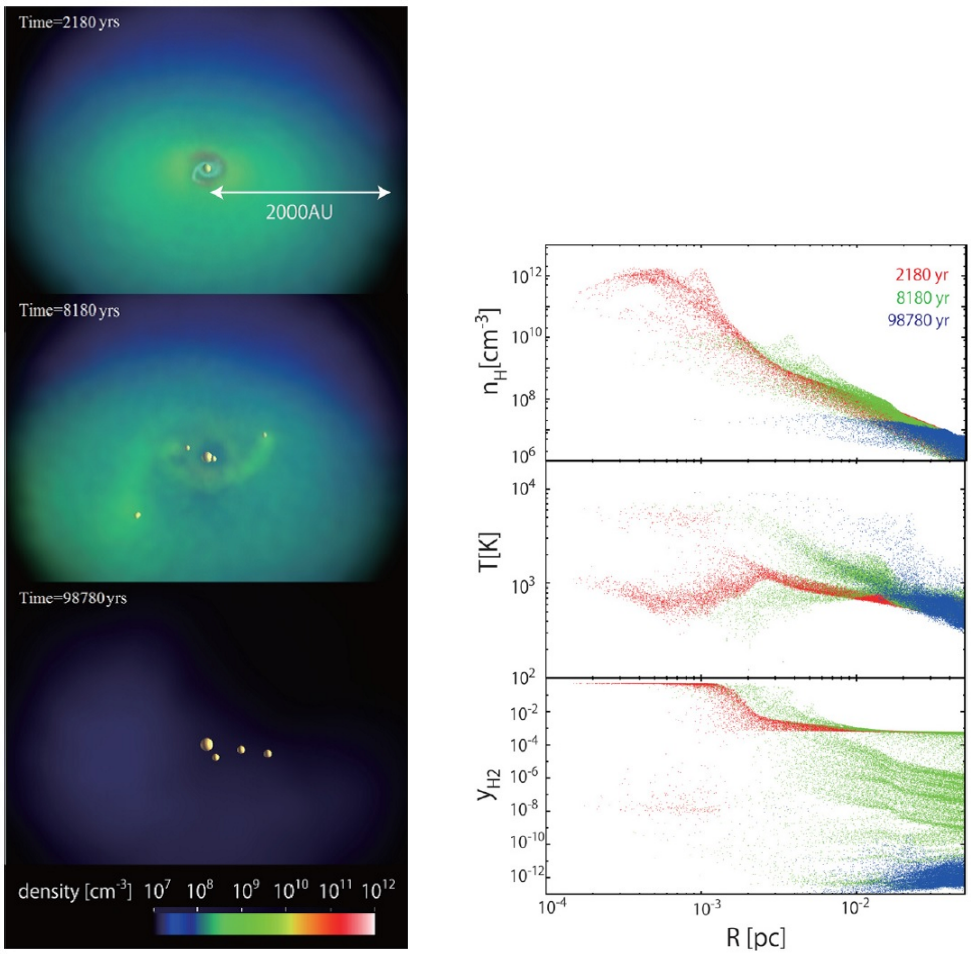

Fig. 1.8 The left and right panels show the results of the simulation on the first star formation. Left: Density and formed star distributions at three snapshots: 2180 yr, 8180 yr, 98780 yr after the formation of the primary star. Taken from figure 6 of Susa et al. (2014). Right: Density (top), temperature (middle), and H_2 fraction (bottom) are shown as functions of the distance from the primary star. The red, green, and blue colors correspond to the three snapshots at 2180 yr, 8180 yr, and 98780 yr after the formation of the primary star. Taken from figure 7 of Susa et al. (2014).

primordial galaxy of $\sim 10^8 - 10^9\ M_\odot$ (Tagawa et al., 2015).

Furthermore, mass-accretion onto BHs are also expected while mergers of multiple non-binary BHs proceed by the gas dynamical friction. Therefore, we also elucidate the dominant mechanism, which are the mass accretion or the merger, for the growth of massive BHs. To derive the critical condition that bifurcates the key mechanism of the growth of BHs, we simulate a multiple BH system, including both the gas dynamical friction and the gas accretion (Tagawa et al., 2016).

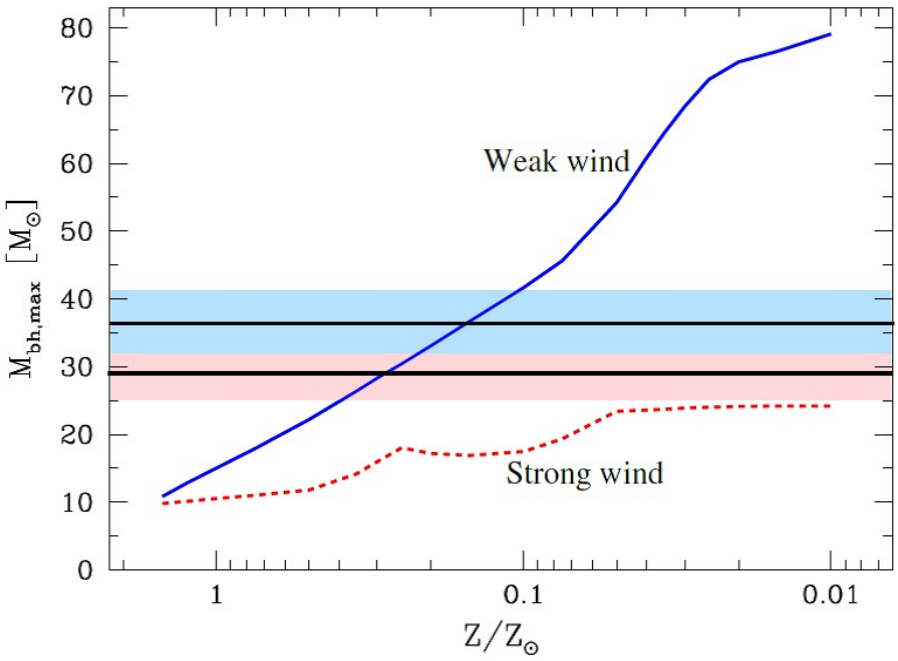

Fig. 1.9 Dependence of maximum BH mass on metallicity Z for strong and weak massive star winds. The masses of GW150914 are indicated by the horizontal bands. Taken from figure 1 of Abbott et al. (2016b).

1.3.2 Detection of the gravitational wave

The merger of BHs may be a potential source of GWs for the Laser Interferometer Space Antenna (LISA) and pulsar timing (Berti et al., 2006; Sesana et al., 2005; Wyithe & Loeb, 2003). Also, the inspiral, merger, and ringdown of binary stellar-mass BH systems can be demonstrated by GWs with the Laser Interferometer Gravitational-Wave Observatory (LIGO), the VIRGO (Abbott et al., 2006; Aasi et al., 2013), the EGO 600 (Lück et al., 2006), or the KAGRA (Aso et al., 2013). Recently, the Advanced LIGO (ALIGO) observatory (LIGO Scientific Collaboration et al., 2015) reported the first direct detection of GWs (Abbott et al., 2016a), aLIGO event GW 150914. The first source of GWs has turned out to be the coalescence of binary BHs. The observed signal in Figure 1.1 indicates that the masses of merged BHs are $m_1 = 36^{+5}_{-4}\ M_\odot$ and $m_2 = 29^{+4}_{-4}\ M_\odot$, and a luminosity distance is 410^{+160}_{-180} Mpc, corresponding to a redshift of $z = 0.09^{+0.03}_{-0.04}$. The GW150914 event is the first observation that can directly confirm the existence of a BH with $\sim 30\ M_\odot$, existence of a merger of a BH binary by GW radiation within the age of the Universe, and existence

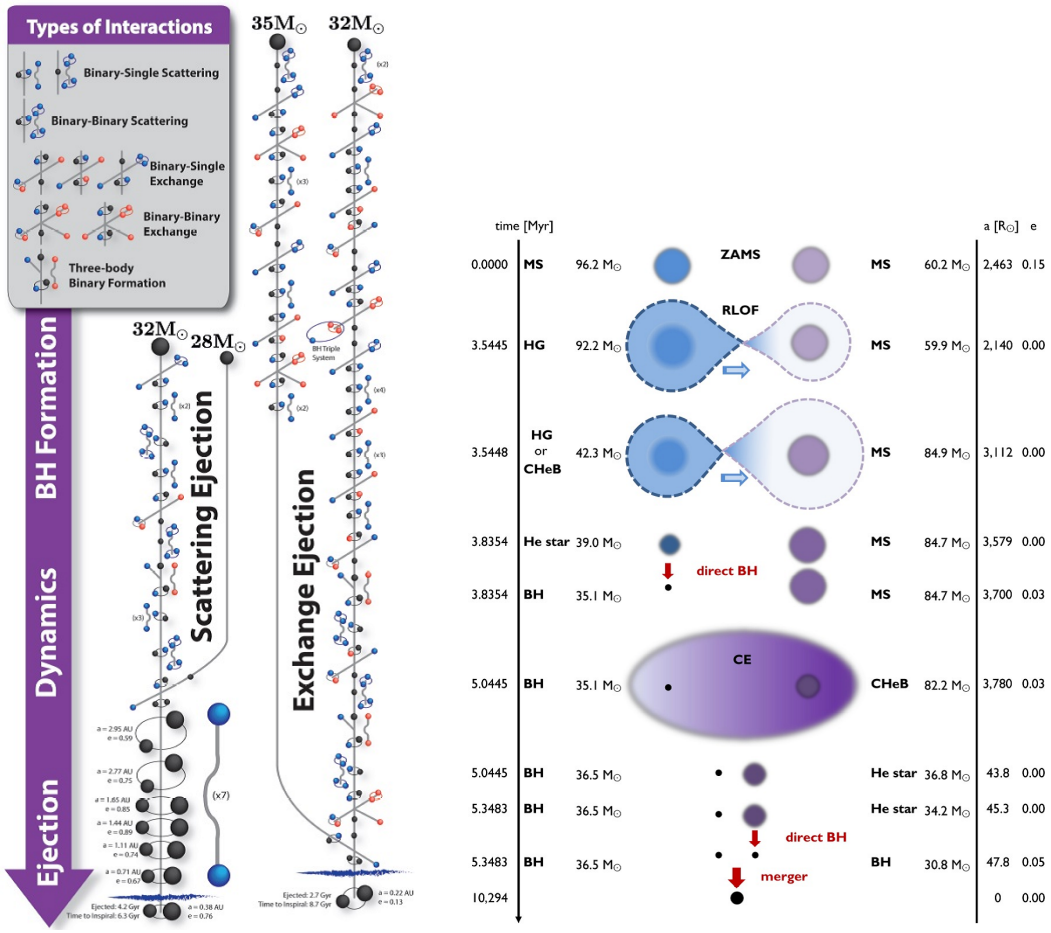

Fig. 1.10 The left and right panels show evolutional tracks of the dynamical formation and classical isolated binary evolution channel leading to the merger similar to the GW150914 events. Left: Interaction diagram of the formation history for two GW150914 progenitors in a single globular cluster model. Taken from figure 1 of Rodriguez et al. (2016). The black, blue, and red sphere represents the GW150914 progenitor BH, other BHs, and stars, respectively. Right: Diagram of binary evolution leading to a BH merger similar to GW150914. This binary stars formed in a low metallicity environment ($Z = 0.03Z_{\odot}$). Taken from figure 1 of Belczynski et al. (2016).

of a heavy stellar mass BH binary. If BHs with $\sim 30\ M_{\odot}$ had been generated as stellar remnants, massive progenitor stars should have taken weak stellar winds. This implies that the progenitor stars formed in a lower metallicity environment, possibly being Pop III stars (Figure 1.9, Abbott et al., 2016b). Also, a weak hard X-ray transient source was detected at 0.4 s after the GW event with *Fermi* Gamma-ray Burst Monitor (Connaughton et al., 2016), although counter arguments are raised.

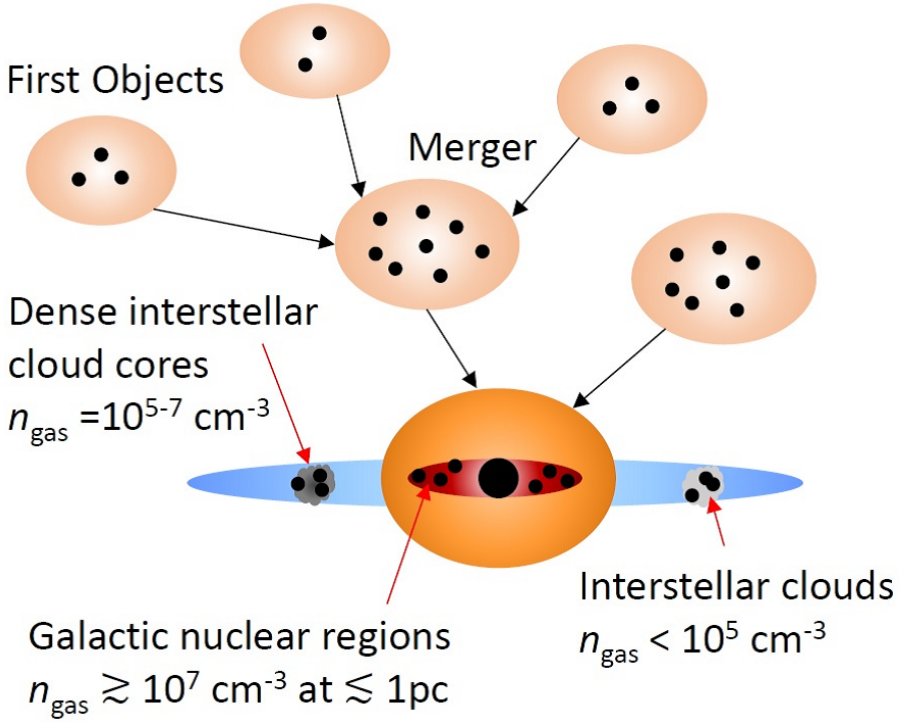

Fig. 1.11 The formation processes of non-binary stellar-mass BHs under gas rich environments in a galaxy.

As the origin of GW150914, several evolutional channels have been proposed. First, the dynamical formation in a globular cluster has been represented (Rodriguez et al., 2016, e.g.). In this channel, the binary separation decays by a number of the three-body interaction, and eventually binary BHs merge to each other due to the GW radiation. Second, the binary evolution has often been considered (Belczynski et al., 2016, e.g.). In this second channel, the massive star binary born in low metallicity environments evolves through mass transfer and/or common envelope phase. After that, the merger is driven by the GW radiation. The left and right panels of Figure 1.10 show evolutional tracks of the first and second channels leading to the merger similar to GW150914. Thus, the merger of stellar-mass BHs has been thought to result from the evolution of binary stars. On the other hand, we have newly proposed a merger scenario from non-binary isolated BHs.

Multiple non-binary stellar-mass BHs are expected to form in first generation objects (left panel of Figure 1.8). Furthermore, according to the hierarchical merger history of galaxies, multiple non-binary stellar-mass BHs are likely to be increased after galaxy mergers as depicted in Figure 1.11.

From our previous study (Tagawa et al., 2015), the multiple non-binary stellar-mass BHs whose typical extension is larger than a thousand AU can merge with each other under gas-rich environments through the gas dynamical friction and the three-body interaction. In galaxies, we can expect several gas rich environments (Figure 1.11) such as galactic center regions of $\lesssim$ 1pc ($n_{\rm gas} \gtrsim 10^7 {\rm cm}^{-3}$, e.g. Namekata & Umemura, 2016), dense interstellar cloud cores ($n_{\rm gas} = 10^{5-7} {\rm cm}^{-3}$, Bergin et al., 1996), and interstellar clouds ($n_{\rm gas} < 10^5 {\rm cm}^{-3}$). In these situations, a considerable amount of gas can accrete onto BHs before the merger (Tagawa et al., 2016). Hence, the initial mass of BHs can be smaller than 30 $M_\odot$, and the initial separation of BHs can be larger than 1 AU. Therefore, mergers of non-binary isolated BHs under gas rich environments may explain the GW150914 event.

In Section 4, to investigate the conditions and environments under which BHs can merge from smaller mass BHs and large separation, we perform post-Newtonian N-body simulations on mergers of stellar-mass BHs. The simulations incorporate such general relativistic effects in the post-Newtonian prescription, the dynamical friction and the mass accretion by ambient gas.

1.3.3 Neutron star mergers as an origin of r-process elements

The astrophysical origin that produces elements heavier than iron by rapid neutron capture reactions (r-process) still remains unsolved. Spectroscopic observations indicate that the r-process rich stars have the same patterns for neutron capture abundances (Figure 1.12, Sneden et al., 2008). These observations imply that r-process elements are mainly produced by one origin. Commonly, probable astrophysical origins of r-process elements are considered to be core-collapse supernovae (CCSNe) and mergers of double neutron stars (NSs) and BH-NS binaries (NSMs), for a long time. However, recent studies of CCSNe nucleosynthesis suggest that the production of heavy r-process elements in CCSNe is difficult to be synthesized (e.g. Reddy et al., 1998; Thompson et al., 2001; Wanajo et al., 2011; Martínez-Pinedo et al., 2012; Wanajo et al., 2013). By contrast, a number of recent nucleosynthesis studies based on hydrodynamical simulations support NSMs as promising sources of r-process elements in the Galaxy (Figure 1.13, Freiburghaus et al., 1999; Korobkin et al., 2012; Wanajo & Janaka, 2012; Wanajo et al., 2014; Bauswein et al., 2014; Foucart et al., 2014; Just et al., 2015).

Nevertheless, the studies of galactic chemical evolution have pointed out that there is a conflict on timescales in the NSM scenario. To reproduce the distribution of r-process elements ([Eu/Fe]) of metal poor stars in the Galactic halo, a very short timescale (1-10 Myr) of NSMs is required (Argast, 2004; Komiya et al., 2014; Matteucci et al., 2014; Tsujimoto & Shigeyama, 2014; Cescutti et al., 2015; van de Voort

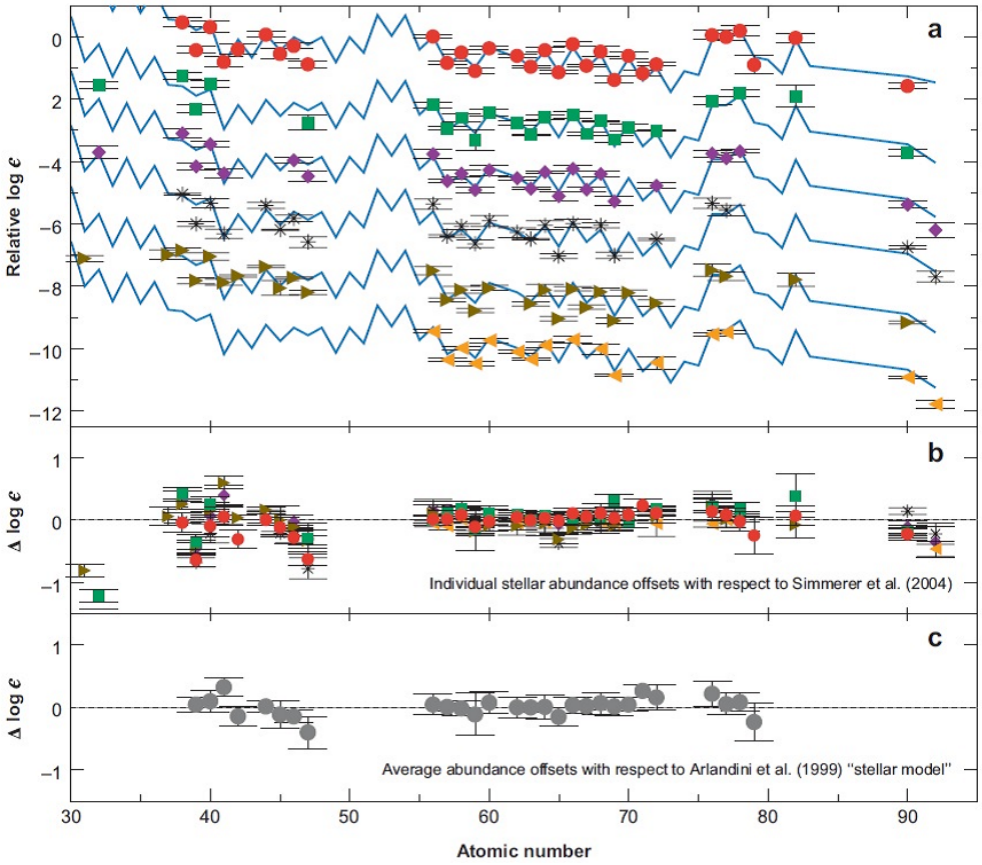

Fig. 1.12 Universality of r-process elements. (a) Comparisons of neutron capture abundances in six r-process rich Galactic halo stars (color plots) with the Solar-system r-process elements-only abundance distribution (blue lines), where $\log\epsilon(A) \equiv \log_{10}(N_{\rm A}/N_{\rm H}) + 12.0$ and $N_{\rm A}$ is abundance of element A. The abundance data of all stars except CS 22892-052 have been vertically displaced downward for display purposes. (b) Difference plot showing the individual elemental abundance offsets; abundance differences are normalized to zero at Eu for each of the six stars with respect to the Solar-system r-process-only abundances. (c) Average stellar abundance offsets. Taken from figure 11 of Sneden et al. (2008).

et al., 2015). On the other hand, the timescale of NSMs is evaluated to be 0.1-1 Gyr from the study of the population synthesis (Portegies et al., 1998; Dominik et al., 2012). Besides, the timescale of NSMs is longer than 100 Myr from the observations of binary pulsars (Lorimer, 2008). Thus, the estimates of the timescale of NSMs are inconsistent with the timescale required by the r-process element distribution of the metal poor stars.

Furthermore, recent study finds Reticulum II as a unique ultra-faint dwarf galaxy (UFD) that shows strong enhancements in r-process elements (Ji et al., 2015). The

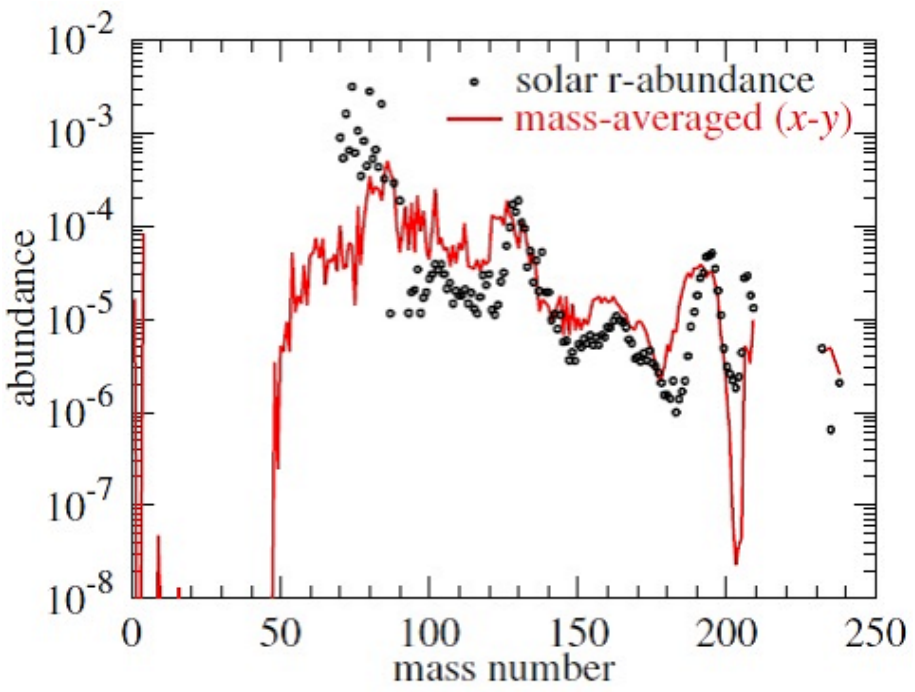

Fig. 1.13 Mass-averaged final nuclear abundances (red line) on the fully general relativistic simulation of a NS-NS merger. Black plots represent the solar r-process abundances. Taken from figure 4 of Wanajo et al. (2014).

r-process enhancement in Reticulum II is 2-3 order of magnitude higher than that in other nine UFDs (Figure 1.14). This observation implies that the origin of r-process elements is a rare event such as NSMs. On the other hand, Bramante & Linden (2016) invokes that the origin of r-process elements is unlikely to be NSMs from these observations of UFDs. Although the r-process enhancement in Reticulum II by NSMs needs the occurrence of NSMs within 0.1-1 Gyr, such merger timescale requires significant supernova natal kicks (50-100 km/s), which remove NS binaries from the weak gravitational potentials of UFDs. Therefore, to explain the origin of the r-process enrichment in Reticulum II by NSMs, any mechanism that can shorten the merger timescale except the significant natal kicks are required.

To solve the problem on the timescales of NSMs, we consider the merger processes in gas-rich first-generation objects at high redshift epochs. As also described in Section 1.3.1, recent radiation hydrodynamic simulations on the formation of first stars show that multiple massive stars form in a primordial gas cloud of $\sim 10^4 - 10^5\ M_\odot$ with the density of around 10^7 cm^{-3} and the extension of 1000 AU, where the gas fraction is 99% (Figure 1.8, Susa et al., 2014). According to the mass function of first stars

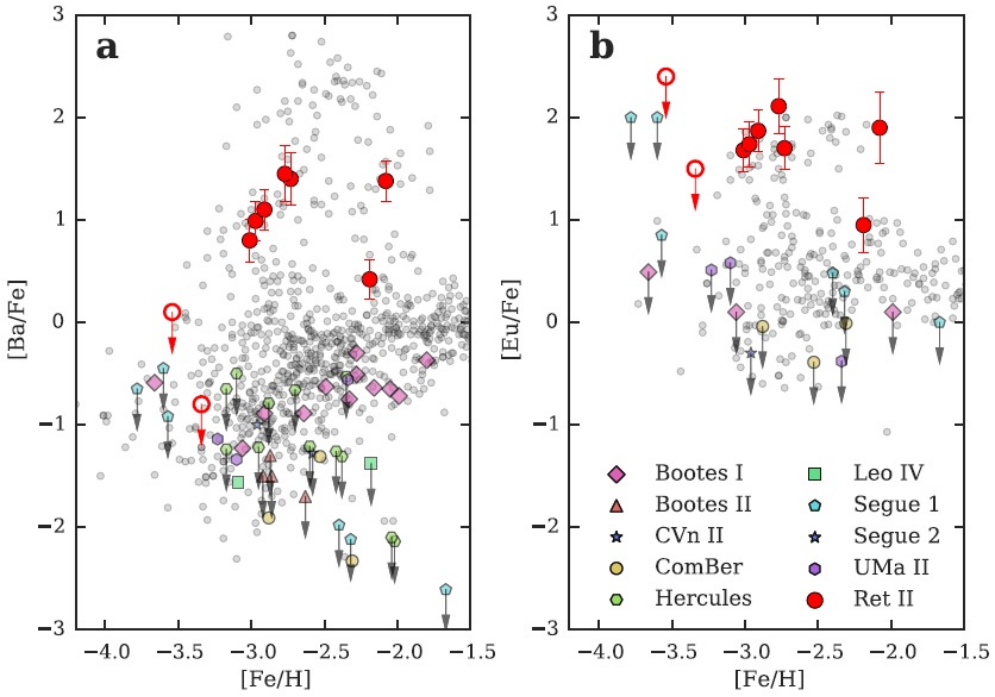

Fig. 1.14 Abundances of r-process elements Ba (a) and Eu (b) for stars in Ret II (large red circles) compared to halo stars (small gray circles) and UFD stars in Segue 1, Hercules, Leo IV, Segue 2, Canes Venatici II, Bootes I, Bootes II, Ursa Major II, and Coma Berenices (medium colored points). Arrows denote upper limits. Taken from figure 2 of Ji et al. (2015).

($\sim 10 - 100\ M_\odot$) (Susa et al., 2014), multiple BHs of a few tens $M_\odot$ and NSs may be born as remnants of supernovae (Figure 1.7, Heger & Woosley, 2002). Recently, Tagawa et al. (2015) have shown that multiple non-binary BHs with separations $\gtrsim 1000$ AU can merge with each other within 100 Myr under gas-rich environments through the three-body interaction and the gas dynamical friction.

Here, to eject the r-process elements by NS-BH mergers, there are the conditions for the properties of the BH. When BH has large spin (dimensionless spin parameter $\alpha \gtrsim 0.7$), the mass of BHs is permitted more than ten $M_\odot$ to release r-process elements (Korobkin et al., 2012; Bauswein et al., 2014; Foucart et al., 2014). From these simulations, in the cases of a large BH mass, these ejection conditions are likely to be concordant with the mass shedding condition as expected in Shibata & Taniguchi (2011). The mass shedding conditions for $\alpha = 0,\ 0.5,\ 0.75,\ 0.9$, and 1 are nearly $m_{\rm BH} = 4.6,\ 7.8,\ 12,\ 19$, and $68\ M_\odot$ (Shibata & Taniguchi, 2011), respectively. As a rough indication for the value of spin parameter, Shibata & Shapiro (2002) indicates that the BH collapsed from supermassive star on fully general relativistic

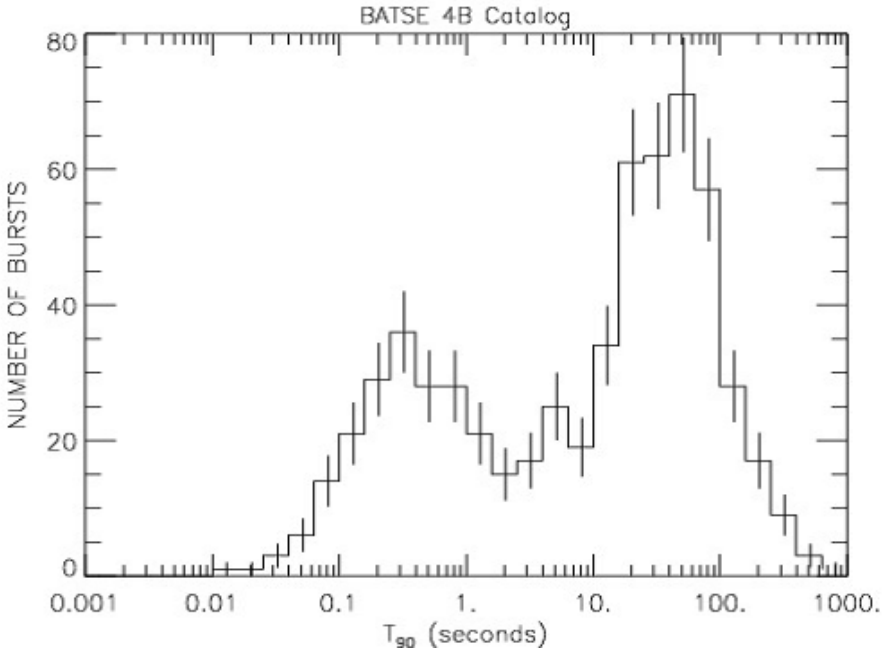

Fig. 1.15 The distribution of duration (T90) for the bursts in the 4B Gamma-Ray Burst Catalog. The T90 is the duration of the period that 90 percent of the burst's energy is emitted. Taken from figure 8 of Paciesas et al. (1999).

simulation has spin of 0.75.

In Section 5.1, to explore the possibility of rapid NSMs in high redshift epochs, we simulate the evolution of a mixed system of BHs and NSs in gas-rich first-generation objects.

1.3.4 Short gamma ray burst

Gamma-ray bursts (GRBs) are short and intense flashes of electromagnetic radiation with typical photon energies of $\sim$ 100keV. GRBs are distributed isotropically on the sky, and no GRB has been observed again. The production of GRBs is thought to require some matter accelerated to relativistic speed (e.g. Meszaros, 2002). The interaction of the relativistic outflow with the surrounding medium will produces synchrotron emission in wide range of wavelength from radio waves to X-rays (e.g. Rees & Meszaros, 1992). This synchrotron emission is called afterglow. The observations of afterglow give the information of distance, energy scales, environments, and progenitors for the GRBs (e.g. Costa et al., 1997).

GRBs are generally classified into two types: long and short GRBs. The classification is based on their spectral hardness and duration. The boundary of the duration

is often given at 2 s because of the bimodal distribution (Figure. 1.15 Paciesas et al., 1999). Besides, the long GRBs and short GRBs have soft and hard spectral, respectively. Due to the difference of properties between long and short GRBs, long and short GRBs are thought to stem from different origins.

The plausible origin of long GRBs is the core collapse supernova of massive stars (Hjorth & Bloom, 2012). From the observation of the afterglow for the long GRBs, a typical opening angle of a jet is $\sim 3-10^{\circ}$ (Frail et al., 2001), and a typical circumburst density is $\sim 1-10\mathrm{cm}^{-3}$ (Yost et al., 2003). Besides, follow-up observations of the hosts have shown that the long GRBs are distributed in bright star-forming regions in their hosts (Fruchter et al., 2006). Furthermore, from the observations of photometry and spectroscopy, long GRBs are likely to be associated with Type Ic SNe (e.g. Woosley & Bloom, 2006).

On the other hand, the origin of short GRBs is still under debate. The plausible origin of short GRBs is the merging of compact objects such as a double NS or NS-BH (Berger, 2014). It is observed that the afterglow of short GRBs are fainter than that of long GRBs. The dimmer afterglows in short GRBs are supposed to result from a lower energy scale and lower circumburst densities (Panaitescu et al., 2001). From the optical and radio observations of afterglows, the circumburst densities are about $\sim 0.1\mathrm{cm}^{-3}$ (Berger, 2014). Perna & Belczynski (2002) has proposed that this low density environments of short GRBs come from the kicks during the binary evolution if compact object mergers produce short GRBs. Meanwhile, recent observation of GRB 130603B indicates that the excess emission in the near-IR matches the predictions for the kilonova with the opacities of r-process elements. This observation favors the compact object binary mergers as an origin of short GRBs.

The evolutional channels of the compact object mergers have been proposed that the evolution of massive star binary in a primordial binary (Narayan et al., 1992) or the evolution by dynamical interactions in globular clusters (Salvaterra et al., 2008). On the other hand, we propose the merger processes evolved from the non-binary stars. Then, we estimate the merger rates of NSMs and event rates of short GRBs from the evolution of non-binary stars, and compare the estimated rates to observed event rates.

1.3.5 Overview of this thesis

Here, we explain the overview of this thesis. The main purpose of this thesis is to elucidate how mergers from multiple BHs in gas-rich environments proceed, and how BHs grow.

In Section 3, we focus on the merger processes of multiple BHs in primordial gas at early cosmic epochs. The investigation of mergers for multiple BHs evolved from

first stars is our first work. For the purpose, we perform post-Newtonian N-body simulations, incorporating the effects of the gas dynamical friction, gas accretion, and GW emission. Our simulations solve the merger of more than three BHs with effects of gas for the first time. Such merger processes are important because a third BH, which decays due to the gas dynamical friction, effectively transports the angular momentum of binary BHs by the three-body interaction. In our study, we investigate how BH mergers proceed by elucidating the merger mechanisms and the merger time. Furthermore, to investigate how BHs grow, we derive a critical accretion rate ($\dot{m}_{\rm c}$), below which the BH growth is promoted faster by mergers, and estimate the effect of the recoil by the GW emission.

In Section 4, we investigate the possibility that the BH merger in GW150914 is evolved from non-binary isolated stars. For the merger scenario of GW150914, the merger stemming from non-binary isolated stars has never been investigated. Then, we elucidate the condition of the BH mergers in the GW150914 event from non-binary isolated BHs with the effects of gas. Besides, we roughly estimate the event rates of BH mergers similar to GW150914 in the non-binary merger scenario.

In Section 5, we apply the merger processes to several issues described in Section 1.3.1, 1.3.3 and 1.3.4. In Section 5.1, to solve the confliction for the NS merger timescale, we consider the mergers in a mixed system of BHs and NSs assuming gas-rich first-generation objects. The investigation of the NS mergers in first-generation objects from multiple stars is our first work. By performing post-Newtonian N-body simulations, we explore the timescale of NS mergers in gas-rich first-generation objects. In Section 5.2, we roughly estimate the event rates of short GRBs by the NS-NS mergers evolved from non-binary stars. In Section 5.3, we discuss the possible environments for the BH growth via BH-BH mergers.

Chapter 2

Numerical model

In this chapter, we describe the framework of numerical simulations. The simulations incorporate the general relativistic effects as the pericentre shift and GW emission (Figure 1.2) as well as the gas dynamical friction and the mass accretion (Figure 1.3), since these effects prompt the merger of multiple BHs under gas rich environments. In our simulations, the three body interaction is also solved precisely, and so the merger processes of three BHs with effects of gas is investigated for the first time.

2.1 Equation of motion

In our simulations, the equations of motion for BHs are given as

$$\frac{d^2\mathbf{r}_i}{dt^2} = \sum_j^{N_{\rm BH}} \left\{ -Gm_j \frac{\mathbf{r}_i - \mathbf{r}_j}{|\mathbf{r}_i - \mathbf{r}_j|^3} + \mathbf{a}_{{\rm PN},ij} \right\} + \mathbf{a}_{{\rm acc},i} + \mathbf{a}^{\rm gas}_{{\rm DF},i} + \mathbf{a}_{{\rm pot},i}, \tag{2.1}$$

where $\mathbf{r}_i$ and $\mathbf{r}_j$ are respectively the positions of i-th and j-th BH, m_j is the mass of j-th BH, $N_{\rm BH}$ is the number of BHs, G is the gravitational constant, $\mathbf{a}_{{\rm PN},ij}$ is the general relativistic acceleration of j-th BH on i-th BH in the post-Newtonian prescription up to 2.5PN term (Kupi et al., 2006). The 1PN and 2PN terms represent the pericenter shift, and 2.5PN term represents the GW emission (shown in Section 2.1.2), $\mathbf{a}^{\rm gas}_{{\rm DF},i}$ is the acceleration on i-th BH by the gas dynamical friction (Section 2.1.3), and $\mathbf{a}_{{\rm pot},i}$ is the acceleration on i-th BH by the gas gravitational potential (Section 2.1.4), and $\mathbf{a}_{{\rm acc},i}$ is the acceleration on i-th BH by the gas accretion (Section 2.1.5),

The integration of the equations of motion is calculated by the fourth-order Hermite scheme with the shared time step (Makino & Aarseth, 1992, Section 2.1.1).

2.1.1 Numerical scheme

For the integration of the equation of motion, we use the fourth-order Hermite scheme with the shared time step (Makino & Aarseth, 1992). We calculate the time derivative of the acceleration by the Newtonian gravity, the relativistic force, and the gas gravitational potential in order to use the Hermite scheme. On the other hand, we treat the dynamical friction and accretion of gas to quadratic order, since the formulae of the dynamical friction and accretion acceleration are not so accurate as that of gravity and also the fourth-order scheme is especially required during the three-body interaction between a close BH binary and an intruding BH. Here, the shared time step is given as

$$\Delta t = \min_i \sqrt{\eta_{\rm ac} \frac{|\mathbf{a}_{{\rm Her},i}||\mathbf{a}^{(2)}_{{\rm Her},i}| + |\mathbf{a}^{(1)}_{{\rm Her},i}|^2}{|\mathbf{a}^{(1)}_{{\rm Her},i}||\mathbf{a}^{(3)}_{{\rm Her},i}| + |\mathbf{a}^{(2)}_{{\rm Her},i}|^2}}, \tag{2.2}$$

where $\mathbf{a}^{(k)}_{{\rm Her},i}$ is the k-th derivative of $\mathbf{a}_{{\rm Her},i}$, $\mathbf{a}_{{\rm Her},i}$ is the acceleration on i-th BH that is treated until the fourth-order, and $\mathbf{a}_{{\rm Her},i}$ is given by

$$\mathbf{a}_{{\rm Her},i} = \sum_j^{N_{\rm BH}} \left\{ -Gm_j \frac{\mathbf{r}_i - \mathbf{r}_j}{|\mathbf{r}_j - \mathbf{r}_j|^3} + \mathbf{a}_{{\rm PN},ij} \right\} + \mathbf{a}_{{\rm pot},i}. \tag{2.3}$$

The $\eta_{\rm ac}$ is the accuracy parameter, and we settle to be $\eta_{\rm ac} = 0.003$.

To avoid cancellation of significant digits at tiny separations of $\sim 100\ r_{\rm sch}$, we calculate the BHs evolution in the coordinate whose origin is always the center of mass for the closest BH pair.

2.1.2 Relativistic effects

We incorporate the general relativistic effects by the post-Newtonian prescription up to 2.5PN term (Kupi et al., 2006). The post-Newtonian approximation is the one of the approximation of the general relativistic effects for weak gravity field. In the post-Newtonian approximation, the Einstein field equation is expressed by the series of powers of v/c. As the relativistic effects on i-th BH by j-th BH, simulations incorporate 1PN ($\mathbf{a}_{\rm 1PN,ij}$) and 2PN ($\mathbf{a}_{\rm 2PN,ij}$) terms corresponding to the first and second order for the pericentre shift, and 2.5PN term ($\mathbf{a}_{\rm 2.5PN,ij}$) corresponding to the

GW emission (Figure 1.2). The post-Newtonian terms are given by

$$\begin{aligned}\mathbf{a}_{\mathrm{1PN,ij}} = \frac{Gm_j}{c^2 r_{ij}^2}[\mathbf{n}[&-{\mathbf{v}_i}^2 - 2{\mathbf{v}_j}^2 + 4\mathbf{v}_i\mathbf{v}_j + \frac{3}{2}(\mathbf{n}\mathbf{v}_j)^2 \\ &+5\left(\frac{Gm_i}{r_{ij}}\right) + 4\left(\frac{Gm_j}{r_{ij}}\right)] \\ &+(\mathbf{v}_i - \mathbf{v}_j)(4\mathbf{n}\mathbf{v}_i - 3\mathbf{n}\mathbf{v}_j)],\end{aligned} \tag{2.4}$$

$$\begin{aligned}\mathbf{a}_{\mathrm{2PN,ij}} = \frac{Gm_j}{c^4 r_{ij}^2}[\mathbf{n}[&-2{\mathbf{v}_j}^4 + 4{\mathbf{v}_j}^2(\mathbf{v}_i\mathbf{v}_j) - (\mathbf{v}_i\mathbf{v}_j)^2 \\ &+\frac{3}{2}{\mathbf{v}_i}^2(\mathbf{n}\mathbf{v}_j)^2 + \frac{9}{2}{\mathbf{v}_j}^2(\mathbf{n}\mathbf{v}_j)^2 - 6(\mathbf{v}_i\mathbf{v}_j)(\mathbf{n}\mathbf{v}_j)^2 \\ &-\frac{15}{8}(\mathbf{n}\mathbf{v}_j)^4 + \left(\frac{Gm_i}{r_{ij}}\right)[-\frac{15}{4}{\mathbf{v}_i}^2 + \frac{5}{4}{\mathbf{v}_j}^2 \\ &-\frac{5}{2}\mathbf{v}_i\mathbf{v}_j + \frac{39}{2}(\mathbf{n}\mathbf{v}_i)^2 - 39(\mathbf{n}\mathbf{v}_i)(\mathbf{n}\mathbf{v}_j) + \frac{17}{2}(\mathbf{n}\mathbf{v}_i)^2] \\ &+\left(\frac{Gm_j}{r_{ij}}\right)[4{\mathbf{v}_j}^2 + 8\mathbf{v}_i\mathbf{v}_j + 2(\mathbf{n}\mathbf{v}_i)^2 \\ &-4(\mathbf{n}\mathbf{v}_i)(\mathbf{n}\mathbf{v}_j) - 6(\mathbf{n}\mathbf{v}_i)^2] + (\mathbf{v}_i - \mathbf{v}_j)[{\mathbf{v}_i}^2(\mathbf{n}\mathbf{v}_j) \\ &+4{\mathbf{v}_j}^2(\mathbf{n}\mathbf{v}_i) - 5{\mathbf{v}_j}^2(\mathbf{n}\mathbf{v}_2) - 4(\mathbf{v}_i\mathbf{v}_j)(\mathbf{n}\mathbf{v}_i) \\ &+4(\mathbf{v}_i\mathbf{v}_j)(\mathbf{n}\mathbf{v}_j) - 6(\mathbf{n}\mathbf{v}_i)(\mathbf{n}\mathbf{v}_j)^2 + \frac{9}{2}(\mathbf{n}\mathbf{v}_j)^3 \\ &+\left(\frac{Gm_i}{r_{ij}}\right)\left(-\frac{63}{4}\mathbf{n}\mathbf{v}_i + \frac{55}{4}\mathbf{n}\mathbf{v}_j\right) \\ &+\left(\frac{Gm_j}{r_{ij}}\right)(-2\mathbf{n}\mathbf{v}_i - 2\mathbf{n}\mathbf{v}_j)]] \\ &+\frac{G^3 m_j}{r_{ij}^4}\mathbf{n}[-\frac{57}{4}{m_i}^2 - 9{m_j}^2 - \frac{69}{2}m_i m_j],\end{aligned} \tag{2.5}$$

$$\begin{aligned}\mathbf{a}_{\mathrm{2.5PN,ij}} = \frac{4}{5}\frac{G^2 m_i m_j}{c^5 r_{ij}^3}[(\mathbf{v}_i - \mathbf{v}_j)[&-(\mathbf{v}_i - \mathbf{v}_j)^2 \\ &+2\left(\frac{Gm_i}{r_{ij}}\right) - 8\left(\frac{Gm_j}{r_{ij}}\right)] + \mathbf{n}(\mathbf{n}\mathbf{v}_i - \mathbf{n}\mathbf{v}_j) \\ &[3(\mathbf{v}_i - \mathbf{v}_j)^2 - 6\left(\frac{Gm_i}{r_{ij}}\right) + \frac{52}{3}\left(\frac{Gm_j}{r_{ij}}\right)]],\end{aligned} \tag{2.6}$$

where

$$\mathbf{n} = \frac{\mathbf{r}_{ij}}{r_{ij}}, \tag{2.7}$$

$$\mathbf{r}_{ij} = (\mathbf{r}_i - \mathbf{r}_j). \tag{2.8}$$

2.1.3 Gas dynamical friction

In the gas dynamical friction, the BH gravity creates density increase within ambient gas, which act as a drag force (left panel of Figure 1.3). Ostriker (1999) derive the analytical formulae for the gas dynamical friction. In the analysis, Ostriker (1999) find that the formulae vary whether a perturber is subsonic of $\mathcal{M} < 1$ or supersonic of $\mathcal{M} > 1$, where $\mathcal{M}$ is the mach number of a perturber. This comes from the shape of a perturbed density. A subsonic perturber generates a density distribution with ellipses contours of constant density. On the other hand, a supersonic perturber generates a density wake within the rear Mach cone of half-opening angle $\theta = \sin^{-1}(1/\mathcal{M})$. Whereas, Escala et al. (2004) indicate that the analytic formula in a supersonic region of $\sim 1.5 > \mathcal{M} > 1$ derived in Ostriker (1999) is overestimated. Then Escala et al. (2004) gives fitting formulae in comparison to the orbital decay using a numerical hydrodynamical simulation. The gas dynamical friction force derived as analytic formulae in Escala et al. (2004) discontinuously varies at $\mathcal{M} = 0.8$. Moreover, Tanaka & Haiman (2009) point out that the gas dynamical friction force prescribed by Escala et al. (2004) in a supersonic region of $\mathcal{M} >\sim 1.5$ is overestimated. Hence, Tanaka & Haiman (2009) use the prescription of Escala et al. (2004) in $\mathcal{M} < \mathcal{M}_{\rm eq}$, and that of Ostriker (1999) in $\mathcal{M} > \mathcal{M}_{\rm eq}$, where $\mathcal{M}_{\rm eq}$ is the Mach number where the acceleration given by these two formulae are equal.

In our simulation, we use the formulae given by Tanaka & Haiman (2009). Here, we adopt $\mathcal{M}_{\rm eq} = 1.5$ as Tanaka & Haiman (2009). Then, the acceleration of the dynamical friction by gas ($\mathbf{a}^{\rm gas}_{{\rm DF},i}$) is given as

$$\mathbf{a}^{\rm gas}_{{\rm DF},i} = -4\pi G^2 m_i m_{\rm H} n_{\rm gas}(r) \frac{\mathbf{v}_i}{{v_i}^3} \times f(\mathcal{M}_i), \tag{2.9}$$

$$f(\mathcal{M}_i) = \begin{cases} 0.5\ln\left(\frac{v_i t}{r_{\rm min}}\right)\left[\mathrm{erf}\left(\frac{\mathcal{M}_i}{\sqrt{2}}\right) - \sqrt{\frac{2}{\pi}}\mathcal{M}_i \exp(-\frac{\mathcal{M}_i^2}{2})\right], \\ (0 \leq \mathcal{M}_i \leq 0.8) \\ 1.5\ln\left(\frac{v_i t}{r_{\rm min}}\right)\left[\mathrm{erf}\left(\frac{\mathcal{M}_i}{\sqrt{2}}\right) - \sqrt{\frac{2}{\pi}}\mathcal{M}_i \exp(-\frac{\mathcal{M}_i^2}{2})\right], \\ (0.8 \leq \mathcal{M}_i \leq \mathcal{M}_{\rm eq}) \\ \frac{1}{2}\ln\left(1 - \frac{1}{\mathcal{M}_i^2}\right) + \ln\left(\frac{v_i t}{r_{\rm min}}\right), \\ (\mathcal{M}_{\rm eq} \leq \mathcal{M}_i) \end{cases} \tag{2.10}$$

where $n_{\rm gas}$ is the gas number density, $m_{\rm H}$ is the mass of the hydrogen atom, v_i is the velocity of i-th BH, and t is the elapsed time. The $r_{\rm min}$ is the minimum scale that the gas dynamical friction work on a BH, and we give $r_{\rm min}$ as Gm_i/v_i^2. Here, $v_i t$ means the effective scale of gaseous medium, and we set an maximum value of $v_i t$ to 0.1 pc. If $v_i t < r_{\rm min}$, we give $f(\mathcal{M}_i) = 0$.

2.1.4 Gas potential

In our study, we postulate uniform background gas to extract the dependence on the gas density, and give the gas density as a parameter. Then, the acceleration by gas gravitational potential ($\mathbf{a}_{{\rm pot},i}$) and its time derivative ($\dot{\mathbf{a}}_{{\rm pot},i}$) are given by

$$\mathbf{a}_{{\rm pot},i} = -\frac{4}{3}\pi G m_{\rm H} n_{\rm gas} \mathbf{r}_i, \tag{2.11}$$

$$\dot{\mathbf{a}}_{{\rm pot},i} = -\frac{4}{3}\pi G m_{\rm H} n_{\rm gas} \mathbf{v}_i. \tag{2.12}$$

2.1.5 Gas accretion

We envisage the Hoyle-Lyttleton accretion as an accretion mechanism onto BHs. The Eddington luminosity does not limit the mass accretion rate in a BH accretion disk. This is because photons are trapped within innermost optically-thick regions without diffusing away from the disk surface (so-called photon trapping effects, Abramowicz et al., 1988). Here, we use a model for such a super-Eddington accretion. The luminosity

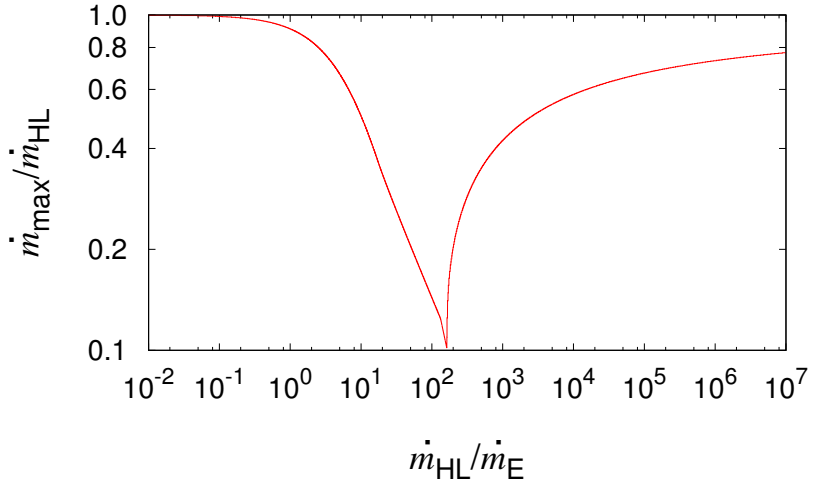

Fig. 2.1 The maximum gas accretion rate ($\dot{m}_{\rm max}$) with the reduction by radiation pressure as a function of the Eddington accretion rate ($\dot{m}_{\rm E}$), where $\dot{m}_{\rm HL}$ is the Hoyle-Lyttleton accretion rate. A viscous accretion disk with viscosity parameter $\alpha = 0.1$ is assumed. Taken from figure 1 of Tagawa et al. (2016).

of a super-Eddington (slim) disk is fitted as

$$\begin{aligned}\Gamma &\equiv L/L_{\rm E} \\ &\simeq \begin{cases} 2\left[1+\ln\left(\frac{\eta\dot{m}}{20\dot{m}_{\rm E}}\right)\right] & \text{for } \dot{m} \geq 20\ \dot{m}_{\rm E}/\eta \\ \left(\frac{\eta\dot{m}}{10\dot{m}_{\rm E}}\right) & \text{for } \dot{m} < 20\ \dot{m}_{\rm E}/\eta \end{cases}\end{aligned} \tag{2.13}$$

for the viscosity parameter of $\alpha = 0.1$ (Watarai et al., 2000), where $\dot{m}$ is the mass accretion rate, $L_{\rm E}$ is the Eddington luminosity, $\dot{m}_{\rm E}$ ($= L_{\rm E}/\eta c^2$) is the Eddington accretion rate, η is the radiative energy conversion efficiency ($\eta = 0.1$ in this study), and c is the speed of light.

We also consider the effect of the radiation pressure on the Hoyle-Lyttleton accretion. The accretion rate is reduced by the radiation pressure as

$$\frac{\dot{m}}{\dot{m}_{\rm HL}} = \begin{cases} (1-\Gamma) & (0 \leq \Gamma \leq 0.64) \\ (1-\Gamma-\frac{2}{\pi}\psi_0+\Gamma{\rm sin}\psi_0) & \\ & (0.64 \leq \Gamma \leq 1.65) \\ \frac{2}{\pi}\tan^{-1}\left(\frac{\Gamma}{0.75{\rm ln}10^5}\right) & (1.65 \leq \Gamma) \end{cases} \tag{2.14}$$

(Hanamoto et al., 2001), where $\dot{m}_{\rm HL}$ is the Hoyle-Lyttleton accretion rate, and $\cos\psi_0 = 2/(\pi\Gamma)$. By combining equations (2.13) and (2.14), the maximum gas accretion rate ($\dot{m}_{\rm max}$), which is shown in Fig. 2.1, is derived. Fig. 2.1 shows

the Hoyle-Lyttleton accretion rate is maximally reduced until $\sim 0.1\dot{m}_{\rm HL}$ around $\dot{m}_{\rm HL}/\dot{m}_{\rm E} \approx 10^2$. For $\dot{m}_{\rm HL}/\dot{m}_{\rm E} > 10^2$, the reduction becomes smaller due to the photon trapping effect.

To parameterize the accretion rate, the gas mass accretion rate is given as

$$\dot{m}_i = \epsilon \dot{m}_{{\rm HL},i} = \epsilon \frac{4\pi G^2 m_{\rm H} n_{\rm gas} m_i^2}{(C_{\rm s}^2 + v_i^2)^{3/2}}. \tag{2.15}$$

The v_i is the velocity of ith BH, and $\epsilon(\leq 1)$ is the accretion efficiency. In our study, considering another feedback effects, we investigate the range of $10^{-7} \leq \epsilon \leq 1$ or $\epsilon = 0$. For a given $\dot{m}_i$, it is further limited by the maximum accretion rate shown in Fig. 2.1. As for the back reaction against gas accretion, the acceleration due to gas accretion is incorporated. We assume that the relative velocity between BH and gas is the BH velocity (i.e., static ambient gas in the Hoyle-Lyttleton accretion scales). Then, the acceleration due to gas accretion on ith BH $a_{{\rm acc},i}$ is given by

$$a_{{\rm acc},i} = -\frac{\dot{m}_i v_i}{m_i}. \tag{2.16}$$

Also, when the gas accretes onto BHs, the gas mass and the gas number density is reduced to conserve the total mass of the system.

2.1.6 Recoil kick

In the study for an origin of the r-process elements, we incorporate the effect of GW radiation recoil for the merged BH. When the recoil kick velocity for the merged BH due to the anisotropic emission of GW radiation is calculated, we randomly give the spin magnitude in an uniform probability and the isotropic direction for each BH on the occasion of the merger. In the cases of the NS-BH mergers, we simply give the recoil velocity in the same manner as the BH-BH mergers. We employ the model of

the recoil velocity given by

$$\begin{aligned}
\boldsymbol{V}_{\rm recoil}(q,\boldsymbol{\alpha}) &= v_m\hat{\boldsymbol{e}}_1 \\
&\quad + v_\perp(\cos\xi\hat{\boldsymbol{e}}_1 + \sin\xi\hat{\boldsymbol{e}}_2) + v_\parallel\hat{\boldsymbol{e}}_z, \\
v_m &= A\frac{q^2(1-q)}{(1+q)^5}\left(1+B\frac{q}{(1+q)^2}\right), \\
v_\perp &= H\frac{q^2}{(1+a)^5}(\alpha_2^\parallel - q\alpha_1^\parallel), \\
v_\parallel &= K\cos(\Theta-\Theta_0)\frac{q^2}{(1+q)^5}(\alpha_2^\perp - q\alpha_1^\perp)
\end{aligned} \tag{2.17}$$

(Campanelli et al., 2007a), where $\boldsymbol{\alpha}_i = \boldsymbol{S}_i/m_i^2$, $\boldsymbol{S}_i$ is the spin of BH i, q is the mass ratio of the smaller to larger mass BH, and the indices $\parallel$ and $\perp$ refer to parallel and perpendicular to the orbital angular momentum, respectively, $\hat{\boldsymbol{e}}_1$, $\hat{\boldsymbol{e}}_2$ are orthogonal unit vectors in the orbital plane, ξ represents the angle between the unequal-mass and spin contributions to the recoil velocity in the orbital plane, Θ is the angle between the infall direction and the in-plane component of $\boldsymbol{\Delta} \equiv m(\boldsymbol{S}_2/m_2 - \boldsymbol{S}_1/m_1)$ at the merger. Since our simulations cannot resolve the moment of the merger, we simply use the infall direction of Θ by the relative direction for a larger BH from a smaller BH at our merger condition, and $\Theta_0 = 0^\circ$. The constants are given as $A = 1.2\times10^4$ km s^{-1}, $B = -0.93$, $H = 7.3\times10^3$km s^{-1}, and $K = 6.0\times10^4$ km s^{-1} (Campanelli et al., 2007a). Referring to $\xi = 90^\circ$ for head-on collisions in Choi et al. (2007) and $\xi = 88^\circ$ for SP6 run in Campanelli et al. (2007b), we give $\xi = 90^\circ$.

2.2 Key parameters

Parameters for merger processes of multiple black holes

The four key parameters in the simulations of Section 3 are the initial BH mass, the BH density, the gas number density, the accretion efficiency, and the BH number. Initially, we set ten BHs of equal mass.

As fiducial conditions, we consider two cases for the BH mass of 30 $M_\odot$ and 10^4 $M_\odot$. The 30 $M_\odot$ BHs is assumed to be first star remnants, which are born in a first-generation object of $\sim 10^5 - 10^6$ $M_\odot$, or to be massive star remnants, which stray into gas rich environments. The 10^4 $M_\odot$ BHs is formed from supermassive stars, which are incorporated in a primordial galaxy of $\sim 10^8 - 10^9$ $M_\odot$

As a key parameter, we vary the BH density, $\rho_{\rm BH}$, at the initial epoch. To vary the BH density, we change the typical extension of the BH spatial distribution at the initial epoch, $r_{\rm typ}$. The relation between $\rho_{\rm BH}$ and $r_{\rm typ}$ is given by

$$\rho_{\rm BH} = \frac{3}{4\pi r_{\rm typ}^3} \sum_i m_i. \tag{2.18}$$

We alter $r_{\rm typ}$ from 0.01 pc to 1 pc for 30 $M_\odot$ mass BH referring to the simulations on first star formation (Greif et al., 2011; Umemura et al., 2012; Susa, 2013; Susa et al., 2014), and $r_{\rm typ}$ from 0.1 pc to 10 pc for 10^4 $M_\odot$ mass BH.

Additionally, the gas number density ($n_{\rm gas}$) is a key parameter. Simulations of first star formation show that the gas density in a first object is settled at $\sim 10^{7-8}$ cm^{-3} in a primordial cloud of $\sim$ 0.01 pc (Susa et al., 2014). Besides, the $n_{\rm gas}$ of dense interstellar cloud cores is from 10^5cm^{-3} to 10^7cm^{-3} (e.g. Bergin et al. (1996)), and the $n_{\rm gas}$ of galactic nuclear regions is $n_{\rm gas} \gtrsim 10^7$cm^{-3} at $\lesssim$ 1pc (e.g. Namekata & Umemura, 2016). Anyhow the gas density is less than 10^{10} cm^{-3} for the scale of 0.01 pc in realistic environments. Nevertheless, to elucidate the merger processes in a wide variety of environments, we consider the gas density from 10^4 cm^{-3} to 10^{12} cm^{-3}.

Furthermore, we change the gas accretion efficiency, ϵ. The relation between the accretion rate and accretion efficiency is described in Section 2.1.5. Because the gas accretion rate in first-generation objects is not elucidated, we consider a wider range of gas accretion efficiency as $10^{-7} \leq \epsilon \leq 1$ or $\epsilon = 0$.

The simulations are evolved for 100 Myr, because the background environments of the host objects are likely to change in 100 Myr. Also, we terminate simulations, if the number of BHs becomes less than two due to the merger or escape.

Parameters for non-binary merger in GW150914

The key parameters in the simulations of Section 4 are the BH density, the initial BH mass, the gas number density, and the gas accretion efficiency.

One key parameter in our simulations is the BH density, $\rho_{\rm BH}$, at the initial epoch. Simulations on the formation of the first stars shows that several or more stars are born in a disk of ~ 1000 AU. Referring to these results, we investigate the range of $r_{\rm typ}$ from 0.01 pc to 1 pc.

Additionally, assuming first star remnants or massive stars born in low-z, we set up five BHs of equal mass of 20, 25 and 30 $M_\odot$ initially.

Considering the various environments such as interstellar clouds, dense interstellar cloud cores, and galactic nuclear regions, we give the range of the gas density from 10^2 cm^{-3} to 10^{10} cm^{-3}.

Furthermore, we change the gas accretion efficiency, ϵ, from 10^{-3} to 1.

The simulations are evolved for 10 Gyr, since we consider the merger within the cosmic time. Also, we terminate the simulation, if one merger of BHs occurs.

Parameters for origin of r-process elements by neutron star mergers

The key parameters in the simulations of Section 5.1 are the BH density, the gas number density, the gas accretion efficiency, and the initial compact star mass distribution.

The simulation for the origin of r-process elements incorporates the effect of the recoil kick due to the anisotropic emission of GW radiation (Section 2.1.6).

One key parameter in our simulations is the BH density, $\rho_{\rm BH}$, at the initial epoch. Recent radiation hydrodynamic simulations on the formation of the first stars have shown that several or more stars are born in a disk of ~ 1000 AU (Susa et al., 2014). From these results, we change the typical extensions of BH spatial distributions at the initial epoch, $r_{\rm typ}$, from 0.001 pc to 3 pc.

Another key parameter is the gas number density, $n_{\rm gas}$. Referring to the simulations of the first star formation, we consider the gas density from 10^5 cm^{-3} to 10^{10} cm^{-3}.

Furthermore, we change the gas accretion efficiency, ϵ, as $10^{-4} \leq \epsilon \leq 1$ or $\epsilon = 0$.

As the initial compact star mass distribution, we give the next three patterns.

$$\begin{aligned}
&\text{(a)} 30 M_\odot \times 1,\ 10\ M_\odot \times 2,\ 1.3\ M_\odot \times 2 \\
&\text{(b)} 10\ M_\odot \times 2,\ 1.3\ M_\odot \times 3 \\
&\text{(c)} 10\ M_\odot \times 3,\ 1.3\ M_\odot \times 2
\end{aligned}$$

In our simulations, we assume that the compact stars of $\lesssim 1.4\ M_\odot$ are NSs and others are BHs.

The evolution is pursued for 100 Myr, which is sufficiently longer than the required time ($\sim$ 10 Myr) to explain the distribution of r-process elements for metal poor stars in the MW halo. We also terminate simulations if NSMs satisfy the conditions for the mass ejection of r-process elements, or all BHs merge into one BH. Here, we set the conditions for the mass ejection of r-process elements to the mergers of NS-NS or light BH($m_{\rm BH} \leq 68\ M_\odot$)-NS. This condition for the BH mass at NS-BH mergers accords with the mass shedding condition for the Kerr BH (Shibata & Taniguchi, 2011).

2.3 Conditions for simulations

2.3.1 Initial condition of the BH distribution

The initial positions of BHs are given randomly in the $x-y$ plane within $r_{\rm typ}$ and the velocities of BHs are given as the sum of a circular component and a random component. The circular velocities are given to balance against the gravity of gas in the $x-y$ plane and the random velocities are given in the xyz space according to a Gaussian distribution with the same dispersion as the circular velocity.

In Section 3 and 5.1, we consider the mergers of first star remnants. First stars are supposed to born in the gas disk, which is supposed to have circular and random velocities due to the turbulence and/or the cold accretion. Besides, multiple first stars presumably receive the kicks due to the three-body interaction. Thus, we give the random and circular velocities initially.

On the other hand, in Section 4, we consider the mergers of first star remnant BHs and Pop I/II BHs. The velocities of the Pop I/II BHs are thought to be randomly distributed. Here, we verify that the dependence of the ratio of the circular velocities to the total velocities on the merger time and the merger type is negligible. Then, we give the same initial velocity distribution for the run of Section 4 as the velocity distribution for Section 3 and 5.1 described above. Other discussions for the validation of an initial condition for Section 4 is described in Section 4.1.

2.3.2 Merger condition

We assume that two MBHs merge, when their separation is less than 100 times the sum of their Schwarzschild radii:

$$|\boldsymbol{r}_i - \boldsymbol{r}_j| < 100\,(r_{{\rm sch},i} + r_{{\rm sch},j})\,, \tag{2.19}$$

where $r_{{\rm sch},i} = 2Gm_i/c^2$ is the Schwarzschild radius of i-th BH. Therefore, the simulations do resolve the scales of 100 $r_{\rm sch}(M_{\rm BH} = 30M_\odot) \simeq 2 \times 10^9$cm. To avoid

cancellation of significant digits and resolve such tiny scales of 100 $r_{\rm sch}$, the BHs evolution is calculated in the coordinate whose the origin is always set to the center of mass for the closest pair of BHs. Due to this prescription, we can calculate the orbit of the BHs accurately until the merger condition is satisfied. When BHs are merge, we give the sum of their masses for the merged BHs.

2.3.3 Setups of gas distribution

In realistic environments, the gas density distributions are likely to be complex. In first-generation objects, the axis ratios of gas disks are from one to five (Hirano et al., 2014). Besides, the gas distribution may be changed significantly due to the gas flow by cold accretion along filaments at high redshifts (e.g. Yajima et al., 2015). In dense molecular cloud cores, the gas density distributions are sometimes nearly spherical and sometimes elongated. Thus, since the gas distributions depend on objects and are complex, we assume a spherical cloud just for simplicity.

In our simulations, we settle the finite gas mass in a sphere with $M_{\rm gas,tot} = 10^5\ M_\odot$. Outside this gas sphere, BHs do not receive the effects of the gas dynamical friction and gas accretion. On the other hand, we assume that gas is distributed infinitely in Section 3.2.1 for simplicity.

2.3.4 Setups of gas temperature

The heating rate by the gas dynamical friction is estimated as follows (Kim et al., 2005):

$$\begin{aligned}\Lambda_{\rm DF} = 7.3\times10^{-25}\ {\rm erg\ cm^{-3}\ s^{-1}} &\left(\frac{n_{\rm gas}}{10^4\ {\rm cm^{-3}}}\right)\\ &\times\left(\frac{M_{\rm BH}}{30\ M_\odot}\right)^2\left(\frac{<f(\mathcal{M})/\mathcal{M}>}{2}\right)\\ &\times\left(\frac{T}{1000\ K}\right)^{-1/2}\left(\frac{n_{\rm BH}}{10\ {\rm pc^{-3}}}\right)\end{aligned} \tag{2.20}$$

where $n_{\rm BH}$ is the number density of BHs, and the angular brackets denote the average over the Maxwellian distribution,

$$f(v) = \frac{4\pi N_{\rm BH}}{(2\pi\sigma_r^2)^{3/2}} v^2 e^{-v^2/(2\sigma_r^2)}, \tag{2.21}$$

where σ_r is the one-dimensional velocity dispersion.

In a first object, the cooling by hydrogen molecules (H_2) is dominant at $T \approx 10^3$ K (e.g. Omukai, 2000). The H_2 cooling rate by $H - H_2$ collision (Hollenbach & McKee,

1989) and the HI cooling rate (Thoul & Weinberg, 1995) are given by

$$\Lambda_{\rm H2}(10^3\ K) = 2.8\times10^{-21}\ {\rm erg\ cm^{-3}\ s^{-1}} \times\left(\frac{n_{\rm gas}}{10^4\ {\rm cm^{-3}}}\right)\left(\frac{f_{\rm H_2}}{3\times10^{-4}}\right) \tag{2.22}$$

$$\Lambda_{\rm HI}(10^4\ K) \sim 1.0\times10^{-14}\ {\rm erg\ cm^{-3}\ s^{-1}} \times\left(\frac{n_{\rm gas}}{10^4\ {\rm cm^{-3}}}\right)^2 f_{\rm HI}^2 \tag{2.23}$$

where $f_{\rm H_2}$ and $f_{\rm HI}$ are the fraction of H_2 molecules and neutral hydrogen atoms, respectively. In the range of $n_{\rm gas} \gtrsim 10^4\ {\rm cm^{-3}}$, $f_{\rm H_2} \gtrsim 3\times10^{-4}$ (Palla et al., 1983).

We find that the cooling rate is higher than the heating rate over the ranges of parameters in which the simulations are performed. Therefore, since the gas temperature is expected to be settled at $T \approx 10^3$ K, we assume the gas temperature to be 1000 K. Accordingly, the sound speed ($C_{\rm s}$) is 3.709 [km/s].

Chapter 3

Merger processes of multiple black holes

In this chapter, we investigated the merger processes of multiple BHs with the effects of gas. In Section 3.1, we categorize the merger mechanisms (Tagawa et al., 2016). In Section 3.2.1 and 3.2.2, we elucidate the dependence of merger timescale without the effect of gas accretion (Tagawa et al., 2015) and with the effect of gas accretion (Tagawa et al., 2016). In Section 3.3, we derive the critical accretion rate below which the merger precedes (Tagawa et al., 2016). In Section 3.4, we consider the effect of the recoil kick due to the anisotropic radiation of GW radiation (Tagawa et al., 2016).

3.1 Merger mechanisms of multiple black holes

First, we present the merger mechanisms of multiple BHs with gas accretion. The classification of the merger mechanisms without gas accretion is described in Appendix A.1.

The merger mechanisms are classified by the manner of orbit decay just before the GW emission drives the merger. We categorize the merger mechanisms into four types: a gas drag-driven merger (type A), an interplay-driven merger (type B), a three body-driven merger (type C), and an accretion-driven merger (type D). The classification with gas accretion between type A, type B, and type C is the same as that without gas accretion indicated in Appendix A.1.

In type A, the separation of BHs monotonically shrinks due to the gas dynamical friction before the GW works. In both of types B and C, there are the discontinuous changes of the orbit during the first merger. This disturbance is induced by the three-body interaction. These disturbance is verified by eye. Note that early decay is usually caused by the gas dynamical friction in the first merger of types B and C. On the other hand, in type B, after first few mergers that are promoted by the

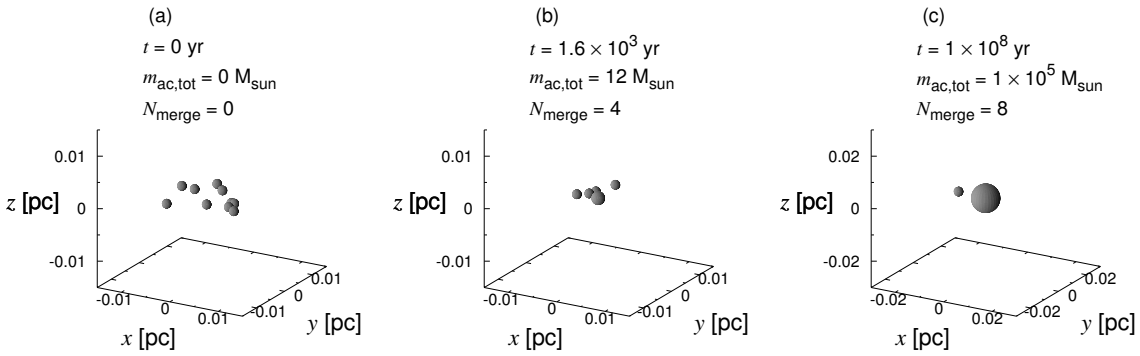

Fig. 3.1 Snapshots of the distributions of the multiple BHs for a gas drag-driven merger (type A). The initial parameters are a typical extension of BH spatial distributions, $r_{\rm typ} = 0.01$ pc, the gas number density, $n_{\rm gas} = 10^{12}$ cm^{-3}, and the accretion rate, $\epsilon = 10^{-4}$. In each snapshot, the elapsed time t, the total accreted mass $m_{\rm ac,tot}$ onto BHs, and the number of merged BHs $N_{\rm merge}$ are presented. The sizes of spheres represent the mass of the BH in logarithmic scales, where the smallest one corresponds to the initial BH mass, $m_i = 30M_\odot$. Taken from figure 2 of Tagawa et al. (2016).

three-body interactions, the separations of BHs are increased by the slingshot mechanism. Thereafter, the separation of BHs shrinks slowly for long time due to the gas dynamical friction. Whether the slow mergers take place from increased separations is the criterion on which type B is discriminated from type C. Therefore, in type B, there are both mergers that are prompted by the gas dynamical friction and the three-body interaction just before the GW works. In type C, the strong disturbance of the orbit by the three-body interactions continues until the final merger. There are no merger that is prompted mainly by the gas dynamical friction just before the GW works in type C. In type D, significant accretion takes place before the first merger. In the following, we describe the characteristics of each merger mechanism.

3.1.1 Gas drag-driven merger (type A)

Fig. 3.1 shows the snapshots of the multiple BH distribution for a gas drag-driven merger (type A), where a initial typical extension of BH spatial distributions is $r_{\rm typ} = 0.01$ pc, the gas number density is $n_{\rm gas} = 10^{12}$ cm^{-3}, and the accretion efficiency is $\epsilon = 10^{-4}$. The sizes of spheres represent the BH mass in logarithmic scales, where the smallest size corresponds to the initial BH mass of $30M_\odot$. In each snapshot, the elapsed time t, the total accreted mass $m_{\rm ac,tot}$, and the merged BH number $N_{\rm merge}$ are represented. From this figure, several BH mergers occurs without considerable mass accretion before 1.6×10^3yr. Thereafter, subsequent mergers proceed and eventually

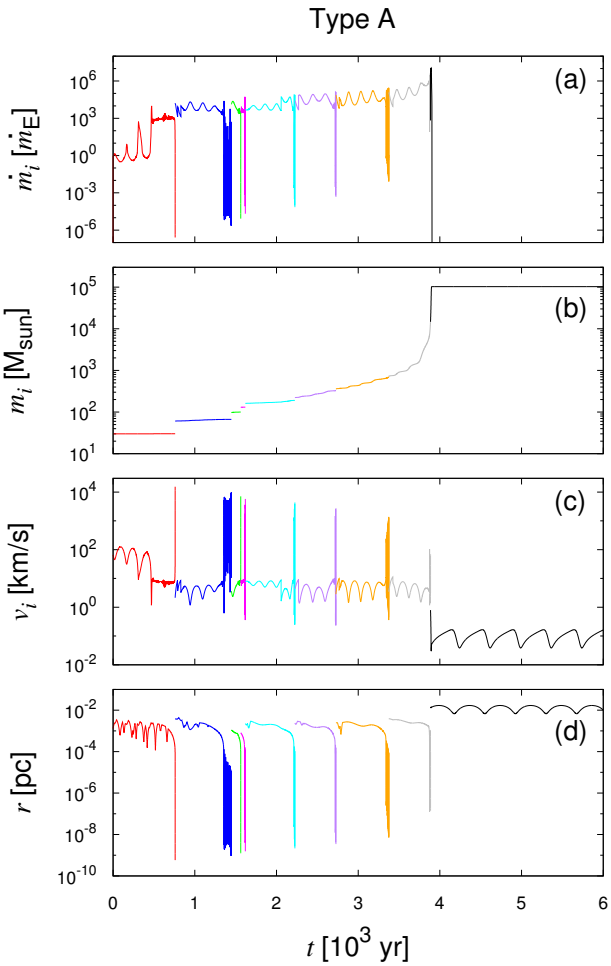

Fig. 3.2 The time evolution of the physical quantities for a gas drag-driven merger (type A). The initial parameters are the same as Figure 3.1. Panels (a), (b), and (c) represent the mass accretion rate in units of the Eddington mass accretion rate for $30M_{\odot}$, the mass and the velocity of the first merged BH, respectively. Panel (d) represents the separation of the closest pair within all BHs, where the colors of lines change at every event of the BH merger. Taken from figure 3 of Tagawa et al. (2016).

considerable amount of gas accretes onto the most massive BH before 10^8yr.

To see the detailed physical processes, Fig. 3.2 shows the time evolution of the mass accretion rate, the mass and the velocity of the first merged BH, and the separation of the closest pair among all BHs. In a type A merger, the separation of BHs decays smoothly due to the dynamical friction. The dynamical friction timescale is given as

$$t_{\rm DF} \simeq \frac{v^3}{4\pi G^2 m_{\rm BH} m_{\rm H} n_{\rm gas}}. \tag{3.1}$$

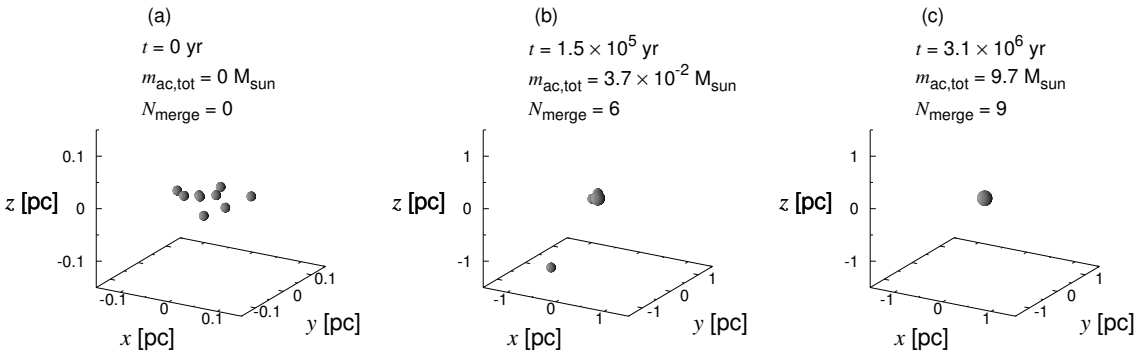

Fig. 3.3 Same as Fig. 3.1, but for an interplay-driven merger (type B). $r_{\rm typ}$ = 0.1 pc, $n_{\rm gas} = 10^9$ cm^{-3}, and $\epsilon = 10^{-6}$. Taken from figure 4 of Tagawa et al. (2016).

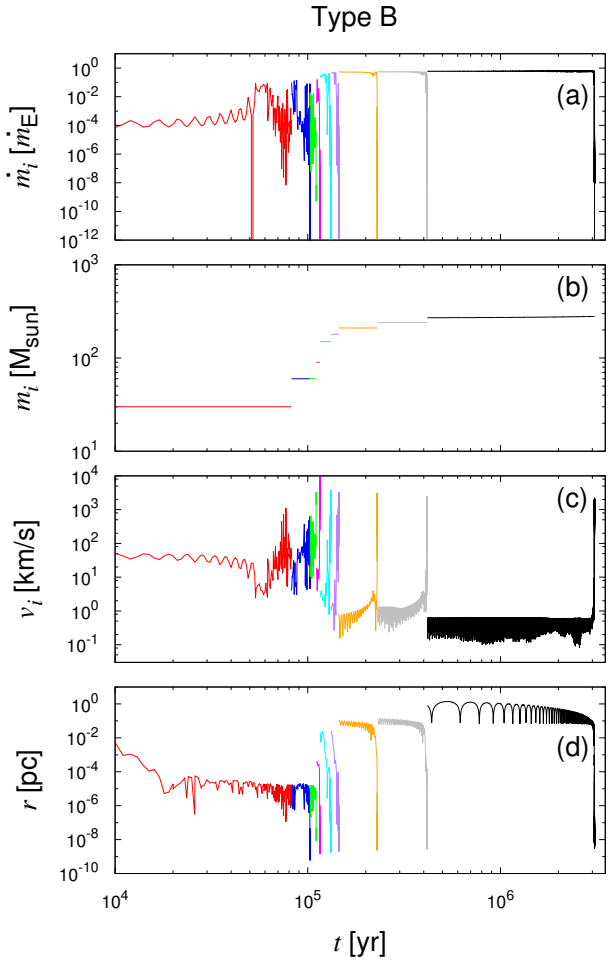

Fig. 3.4 Same as Fig. 3.2, but for an interplay-driven merger (type B). $r_{\rm typ}$ = 0.1 pc, $n_{\rm gas} = 10^9$ cm^{-3}, and $\epsilon = 10^{-6}$. Taken from figure 5 of Tagawa et al. (2016).

On the other hand, the accretion timescale, at which the accretion rate diverges, is given by

$$t_{\rm ac} = \frac{(v^2 + C_{\rm s}^2)^{3/2}}{4\pi G^2 m_{\rm BH} m_{\rm H} n_{\rm gas} \epsilon}. \tag{3.2}$$

Note that the dynamical friction timescale has the same dependence as the accretion timescale on the BH mass and the gas density, because both the dynamical friction and the Hoyle-Lyttleton accretion are caused by the change of the streamline due to the BH gravity. However, the dependence on the BH velocity is different from each other. The dynamical friction timescale is shorter than the accretion timescale, since the accretion timescale depends on the sound velocity and the accretion efficiency $\epsilon(\leq 1)$. But, as in the first merger shown in panel (c) of Fig.3, the accretion timescale is independent of the sound speed, if the BH velocity is supersonic. On the other hand, the accretion timescale is raised because of a low ϵ $(= 10^{-4})$. Hence, the decay of orbit is firstly driven by the gas dynamical friction (panel (d)) before significant gas accretes. As a result, a close BH binary forms and subsequently merges into one BH due to the GW radiation before 10^3 yr. After that, although there is a long phase when the BH velocity is low and the accretion rate is accordingly increased, the accretion timescale is still larger than the dynamical friction timescale. Hence, several mergers are induced by the dynamical friction. Eventually, after all gas instantly accretes onto the most massive BH, the merger halts and a binary BH is left in the system as seen in panel (c) of Fig. 3.1.

3.1.2 Interplay-driven merger (type B)

An example of an interplay-driven merger (type B) is illustrated in Fig. 3.3 and Fig. 3.4. In this example, the accretion efficiency is $\epsilon = 10^{-6}$. In panel (d) of Fig. 3.4, the pericenter and apocenter instantly change many times in the first few mergers. Such discontinuous changes of the pericenter and apocenter are induced by the three-body encounters. Hence, the successive mergers are promoted by the three-body interaction. On the other hand, in the last few mergers, the orbit evolves from a larger separation than the initial typical separation ($r_{\rm typ}$) and the separation of BHs is decayed smoothly due to the dynamical friction. This increasement of separation is a negative effect of three-body interaction. The panel (b) of Fig. 3.3 indicates that a BH is kicked out by the slingshot mechanism. Because of this negative effect, the velocity becomes much lower than the sound velocity due to the deceleration by the gas potential (see panel (c) in Fig. 3.4), so that the accretion rate is increased in the later phase. However, mergers by the dynamical friction proceed faster than the significant accretion, since the accretion rate is quite low compared to the Hoyle-

Lyttleton accretion. Eventually, all BHs merge into one BH within 3×10^6yr, and all the accreted gas mass is $9.7 M_\odot$.

3.1.3 Three body-driven merger (type C)

In a three body-driven merger (type C), the discontinuous changes of the orbit continues until the final merger. An example of type C is illustrated in Fig. 3.5 and Fig. 3.6. The initial parameters are the same as those for the example of the type B merger in above, excepting for the lower gas density. Strong disturbance of separation of BHs seen in panels (c) and (d) of Fig. 3.6 is induced by the three-body encounters. In a type C, because each BH in a closest pair receives the gravity primarily from another BH, the BH velocities in a closest pair increase according to the decay of the separation. Therefore, the accretion rates of the BHs in closest pair for type C are much lower than those for type B. On the other hand, several BHs are kicked out from the central regions due to the slingshot mechanism and accordingly escape from the system. As a result, BHs left in the system merge into one BH.

3.1.4 Accretion-driven merger (type D)

In an accretion-driven merger (type D), significant amount of gas accretes before the first merger. Fig. 3.8 shows the example of type D. In this model, the mass accretion rate is not high on the closest pair of BHs, because the accretion rate is reduced by their high velocities. On the other hand, an isolated BH grows first by accretion because such a BH drifts in the outer regions for long time and has low velocity. In this model, all gas accretes onto the BH within 2×10^5yr. Thereafter, the most massive BH gravitationally interacts with other smaller BHs. Since the massive BH has a larger Schwarzschild radius, the merger condition (2.19) is easy to be satisfied. Shortly after the significant accretion, two BHs approaching the most massive BH merge by the GW radiation. Then, several BHs remain being bound in the system without merger until the end of simulation (Fig. 3.7). Hence, it is hard to occur that all BHs merge into one BH in a type D.

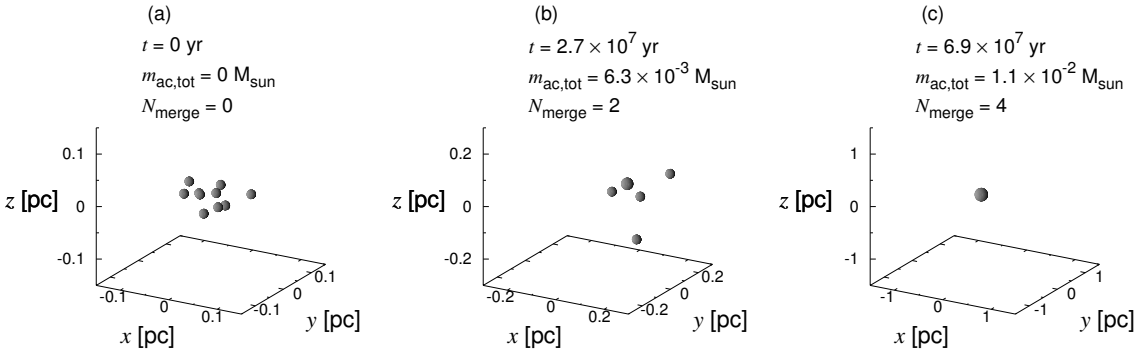

Fig. 3.5 Same as Fig. 3.1, but for a three-body-driven merger (type C). $r_{\rm typ} = 0.1$ pc, $n_{\rm gas} = 10^6$ cm^{-3}, and $\epsilon = 10^{-6}$. Taken from figure 6 of Tagawa et al. (2016).

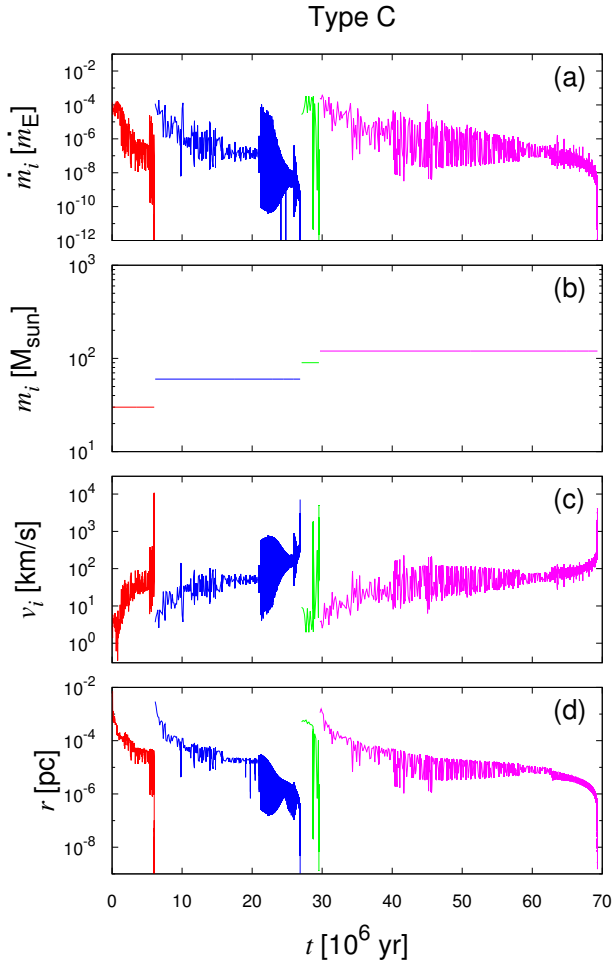

Fig. 3.6 Same as Fig. 3.2, but for a three-body-driven merger (type C). $r_{\rm typ} = 0.1$ pc, $n_{\rm gas} = 10^6$ cm^{-3}, and $\epsilon = 10^{-6}$. Taken from figure 7 of Tagawa et al. (2016).

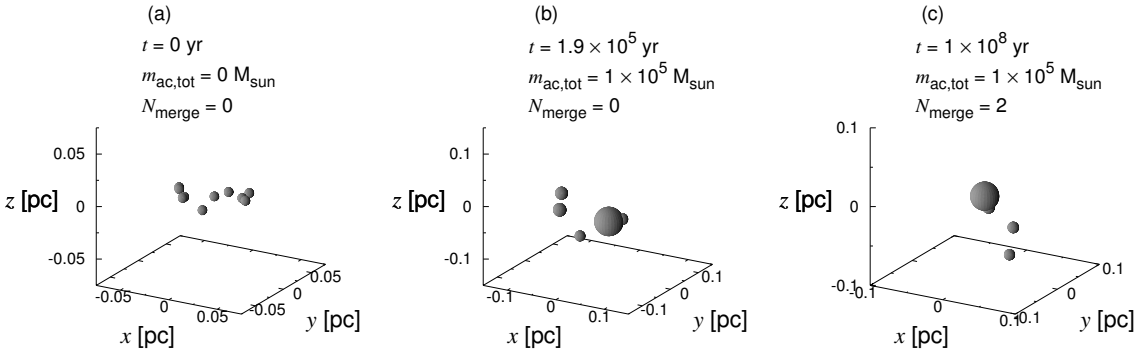

Fig. 3.7 Same as Fig. 3.1, but for an accretion-driven merger (type D). $r_{\rm typ}$ = 0.04 pc, $n_{\rm gas} = 10^7$ cm^{-3}, and $\epsilon = 10^{-1}$. Taken from figure 8 of Tagawa et al. (2016).

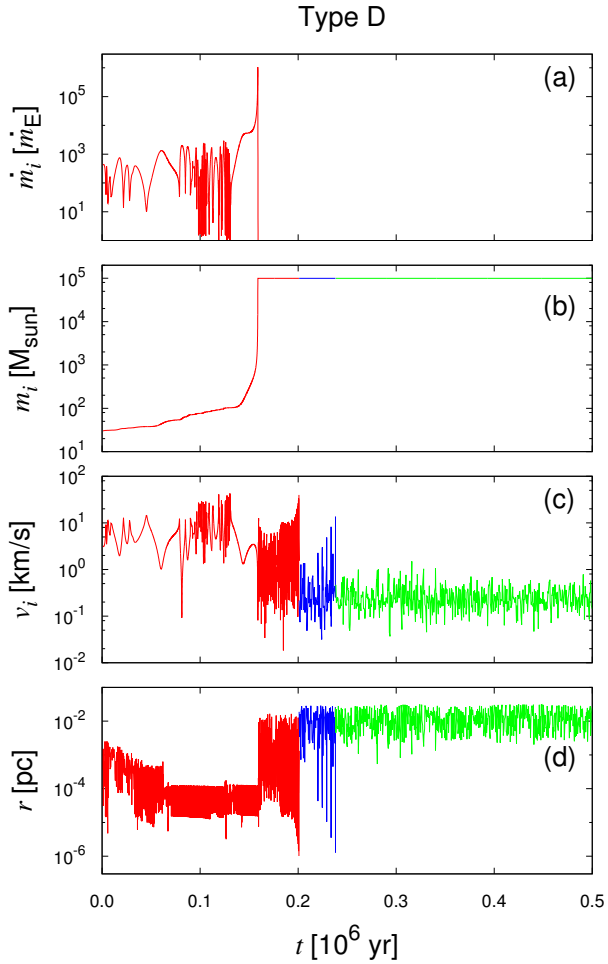

Fig. 3.8 Same as Fig. 3.2, but for an accretion-driven merger (type D). $r_{\rm typ}$ = 0.04 pc, $n_{\rm gas} = 10^7$ cm^{-3}, and $\epsilon = 10^{-1}$. Taken from figure 9 of Tagawa et al. (2016).

Table 3.1 The results with $M_{\rm BH} = 30\ M_\odot$ and $N_{\rm BH} = 10$.

$r_{\rm typ}$[pc]	1.0		0.464		0.215		0.1		0.0464		0.0215		0.01	
$\rho_{\rm BH}[M_\odot {\rm pc}^{-3}]$	7.2×10^1		7.2×10^2		7.2×10^3		7.2×10^4		7.2×10^5		7.2×10^6		7.2×10^7	
	$N_{\rm m}$	type	$N_{\rm m}$	type	$N_{\rm m}$	type	$N_{\rm m}$	type	$N_{\rm m}$	type	$N_{\rm m}$	type	$N_{\rm m}$	type
$n_{\rm gas}[{\rm cm}^{-3}]$	$t_{\rm fin}$[yr]		$t_{\rm fin}$[yr]		$t_{\rm fin}$[yr]		$t_{\rm fin}$[yr]		$t_{\rm fin}$[yr]		$t_{\rm fin}$[yr]		$t_{\rm fin}$[yr]	
10^{12}	0	-	5	A	**9**	A	**9**	A	**9**	A	**9**	A	**9**	B
	1.0×10^8		1.0×10^8		3.6×10^7		4.4×10^6		1.7×10^6		7.0×10^5		4.3×10^5	
10^{11}	2	A	8	A	**9**	A	**9**	A	**9**	A	**9**	A	**9**	B
	1.0×10^8		1.0×10^8		1.3×10^7		1.8×10^5		1.8×10^5		2.3×10^4		2.8×10^4	
10^{10}	5	A	**9**	A	**9**	A	**9**	A	**9**	A	**9**	B	**9**	B
	1.0×10^8		4.5×10^7		5.1×10^6		5.9×10^5		7.4×10^4		6.3×10^4		1.7×10^5	
5×10^9	5	A	**9**	A	**9**	A	**9**	A	**9**	B	**9**	B	**9**	B
	1.0×10^8		2.9×10^7		3.1×10^6		4.5×10^5		1.6×10^5		3.4×10^5		7.7×10^4	
10^9	8	A	**9**	A	**9**	A	**9**	B	**9**	B	**9**	B	**9**	B
	1.0×10^8		2.4×10^7		3.5×10^6		2.6×10^5		4.3×10^5		3.5×10^5		3.0×10^5	
5×10^8	8	A	**9**	A	**9**	A	**9**	B	**9**	B	**9**	B	**9**	B
	1.0×10^8		1.2×10^7		1.3×10^6		6.5×10^5		4.3×10^5		5.5×10^5		5.1×10^5	
10^8	**9**	A	**9**	A	**9**	B	**9**	B	**9**	B	**9**	B	**9**	B
	3.0×10^7		5.1×10^6		4.0×10^6		5.5×10^6		3.6×10^6		4.2×10^6		1.2×10^7	
5×10^7	**9**	A	**9**	B	**9**	B	**9**	B	**9**	B	**9**	B	**9**	B
	4.5×10^7		3.7×10^6		2.2×10^7		3.2×10^7		1.3×10^7		4.7×10^6		3.6×10^6	
10^7	**9**	B	**9**	B	**9**	B	**9**	B	**9**	B	**9**	B	**9**	B
	3.8×10^7		2.3×10^7		1.7×10^7		3.3×10^7		1.8×10^7		2.9×10^7		1.7×10^7	
5×10^6	**9**	B	**9**	B	**9**	B	**9**	B	**9**	B	**9**	B	**9**	B
	4.2×10^7		3.9×10^7		4.2×10^7		4.7×10^7		6.3×10^7		3.5×10^7		3.1×10^7	
10^6	6	B	6	B	8	B	6	C	8	C	6	C	6	C
	1.0×10^8		1.0×10^8		1.0×10^8		1.0×10^8		1.0×10^8		1.0×10^8		1.0×10^8	
5×10^5	2	C	6	C	6	C	4	C	5	C	3	C	4	C
	1.0×10^8		1.0×10^8		1.0×10^8		1.0×10^8		1.0×10^8		1.0×10^8		1.0×10^8	
10^5	0	-	0	-	1	C	0	-	1	C	2	C	0	-
	1.0×10^8		1.0×10^8		1.0×10^8		1.0×10^8		1.0×10^8		1.0×10^8		1.0×10^8	
10^4	0	-	0	-	0	-	1	C	0	-	0	-	0	-
	1.0×10^8		1.0×10^8		1.0×10^8		1.0×10^8		1.0×10^8		1.0×10^8		1.0×10^8	

Table 3.2 The results with $M_{\rm BH} = 10^4\ M_\odot$ and $N_{\rm BH} = 10$.

$r_{\rm typ}$[pc]	10.0		4.64		2.15		1.0		0.464		0.215		0.1	
$\rho_{\rm BH}[M_\odot{\rm pc}^{-3}]$	2.4×10^1		2.4×10^2		2.4×10^3		2.4×10^4		2.4×10^5		2.4×10^6		2.4×10^7	
	$N_{\rm m}$	type	$N_{\rm m}$	type	$N_{\rm m}$	type	$N_{\rm m}$	type	$N_{\rm m}$	type	$N_{\rm m}$	type	$N_{\rm m}$	type
$n_{\rm gas}[{\rm cm}^{-3}]$	$t_{\rm fin}$[yr]		$t_{\rm fin}$[yr]		$t_{\rm fin}$[yr]		$t_{\rm fin}$[yr]		$t_{\rm fin}$[yr]		$t_{\rm fin}$[yr]		$t_{\rm fin}$[yr]	
10^{12}	0	-	4	A	7	A	**9**	A	**9**	A	**9**	A	**9**	A
	1.0×10^8		1.0×10^{10}		1.0×10^{10}		1.3×10^7		1.5×10^6		1.7×10^5		2.2×10^4	
10^{11}	0	-	5	A	**9**	A	**9**	A	**9**	A	**9**	A	**9**	B
	1.0×10^8		1.0×10^8		4.6×10^7		5.0×10^6		5.8×10^5		7.2×10^4		1.6×10^4	
10^{10}	4	A	8	A	**9**	A	**9**	A	**9**	A	**9**	A	**9**	B
	1.0×10^8		1.0×10^8		1.7×10^7		2.0×10^6		2.5×10^5		9.3×10^4		4.1×10^4	
10^9	5	A	**9**	A	**9**	A	**9**	A	**9**	B	**9**	B	**9**	B
	1.0×10^8		5.8×10^7		7.0×10^6		9.6×10^5		7.6×10^5		9.0×10^5		2.4×10^6	
5×10^8	5	A	**9**	A	**9**	A	**9**	B	**9**	B	**9**	B	**9**	B
	1.0×10^8		5.0×10^7		1.0×10^7		1.5×10^6		9.5×10^5		7.6×10^5		6.7×10^5	
10^8	7	A	**9**	A	**9**	B	**9**	B	**9**	B	**9**	B	**9**	B
	1.0×10^8		2.5×10^7		3.7×10^6		8.3×10^6		4.9×10^6		5.6×10^6		7.9×10^6	
5×10^7	**9**	A	**9**	A	**9**	B	**9**	B	**9**	B	**9**	B	**9**	B
	7.3×10^7		2.0×10^7		1.3×10^7		7.1×10^6		1.2×10^7		3.5×10^6		9.4×10^6	
10^7	**9**	B	**9**	B	**9**	B	**9**	B	**9**	B	**9**	B	**9**	B
	7.7×10^7		3.5×10^7		9.3×10^7		6.0×10^7		3.3×10^7		3.6×10^7		4.1×10^7	
5×10^6	8	B	**9**	B	**9**	B	**9**	B	**9**	B	**9**	B	**9**	B
	1.0×10^8		8.3×10^7		3.9×10^7		8.5×10^7		4.6×10^7		4.8×10^7		7.9×10^7	
10^6	5	B	7	B	4	B	**9**	B	5	C	5	C	6	C
	1.0×10^8		1.0×10^8		1.0×10^8		6.5×10^7		1.0×10^8		1.0×10^8		1.0×10^8	
5×10^5	3	B	3	C	3	C	3	C	6	C	4	C	4	C
	1.0×10^8		1.0×10^8		1.0×10^8		1.0×10^8		1.0×10^8		1.0×10^8		1.0×10^8	
10^5	0	-	0	-	0	-	0	-	0	-	1	C	0	-
	1.0×10^8		1.0×10^8		1.0×10^8		1.0×10^8		1.0×10^8		1.0×10^8		1.0×10^8	
5×10^4	0	-	0	-	1	C	0	-	1	C	1	C	1	C
	1.0×10^8		1.0×10^8		1.0×10^8		1.0×10^8		1.0×10^8		1.0×10^8		1.0×10^8	
10^4	0	-	0	-	0	-	0	-	0	-	0	-	1	C
	1.0×10^8		1.0×10^8		1.0×10^8		1.0×10^8		1.0×10^8		1.0×10^8		1.0×10^8	

3.2 Merger time of multiple black holes

3.2.1 Merger time without gas accretion

Here, we elucidate the dependence of the merger timescale on the gas density, BH density, BH mass and BH number. For simplicity, the gas accretion is not incorporated in Section 3.2.1. The dependence of the merger timescale for all parameter sets in the case of ten BHs is shown in Tables 3.1 and 3.2. Table 3.1 represents the results for $M_{\rm BH} = 30\ M_\odot$ and Table 3.2 dose for $M_{\rm BH} = 10^4\ M_\odot$. The column is the initial extension of the BH spatial distribution ($r_{\rm typ}$) and the corresponding BH density ($\rho_{\rm BH}$), and the row is the gas density ($n_{\rm gas}$). As results of simulations, the number of the merged BHs ($N_{\rm m}$), the merger mechanisms and the termination time of simulations ($t_{\rm fin}$) are shown.

From Tables 3.1 and 3.2, for lower BH density (higher $r_{\rm typ}$), type A is seen in a wider range of the gas density. For higher BH density, type B is distributed dominantly in higher gas density environments. On the other hand, type C is seen in lower gas density. But, when the gas density is very low ($< 5 \times 10^5 {\rm cm}^{-3}$), few merger occurs even in the high BH density of $7.2 \times 10^7 M_\odot {\rm pc}^{-3}$. This implies that the gas dynamical friction plays an important role even for type C.

In the case of $M_{\rm BH} = 30\ M_\odot$ (Table 3.1), if $n_{\rm gas}$ is from 5×10^6 to 10^8 cm^{-3}, ten BHs merge into one massive BH over six orders of the BH density ($\rho_{\rm BH} = 72 - 7.2 \times 10^7\ M_\odot {\rm pc}^{-3}$). Also, if the gas density is higher than 5×10^5 cm^{-3}, at least one BH merger occurs within 100 Myr.

In the case of $M_{\rm BH} = 10^4\ M_\odot$ (Table 3.2), if $n_{\rm gas}$ is from 5×10^6 to $10^9 {\rm cm}^{-3}$, ten BHs merge into one massive BH over five orders of BH density ($\rho_{\rm BH} = 2.4 \times 10^2 - 2.4 \times 10^7\ M_\odot {\rm pc}^{-3}$). Interestingly, in the high gas density of $n_{\rm gas} \geq 5 \times 10^6$ cm^{-3}, multiple BHs can merge into one BH even if the typical extention is greater than several pc. Similar to the case of $M_{\rm BH} = 30\ M_\odot$, if the gas density is higher than 5×10^5 cm^{-3}, at lease one BH can merge.

In both cases of BH mass, when the gas density is very high and the BH density is very low (upper left in Table 3.1 and Table 3.2), no merger occurs. This is because the deep gas gravitational potential enhances the circular velocities of BHs and therefore the separation of BHs hardly decays. From Table 3.1 and Table 3.2, the merger mechanism varies systematically with the gas density and the BH density.

To investigate the physics of BH merger, we performed reference simulations with the different BH number. In Fig. 3.9, the averaged merger time in ten BH ($t_{N=10}$), three BH ($t_{N=3}$) and two BH systems ($t_{N=2}$) are shown. We set the averaged merger time as the vertical axis of Fig. 3.9 to show the difference according to the BH number.

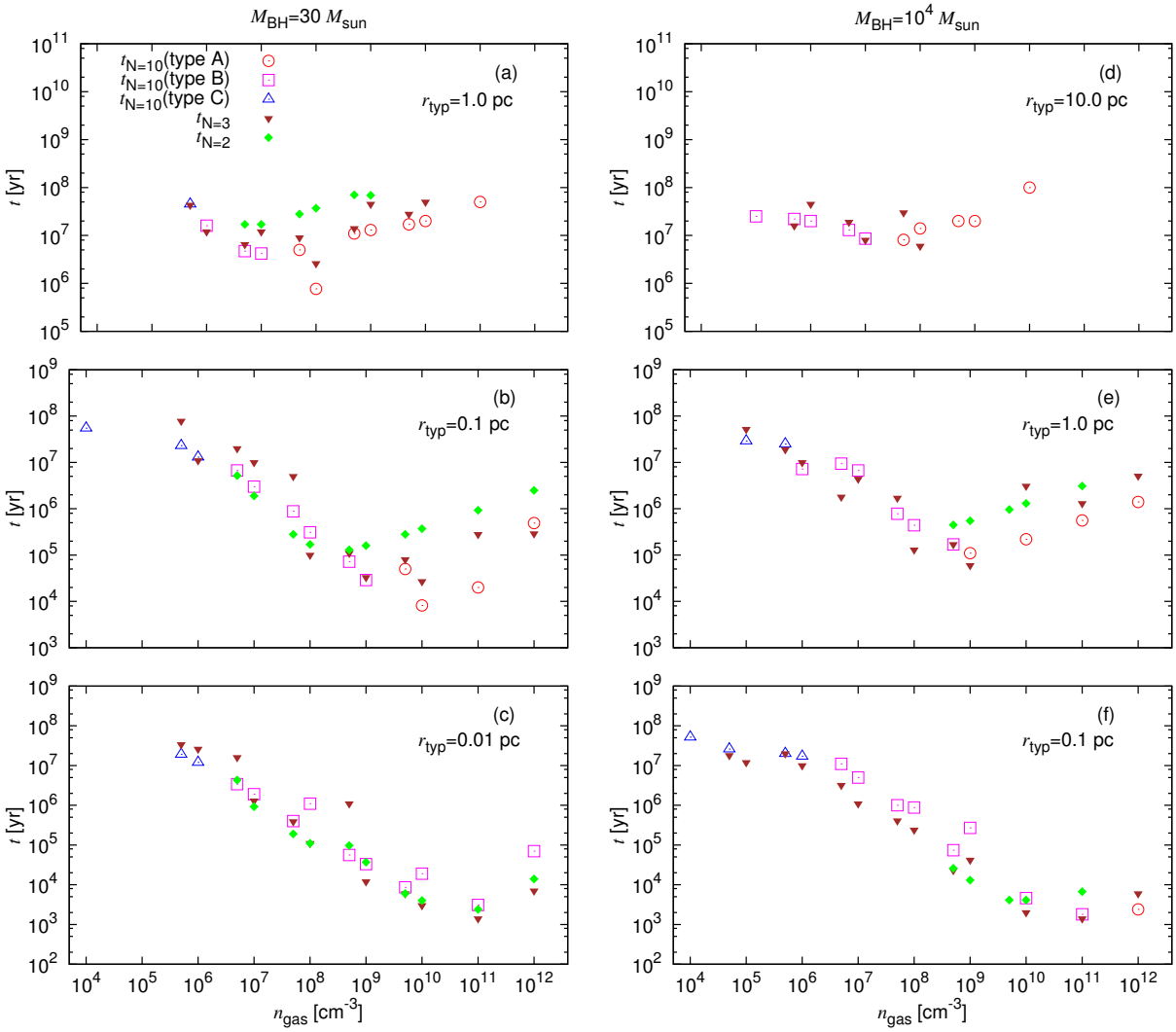

Fig. 3.9 Averaged merger time in ten-BH systems ($t_{N=10}$) as a function of gas number density $n_{\rm gas}$. The left panels are the cases with low-mass BHs ($M_{\rm BH}$ = 30 $M_\odot$), and right panels are those with high-mass BHs ($M_{\rm BH} = 10^4$ $M_\odot$). The top, middle and bottom panels show the results for lower, intermediate, and higher BH density, respectively. Red, pink, and blue open symbols represent the results of the types A, B, and C mergers, respectively. Green- and brown-filled symbols are the results of two-BH ($t_{N=2}$) and three-BH ($t_{N=3}$) systems, respectively. Taken from figure 6 of Tagawa et al. (2015).

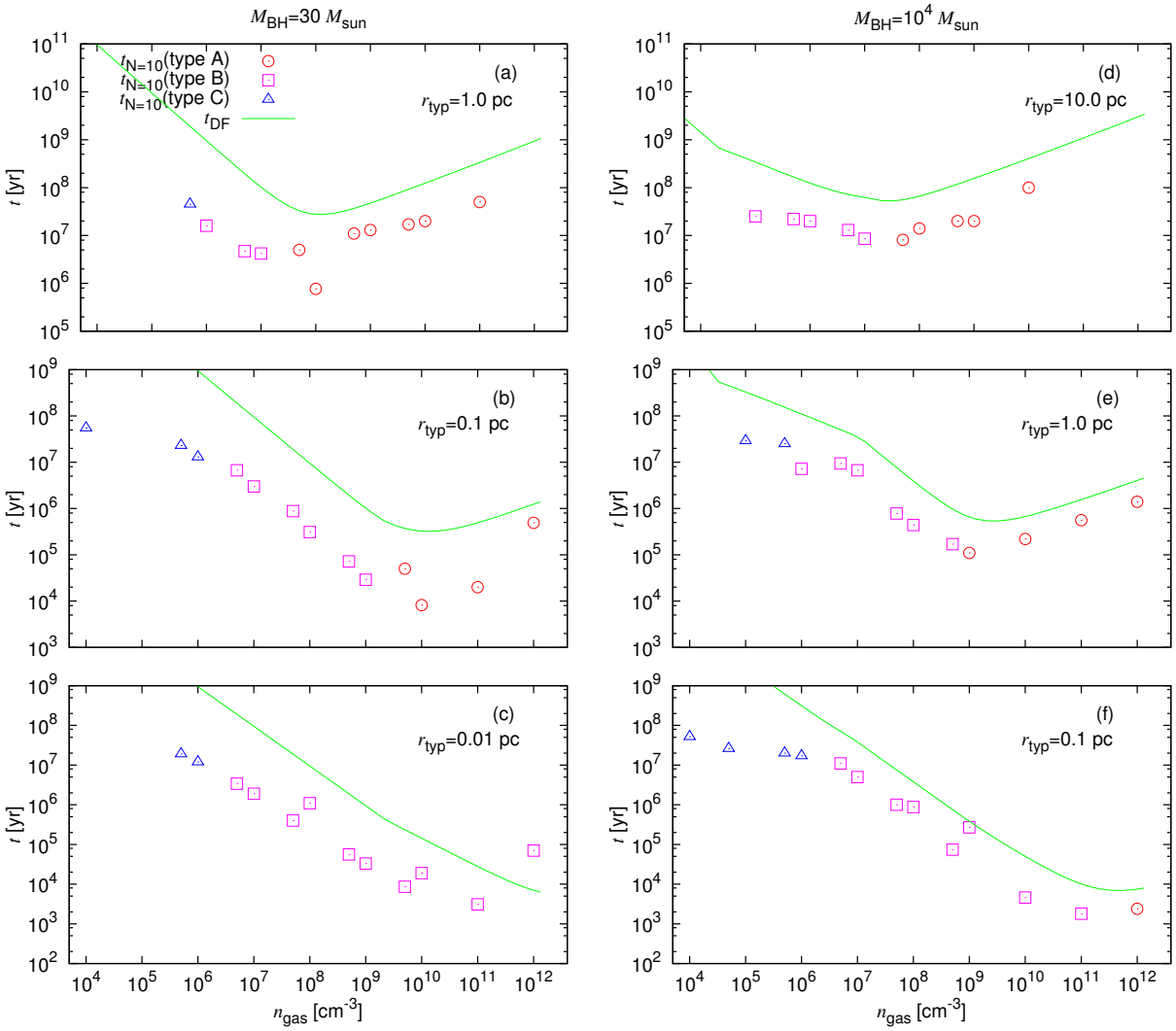

Fig. 3.10 Same as Fig. 3.9, but the analytic estimates of gas dynamical friction timescale, $t_{\rm DF}$, are plotted by green lines, instead of the results of two-BH and three-BH systems. Taken from figure 7 of Tagawa et al. (2015).

Each panel represents a different set of parameters. Red, pink, and blue open symbols respectively corresponds to the types A, B, and C mergers in ten-BH systems. Brown and green filled symbols show the results for three and two BH systems, respectively. Note that the initial setup of random number gives the variance of about a factor of two for the averaged merger time ($t_{\rm fin}$).

For two BH systems, BHs have only circular velocity initially. Since no three-

body interaction occurs in two BH systems, the mergers are always driven by the gas dynamical friction. On the other hand, for three BH systems, the mergers are induced by the combination of the three-body interaction and the gas dynamical friction. The merger timescales in type C almost accord with those in three BH systems. Additionally, in the parameter regions of type C, no merger occurs in two-BH systems. These results are consistent with the classification of type C where the merger is driven by the three-body interaction.

On the other hand, in the parameter regions of types A and B, the mergers occur in both two BH and three BH systems. In the parameter regions of type A, the averaged merger time in ten BH systems is systematically shorter than that in three BH systems. This is because more BHs suffer from the gas dynamical friction simultaneously in the ten BH systems. As seen in top left and top right panels, two and three BH systems cannot merge in high gas density environments, whereas ten BHs systems can merge. These results imply that the gas dynamical friction on ten BHs enhances the frequency of the three-body interaction, eventually allowing the merger. In the bottom right panel, the averaged merger time in ten BH systems is slightly longer than that in three BH systems, in the lower gas density cases of $n_{\rm gas} < 10^9$ cm^{-3}. This is expected by the negative feedback due to the three-body interaction.

In Fig. 3.10, we compare the analytic estimate of gas dynamical friction timescale ($t_{\rm DF}$) to the averaged merger time in ten BHs systems ($t_{\rm N=10}$). The dynamical friction timescale is estimated assuming circular rotating BH binary similar to those by Begelman et al. (1980) and Matsubayashi et al. (2007). On the other hand, based on a test simulation for a BH binary, the eccentricity of the binary is assumed to become very high when the BH gravity dominates the gas potential. Then, $t_{\rm DF}$ is estimated as

$$t_{\rm DF} = \int_{100\ r_{\rm sch}}^{r_{\rm typ}} \frac{\tilde{t}_{\rm DF}(r)}{r} dr, \tag{3.3}$$

$$\tilde{t}_{\rm DF}(r) \equiv \frac{v_{\rm circ}(r)}{\max\{a_{\rm DF}^{\rm gas}(r')\}} \ldots r \le r' \le r_{\rm typ}, \tag{3.4}$$

$$\tilde{t}_{\rm DF}(r_{\rm typ}) \simeq \frac{v_{\rm circ}^3}{4\pi G^2 M_{\rm BH} m_{\rm H} n_{\rm gas}}, \tag{3.5}$$

$$\simeq \begin{cases} \frac{(4\pi m_{\rm H} n_{\rm gas})^{1/2} r_{\rm typ}^3}{3^{3/2} G^{1/2} M_{\rm BH}} & (M_{\rm gas,b} \gg M_{\rm BH}) \\ \frac{M_{\rm BH}^{1/2}}{4\pi G^{1/2} m_{\rm H} n_{\rm gas} r_{\rm typ}^{3/2}} & (M_{\rm gas,b} \ll M_{\rm BH}), \end{cases} \tag{3.6}$$

where, $M_{\rm gas,b}$ is the gas mass within the binary orbital radius, and $v_{\rm circ} = [G(2M_{\rm gas,b} + M_{\rm BH})/2r]^{1/2}$ is the circular velocity. In this estimate, the maximum value of $a_{\rm DF}^{\rm gas}$ are used in the range of $r \le r' \le r_{\rm typ}$ because of the assumption of the

high eccentricity, which is also represented in the study considering the effect of the dynamical friction by stars (Fukushige et al., 1992). Green curves in Fig. 3.10 is the estimated timescale of the gas dynamical friction. According to equation (3.6), the estimated timescale of the gas dynamical friction ($t_{\rm DF}$) is inversely proportional to $n_{\rm gas}$ in the limit of low gas density whereas proportional to $n_{\rm gas}^{1/2}$ in the limit of high gas density. According to this change of dependence, a turning point arises in each curve of $t_{\rm DF}$. As seen in Fig. 3.10, the turning point is near to the transition from type A to type B. Also, the trend of merger time ($t_{\rm N=10}$) is similar to the analytic estimate of gas dynamical friction timescale ($t_{\rm DF}$). The longer timescale in the higher gas density is due to the increase in the deepness of gas gravitational potential. The longer timescale in the lower gas density is due to the decrease of the drag-force due to the gas dynamical friction. In addition, there is the difference that the merger time in the simulations is systematically shorter than the analytic estimate. The main reason for the systematic difference is thought to arise from the absence of the GW as well as the three-body interaction effect in the analytic estimate.

Fig. 3.10 shows the dependence of the merger timescale on the BH density (or $r_{\rm typ}$). According to the increase of the BH density, the power law in the right side shifts lower. This shift arises from the decrease of the deepness of the gas gravitational potential within $r_{\rm typ}$. The dependence on the BH density is the same in the numerical results of ten BH systems. Thus, the tendency of the merger time in the type A region is roughly explained by the analytic timescale.

As described above, type A always appears in higher gas density than the turning point of the double power law of $t_{\rm DF}$. This fact implies that the turning point provides the critical gas density, above which the merger is driven by the gas dynamical friction. Here, the power law in the left side is proportional to $M_{\rm BH}^{1/2} n_{\rm gas}^{-1} r_{\rm typ}^{-3/2}$, and the power law in the right side is proportional to $M_{\rm BH}^{-1} n_{\rm gas}^{1/2} r_{\rm typ}^{3}$. Because $t_{\rm DF}$ of the left side power law is same value to that of the right side power law at the turning point, the turning point is given by $M_{\rm BH}^{1/2} n_{\rm gas}^{-1} r_{\rm typ}^{-3/2} = {\rm const} \times M_{\rm BH}^{-1} n_{\rm gas}^{1/2} r_{\rm typ}^{3}$. Therefore, the turning point is at $n_{\rm gas} \rho_{\rm BH}^{-1} r_{\rm typ}^{-1} = {\rm const}$. Hence, the boundary between types A and B is supposed to be also given by $n_{\rm gas} \rho_{\rm BH}^{-1} r_{\rm typ}^{-1} = {\rm const}$. Fig. 3.11 shows the distribution of merger types as functions of $n_{\rm gas} \rho_{\rm BH}^{-1} r_{\rm typ}^{-1}$ and $\rho_{\rm BH}$. We set $\rho_{\rm BH}$ as the horizontal axis in Fig. 3.11, since $\rho_{\rm BH}$ gives different values for each $M_{\rm BH}$ and $r_{\rm typ}$ in the settings of our simulations. Black cross plots represent the average of the minimum values in type A and the maximum values in type B in logarithmic space for each $\rho_{\rm BH}$. Black line represents the line fitted by $n_{\rm gas} \rho_{\rm BH}^{-1} r_{\rm typ}^{-1} = {\rm const}$ in logarithmic space for cross prots. We can fit the results with $n_{\rm gas} \rho_{\rm BH}^{-1} r_{\rm typ}^{-1} = 8 \times 10^4 \ {\rm cm}^{-3} {\rm pc}^2 / M_\odot$ with a standard deviation of a factor of 3. Here, the uncertainties due to the random number for initial conditions are also a factor of a few, which is roughly estimated from the fluctuation

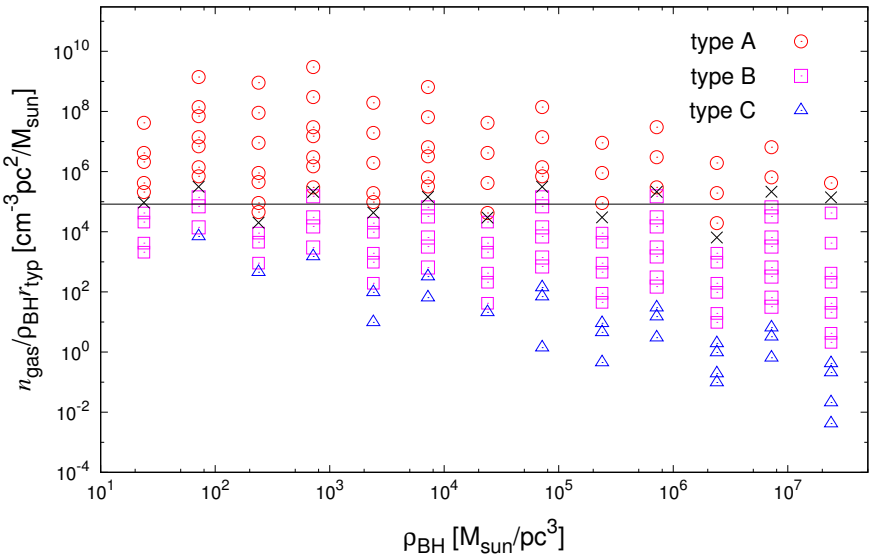

Fig. 3.11 Distribution of merger types as functions of $n_{\rm gas}/r_{\rm typ}\rho_{\rm BH}$ and BH density $\rho_{\rm BH}$. Red, pink, and blue open symbols represent the results of the types A, B, and C mergers respectively. Black cross plots are the boundary between types A and B for each $\rho_{\rm BH}$. A black line is the fitting for black cross plots using $n_{\rm gas}/r_{\rm typ}\rho_{\rm BH} = {\rm const.}$

of the averaged merger time in Fig. 3.9. Hence, the dispersion of the boundary line in Fig. 3.11 can be roughly explained by the uncertainties due to the random number. Thus, we give the boundary between types A and B as

$$\left(\frac{n_{\rm gas}}{10^7\ {\rm cm}^{-3}}\right)\left(\frac{300\ M_\odot/{\rm pc}}{\rho_{\rm BH}}\right)\left(\frac{1\ {\rm pc}}{r_{\rm typ}}\right) = 2.5. \tag{3.7}$$

From this new criteria, in type A, the most of time is spent to remove the gas potential energy. In this phase, the BHs receive gravity mainly from gas. Hence, the angular momentum transport due to the three-body interaction is not efficient because the efficient angular momentum transport by the three-body interaction requires hard binary, whose BH receive gravity mainly from another BH (Binney & Tremaine, 2008).

Tagawa et al. (2015) assume that the boundary can be given by the ratio of the gas mass within $r_{\rm typ}$ to the total BH mass, and the boundary is drived by the average of the ratio for four cases. However, there is no physical explanation for the boundary derived in Tagawa et al. (2015) and this criteria cannot explain the boundary for all

$\rho_{\rm BH}$ well. On the other hand, the boundary of equation (3.7) can be understood from the timescale of the dynamical friction, and gives the criteria between types A and B for all $\rho_{\rm BH}$ well.

3.2.2 Effects of gas accretion and boundary conditions

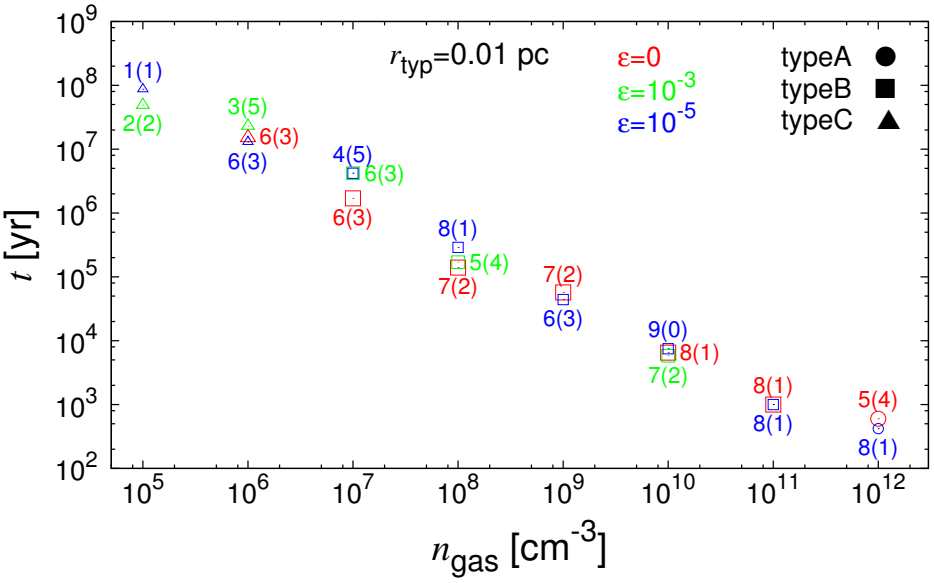

Fig. 3.12 First merger time as a function of gas number density $n_{\rm gas}$ for $r_{\rm typ}$ = 0.01 pc in the case that the merger dominantly contribute to the first growth of the BHs (Tagawa et al., 2016). Red, green, and blue plots represent the merger time in the cases of no accretion ($\epsilon = 0$), intermediate accretion ($\epsilon = 10^{-3}$), and lower accretion ($\epsilon = 10^{-5}$), respectively. Also, circle, square, and triangle symbols represent the types A, B, and C mergers, respectively. The number (in parentheses) described beside each symbol represent the number of merged (escaped) BHs. Taken from figure 13 of Tagawa et al. (2016).

In Section 3.2.1, the gas mass is set to be infinite. Here, by performing the simulations with accretion in the finite gas mass of 10^5 $M_\odot$, we investigate the influences of the gas accretion and the finiteness of gas mass on the merger timescale and mechanisms. Fig. 3.12 shows that the merger timescale for no accretion ($\epsilon = 0$, red symbols), that for intermediate accretion ($\epsilon = 10^{-3}$, green symbols), and for lower accretion ($\epsilon = 10^{-5}$, blue symbols) in the cases in which the merger dominantly contributes to the first growth of BHs. In those cases, the finiteness of the gas mass and the gas accretion do not bring significant influence on the merger timescale within

variances of a factor of 2 and on the merger mechanisms.

Fig. 3.12 also shows the number of escaped BHs for each parameter. The averaged number of escapers is $2 \sim 3$ from assumed systems of $M_{\rm gas,tot} = 10^5\ M_\odot$. The number of escaped BHs is thought to increase in a shallower gravitational potential. Therefore, a deep potential is requisite for the efficient merger of multiple BHs via type B or C mechanism.

3.3 Critical accretion rate for the black hole growth

A significant measure for the BH growth is provided by the conditions in which the predominant mechanism of the BH growth is bifurcated between the merger and the accretion. Fig. 3.13 shows resultant merger types and the contribution of the accreted mass $m_{\rm ac}$ to the final mass $m_{\rm fin}$ at the end of simulations. This figure indicates that the fractions of accreted mass are steep functions of two parameters (ϵ and $n_{\rm gas}$), depending on the initial extension of BH spatial distributions ($r_{\rm typ}$). This behavior arises from the fact that the Hoyle-Lyttleton accretion rate is a nonlinear function of mass as shown in equation (2.15) and so diverges at the finite time as

$$m_i = \frac{1}{m_0^{-1} - \alpha t}, \tag{3.8}$$

where m_0 is the initial mass and $\alpha = \epsilon 4\pi G^2 m_{\rm H} n_{\rm gas}/(C_{\rm s}^2 + v_i^2)^{3/2}$.

From the results in Fig. 3.13, we derive the critical condition that bifurcates the key mechanism of the growth of BHs. In the cases of the low gas density, $t_{\rm DF}$ and $t_{\rm ac}$ does not depend on the BH density, $\rho_{\rm BH}$. Furthermore, the dependence of $t_{\rm DF}$ on $n_{\rm gas}$ is the same as that of $t_{\rm ac}$. Therefore, the critical accretion efficiency ($\epsilon_{\rm c}$), above which the accretion mass is predominant, is expected to be constant. To assess $\epsilon_{\rm c}$, we use the average ratios of accretion mass to final mass ($m_{\rm ac}/m_{\rm fin}$). Also, the range of the gas density that can be used in this assessment is low-density regions of $n_{\rm gas} < 10^8{\rm cm}^{-3}$. Then, we derive $\epsilon_{\rm c}$ by linearly interpolating $m_{\rm ac}/m_{\rm fin}$ between $\max\{\log\epsilon\}$ for $2m_{\rm ac} < m_{\rm fin}$ and $\min\{\log\epsilon\}$ for $2m_{\rm ac} > m_{\rm fin}$. As a result, we find the critical accretion efficiently for the low density cases is $\epsilon_{\rm c} = 6 \times 10^{-3}$. This value is roughly consistent with the condition that the timescale for the merger of ten BHs is a few hundred times larger than the accretion timescale, as required in Tagawa et al. (2015).

On the other hand, in high-density regions, $\epsilon_{\rm c}$ is depending on $n_{\rm gas}$ and $r_{\rm typ}$. To derive the dependence of $\epsilon_{\rm c}$ on $n_{\rm gas}$, we use the results in high-density regions of $n_{\rm gas} \geq 10^8{\rm cm}^{-3}$ for a given $r_{\rm typ}$. Fig. 3.14 shows $\epsilon_{\rm c}$ as a function of $n_{\rm gas}$. As shown in Fig. 3.14, the dependence of $\epsilon_{\rm c}$ on $n_{\rm gas}$ seems almost same irrespective of $r_{\rm typ}$. Actually, if the dependence is assumed to be a power law as $\epsilon_{\rm c} = a n_{\rm gas}^p$, we can fit the results with $p = -1.01 \pm 0.07$, by linearly interpolating $m_{\rm ac}/m_{\rm fin}$ between $\max\{\log n_{\rm gas}\}$ for $2m_{\rm ac} < m_{\rm fin}$ and $\min\{\log n_{\rm gas}\}$ for $2m_{\rm ac} > m_{\rm fin}$. Next, we investigate the dependence on $\rho_{\rm BH}$. Fig. 3.15 shows $\epsilon_{\rm c}$ as a function of $\rho_{\rm BH}$. The dependence on $\rho_{\rm BH}$ also seems to be well fitted by a power law form. If the dependence is assumed to be $\epsilon_{\rm c} = a n_{\rm gas}^{-1.01} \rho_{\rm BH}^q$, the best fit value is $q = 0.74 \pm 0.20$.

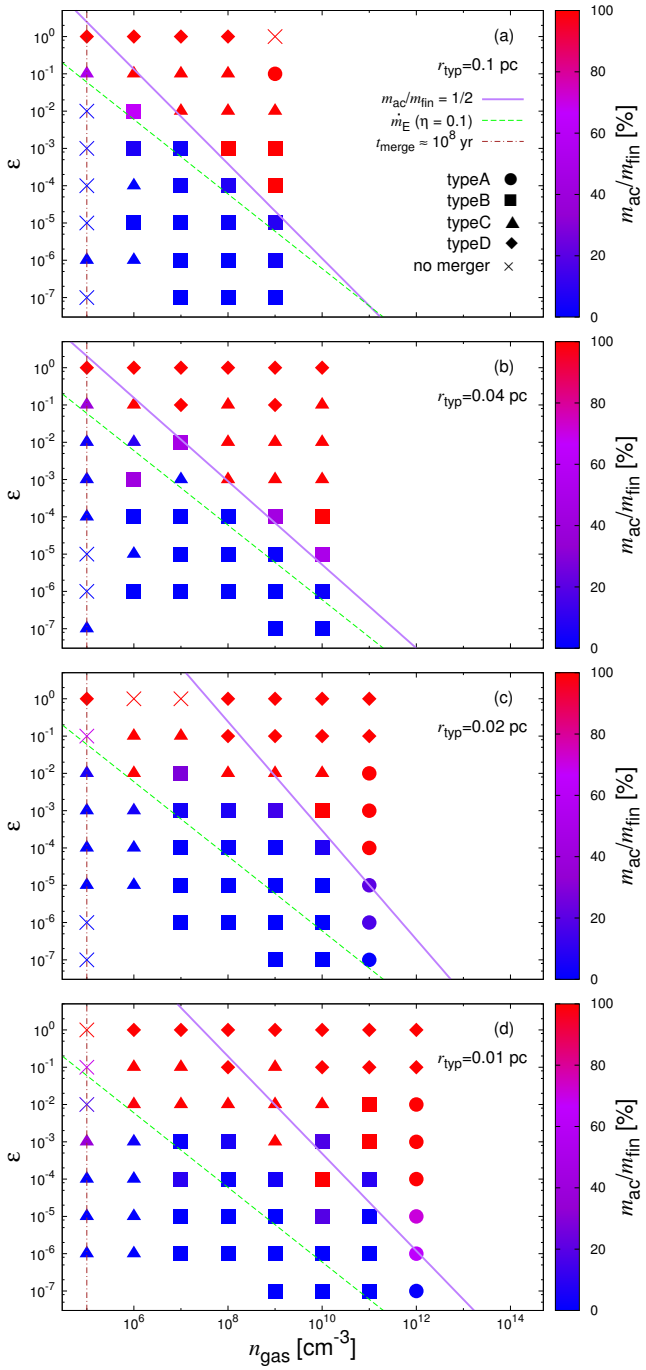

Fig. 3.13 The contribution of the accreted mass to the final mass of the most massive BH as functions of the gas density, $n_{\rm gas}$, and the accretion rate, ϵ. Filled circles, squares, triangles, diamonds, and crosses represent gas drag-driven mergers (type A), interplay-driven mergers (type B), three body-driven mergers (type C), accretion-driven mergers (type D) and no merger, respectively. The initial typical extension of BH spatial distributions is (a) $r_{\rm typ}$ =0.1 pc, (b) 0.04 pc, (c) 0.02 pc, and (d) 0.01 pc. The green dashed line represents the Eddington accretion rate $\dot{m}_{\rm E}$ for the initial mass of the BH. The purple line represents the critical condition that bifurcates the key mechanisms for the growth of the BH. The brown dot-dashed line represents the lower limit of gas density for the occurrence of merger within 10^8 yr, which is roughly estimated from Fig. 6 in Tagawa et al. (2015). Taken from figure 10 of Tagawa et al. (2016).

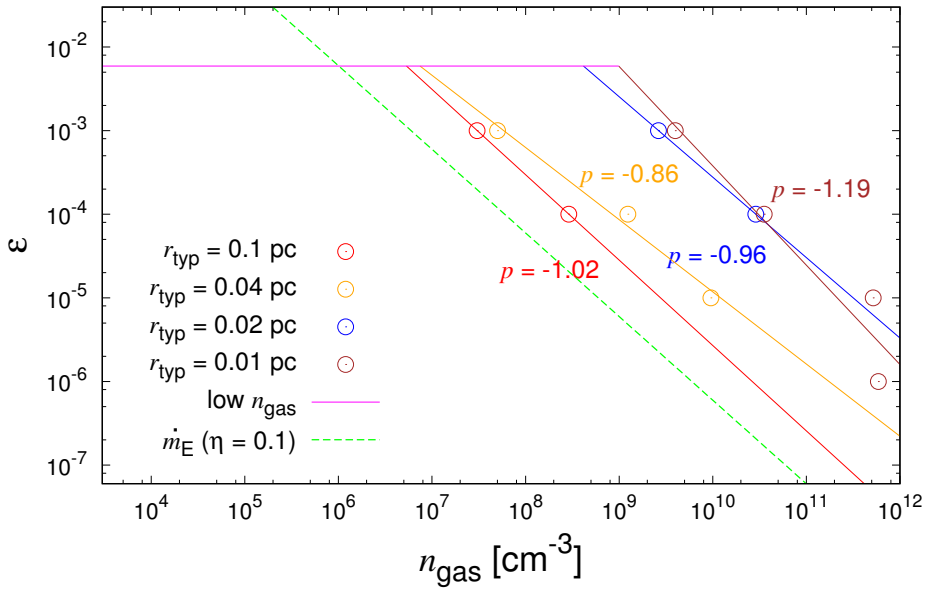

Fig. 3.14 The critical accretion efficiency, ϵ_c, as a function of ambient gas density, n_{gas}. Red, orange, blue, and brown plots represent the critical condition in high-density regions for $r_{typ} = 0.1,\ 0.04,\ 0.02$, and 0.01 pc, respectively. Red, orange, blue, and brown lines represent the curves fitted by $n_{gas,c} = a\epsilon^p$ for $r_{typ} = 0.1,\ 0.04,\ 0.02$, and 0.01 pc. Pink line represents the critical condition in low-density regions. The green dashed line represents the Eddington accretion rate $\dot{m}_E$. Taken from figure 11 of Tagawa et al. (2016).

As the results for high and low gas density cases, ϵ_c is given as

$$\epsilon_c = \begin{cases} 6 \times 10^{-3} \\ \qquad \text{for } n_{gas} \lesssim 10^8 \text{cm}^{-3} \\ 2 \times 10^{-3} \left(\frac{n_{gas}}{10^8 \text{cm}^{-3}}\right)^{-1.0} \left(\frac{\rho_{BH}}{10^6 M_\odot \text{pc}^{-3}}\right)^{0.74} \\ \qquad \text{for } n_{gas} \gtrsim 10^8 \text{cm}^{-3}. \end{cases} \tag{3.9}$$

The accretion efficiency of 6×10^{-3} corresponds to a super-Eddington accretion rate with the Eddington ratio of ~ 10 at first generation objects of $n_{gas} = 10^7 \text{cm}^{-3}$. The equation (3.9) is basically the condition of $t_{DF} \sim t_{ac}$. This condition leads to $\epsilon_c = \text{const}$ in a low-density limit and $\epsilon_c \propto n_{gas}^{-3/2} \rho_{BH}$ in a high-density limit.

The difference in the dependence of ϵ_c between an analytic estimate and the numerical results may come from mass accretion in $v \lesssim c_s$ and also from the gradual transition from high-density regions to low-density regions. Equation (3.9) shows that

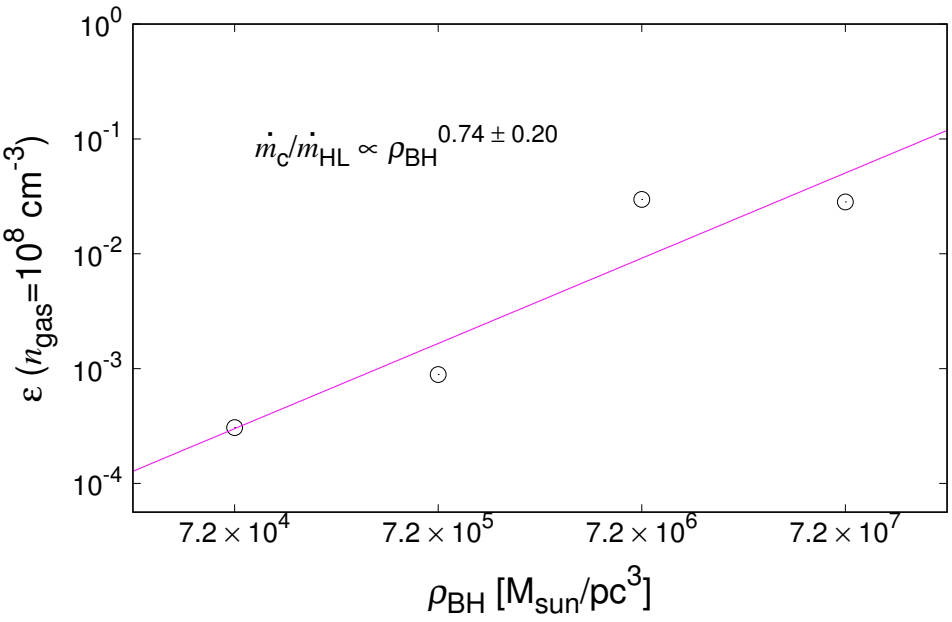

Fig. 3.15 The critical accretion efficiency, ϵ_c, as a function of ρ_{BH}, for $n_{gas} = 10^8$ cm^{-3}. A straight line is the fitting using a power law of $\epsilon(n_{gas} = 10^8 \text{ cm}^{-3}) = a\rho_{BH}^q$. Taken from figure 12 of Tagawa et al. (2016).

if ρ_{BH} is lower (r_{typ} is larger), then the critical accretion efficiency becomes lower in high density environments of $n_{gas} \gtrsim 10^8 \text{cm}^{-3}$.

Here, as seen in Section 2.1.5, ϵ is reduced by the radiation pressure when $\epsilon > 0.1$. However, ϵ_c of equation (3.9) is much smaller than $\epsilon = 0.1$, and so the results are not affected by the radiation pressure.

From the results of our simulations, if the BH merger precedes the significant gas accretion, all BHs merge into one massive BH. This may be concerned to the fact that only one BH resides in the center of each massive galactic bulge. On the other hand, if the significant gas accretion precedes the BH merger, multiple BHs are likely to be left in the system. Interestingly, a number of stellar mass ($\sim 50 M_\odot$) BHs are found in the center region of M31 (Barnard et al., 2014). Although the origin of these stellar mass BHs is not unveiled yet, multiple BHs can be left if the multiple BH systems are evolved by rapid mass accretion.

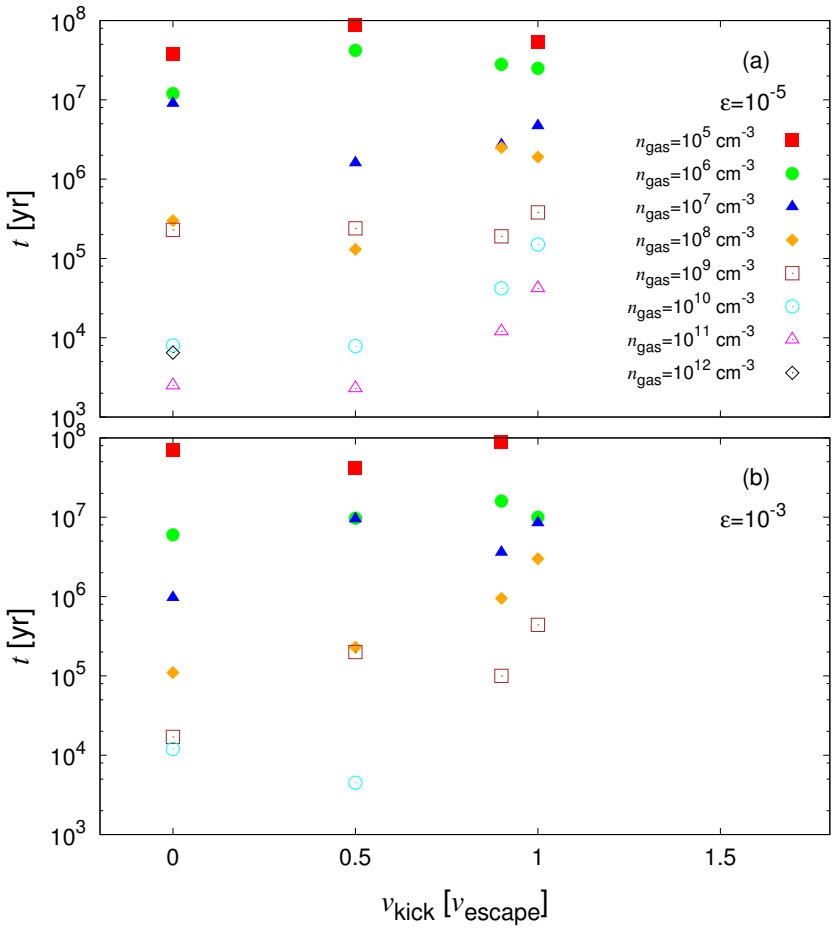

Fig. 3.16 The averaged merger time as a function of the kick velocity in the cases of $r_{\rm typ} = 0.01$ pc and $v_{\rm kick} \leq v_{\rm escape}$. Filled red squares, green circles, blue triangles, orange diamonds, open brown squares, blue circles, magenta triangles, and black diamonds represent the merger time for $n_{\rm gas} = 10^5$, 10^6, 10^7, 10^8, 10^9, 10^{10}, 10^{11}, and 10^{12}, respectively. Panel (a) presents the results for the case of lower accretion ($\epsilon = 10^{-5}$), while panel (b) for intermediate accretion ($\epsilon = 10^{-3}$). Taken from figure 14 of Tagawa et al. (2016).

3.4 Effect of Recoil Kick

In Section 3.4, we estimate the effect of the recoil kick due to the anisotropic emission of GW radiation. The recoil velocity depends strongly on the magnitudes of BH spins and the alignment of BH spins with the orbital angular momentum of a BH binary.

To investigate the effect of the recoil kick on the merger processes, we perform the

simulations incorporating the recoil kick at the merger in the case of $r_{\rm typ} = 0.01$ pc. In these simulations, the kick velocity ($v_{\rm kick}$) are set to be 0, 0.5, 0.9, 1.0, 1.1, and 1.5 times escape velocity ($v_{\rm escape}$). Also, we give the number of BHs as five to spare computational cost. As expected, if $v_{\rm kick} \leq 1.0 \times v_{\rm escape}$, the merged BH is bound in the system, while in the cases of $v_{\rm kick} \geq 1.1 \times v_{\rm escape}$, the merged BH escapes from the system. Fig. 3.16 shows the averaged merger time as a function of $v_{\rm kick}$ for $v_{\rm kick} \leq v_{\rm escape}$. From this figure, the averaged merger times for $v_{\rm kick} \sim v_{\rm escape}$ is mostly the same as that for $v_{\rm kick} = 0$ in low gas density cases as $n_{\rm gas} < 10^8$ cm^{-3}. This is because the merger timescale is almost independent of the initial extension of BH spatial distributions in low BH density cases (Section 3.2.1). On the other hand, in high gas density cases ($n_{\rm gas} \geq 10^8$ cm^{-3}), the averaged merger time for $v_{\rm kick} \sim v_{\rm escape}$ is longer by about ten times than that for $v_{\rm kick} = 0$ km/s. As a result, the critical accretion rate may be reduced by about one order of magnitude in high gas density regions, if the effect of the recoil velocity is non-negligible.

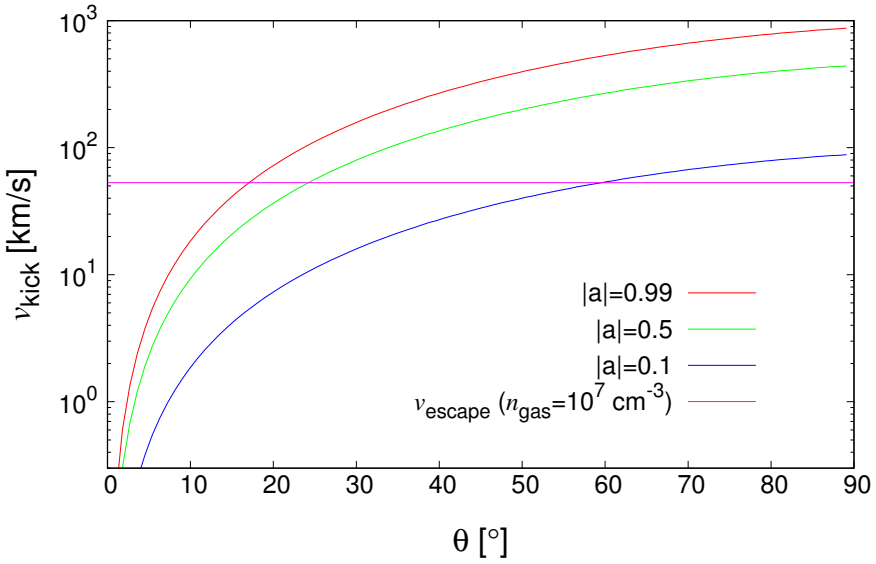

Fig. 3.17 The averaged kick velocity as a function of the angle (θ) between the spin of one BH and the angular momentum of the binary in the cases that two BHs have the same masses and spin magnitude, and the spin direction of another BH is the same as the direction of the angular momentum of the binary. Red, green, and blue lines represent the results for BH spin magnitude of $|a_1| = |a_2| =$ 0.99, 0.5, and 0.1, respectively. The pink line denotes the escape velocity for a gas cloud of $n_{\rm gas} = 10^7$ cm^{-3}. Taken from figure 15 of Tagawa et al. (2016).

Next, we estimate the probability that the kick velocity surpasses the escape velocity

for each gas density. Here, we assume completely random direction and magnitude of BH spins for equal mass BHs. To derive the probability, 10^7 sets of BH spins are calculated. The model of the recoil velocity is used from Campanelli et al. (2007a), and we set the two angle ξ and Θ_0 in equation (1) of Campanelli et al. (2007a) to $\xi = 90^\circ$ and $\Theta_0 = 0^\circ$. Table. 3.3 shows the escape velocity and the probability of $v_{\rm kick} > v_{\rm escape}$ for each gas density. From this table, if we consider a first-generation object of $n_{\rm gas} \sim 10^7$ cm^{-3}, about 90 percent of merged BHs possibly escape from the system. Thus, the effect of recoil velocity can significantly reduce the BH growth rate via the BH merger. This is the prospect in the cases of the random orientation of BH spins. On the other hand, if the BH spins are primitively correlated with each other in a binary, the probability varies. Considering the binary formation, we can expect that the orientations of BH spins are similar to the orientation of the binary angular momentum. To make a simple estimate, we vary the orientation of the spin ($\mathbf{a}_1$) of one BH, assuming that the orientation of the other BH spin ($\mathbf{a}_2$) is the same as the orbital angular momentum orientation, and the spin magnitude is the same with each other ($|\mathbf{a}_1| = |\mathbf{a}_2|$). The resultant kick velocities are averaged over 10^5 sets of the random azimuthal angles between the infall orientation at a merger and the projected orientation of $\mathbf{a}_1$ to the binary orbital plane. In Fig. 3.17, the kick velocity as a function of θ is shown. When the merged BHs are rapidly rotating ($|\mathbf{a}_1| = |\mathbf{a}_2| = 0.99$), the averaged kick velocity surpasses the escape velocity in $\theta > 16.2^\circ$. This means that if θ is randomly given from 0° to 90°, about 82 percent of merged BHs will escape and 18 percent stay in the system. Besides, as the BH spin magnitude decreases, then the escape fraction decreases. Thus, the escape probability of a merged BH born from a star binary becomes lower than that for the cases of the randomly oriented spins. Furthermore, Natarajan & Pringele (1998) have suggested that the BH spins are aligned with the outer accretion disk within $\sim 10^5 - 10^6$ yr due to the Bardeen-Petterson effect, although the large uncertainties in the viscosity may change the alignment timescale (Volonteri et al., 2007).

Table 3.3 The escape velocity and probability for each gas number density in the cases of random spins and equal mass BHs.

$n_{\rm gas}$ ($\rm cm^{-3}$)	$v_{\rm escape}$ (km/s)	$P(v_{\rm kick} > v_{\rm escape})$ (%)
10^5	24.6	95.6
10^6	36.1	93.4
10^7	53.0	90.2
10^8	77.7	85.3
10^9	114	78.0
10^{10}	167	67.2
10^{11}	246	52.5
10^{12}	361	35.8

Chapter 4

Non-binary black hole merger in GW150914

In this section, to investigate the possibility of merger from non-binary BHs in GW150914, we perform post-Newtonian N-body simulations.

4.1 Mergers at GW150914 from smaller mass BHs

We extract the binaries that appear similar to GW150914 from our 264 models. The parameters we investigated are the gas number density ($n_{\rm gas}$), the initial extention of BH distribution ($r_{\rm typ}$), the accretion rate (ϵ) and the initial BH mass (m_0).

In Figure 4.1, the masses of binary BHs just before the first merger in our simulations are shown. We find several sets of parameters, in which the masses in a

Table 4.1 Models merged at the masses of the GW150914 event.

Model	m_0 ($M_\odot$)	$n_{\rm gas}$ ($\rm cm^{-3}$)	ϵ	$r_{\rm typ}$ (pc)	m_1 ($M_\odot$)	m_2 ($M_\odot$)	$t_{\rm merge}$ (yr)	type
1	25.0	10^3	0.1	0.1	37.3	28.2	3.3×10^9	B,C
2	25.0	10^6	0.01	0.1	33.3	31.3	2.8×10^7	B,C
3	25.0	10^7	0.01	0.01	35.8	32.3	1.3×10^7	B,C
4	25.0	10^8	0.01	0.01	33.8	28.7	4.2×10^5	B,C
5	25.0	10^{10}	0.01	0.01	34.5	32.1	5.8×10^3	B,C
6	30.0	10^4	0.01	1	33.3	31.2	1.0×10^9	B,C
7	30.0	10^4	0.01	0.1	35.6	30.8	1.0×10^9	B,C
8	30.0	10^4	0.01	0.01	33.4	32.0	7.7×10^8	B,C
9	30.0	10^5	0.01	0.1	32.4	31.2	1.5×10^8	B,C
10	30.0	10^6	0.01	0.1	34.4	32.7	9.9×10^6	B,C
11	30.0	10^9	0.01	0.1	34.4	32.8	1.7×10^4	B,C
12	30.0	10^{10}	0.001	0.01	32.1	31.9	1.2×10^4	B,C

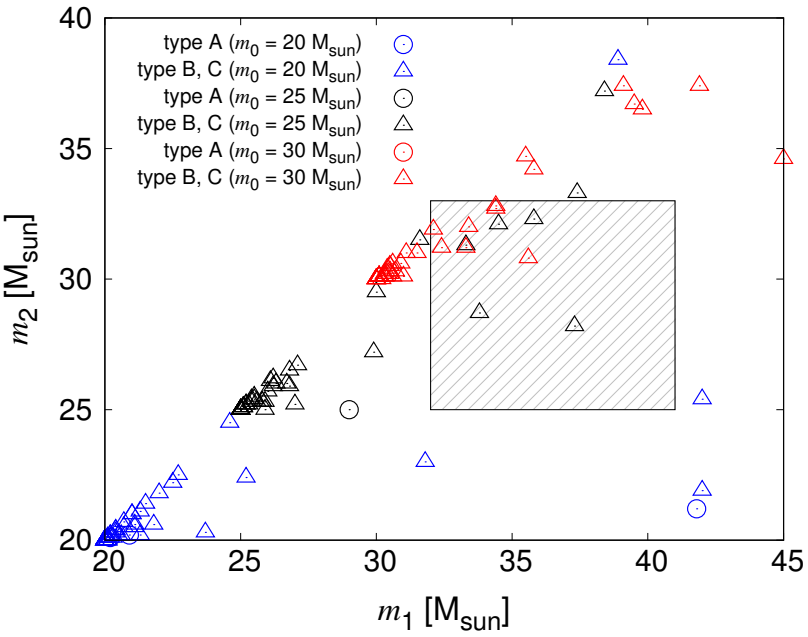

Fig. 4.1 The BH masses ($m_1 > m_2$) in a binary just before the first merger in each run. Blue, black, and red plots represent the initial masses (m_0) of 20, 25 and 30 $M_\odot$, respectively. Circles and triangles represent the gas drag-driven mergers (type A), and interplay-driven mergers (type B) or three body-driven mergers (type C), respectively. The masses of GW150914 with their uncertainties are indicated by the hatched region. The filled symbols in panel (b) are the parameters where the masses of merged BHs match those of GW150914.

binary at first merger match those determined in GW150914 within their uncertainties. All of these parameters show that mergers are driven by interplay or three-body interactions (type B or C). Since the three body-interaction is chaotic mechanism, accreted masses of type B, C are easy to change according to the random number for initial conditions. Therefore, if BH evolution from the similar initial condition to the BHs of GW150914 is occur, the masses at mergers are presumably different from GW150914. This suggests that the masses of following GW events by the BH binary mergers are presumably different masses from the masses of GW150914 in the case of the non-binary BH merger scenario.

Figure 4.2 is the same as Figure 4.1, but the accreted masses are shown. The accreted mass is basically almost less than a several tens percent of the initial mass in the range of $0-30\ M_\odot$. Thus, as the masses of the seed BHs become smaller, then the merger rate at the masses of GW150914 is reduced. Actually, there is no run that BHs merge at the masses of GW150914 from seed masses of 20 $M\odot$ as seen in Figure

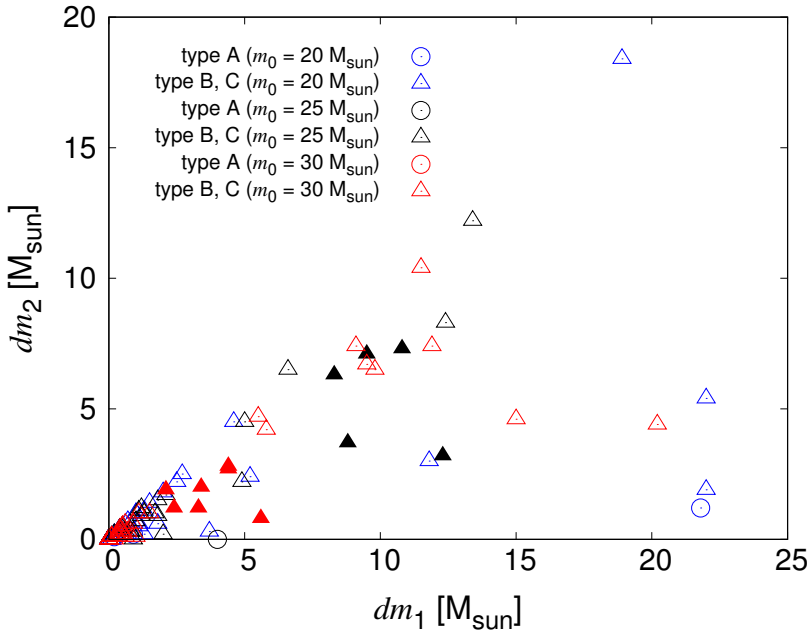

Fig. 4.2 Same as Figure 4.1, but the accreted masses of merged BHs in a binary just before the first merger in each run. The filled symbols are the parameters where the masses of merged BHs match those of GW150914.

4.1.

The sets of parameters in which the masses in a binary match those determined in GW150914 are shown in Table 4.1. The columns are the model number, the initial mass of BHs (m_0), the initial gas number density ($n_{\rm gas}$), the accretion efficiency (ϵ), the initial extension of the BH spatial distribution ($r_{\rm typ}$), the masses of binary BHs just before the merger ($m_1,\ m_2,\ m_1 > m_2$), merger time ($t_{\rm merge}$), and the type of the merger in each run.

As seen in Table 4.1, the accretion rates of those parameters are 0.01 except the Model 1 and 12. These values are roughly consistent with the results of Section 3.3. We derive the critical accretion efficiency for ten mergers in the low density regions ($n_{\rm gas} \lesssim 10^8 {\rm cm}^{-3}$) as $\epsilon_{\rm c} = 0.006$, at which the time passed until most of gas accretes coincides with the time passed until ten BHs merge into one BH. We simply assume that the critical accretion efficiency for one merger is ten times larger than the critical accretion efficiency for ten mergers, and so the critical accretion efficiency for one merger in the low density regions is about 0.06. Besides, the accretion efficiency of the runs whose first mergers are accompanied by few tens percent mass accretion is expected to be just below the critical accretion efficiency for one merger because

the Hoyle-Lyttleton-type accretion is a nonlinear function of mass, and therefore, accreted mass is a steep function of ϵ and $n_{\rm gas}$. In fact, the accretion efficiency of 0.01 indicated in Table 4.1 is just below the critical accretion efficiency for one merger (~ 0.06). The reason of exception for the Model 1 is likely to come from the fact that the effect of the strong three-body interaction at the low gas density shortens the merger time. On the other hand, the accretion efficiency in Model 12 is lower. This is because the gas density in Model 12 is higher, and so the critical accretion efficiency becomes smaller than 0.06.

According to Table 4.1, the initial extension of the BH spatial distribution ($r_{\rm typ}$) of runs in which the merger occurs at the masses of GW150914 is mostly less than 1 pc. This may be relevant to the contribution of the three-body interaction. Since the effect of the three-body interaction becomes weak in the low BH density cases, the growing BHs are easy to continue to be accreted, and so the accreted mass becomes more steep function of parameters such as ϵ and $n_{\rm gas}$. Therefore, the probability of the merger at the masses of GW150914 from smaller seed BHs is reduced in the low BH density cases. Hence, we conclude that higher BH density is preferred for the merger at the masses of GW150914 from smaller seed BHs.

Next, we discuss preferable environments for the non-binary merger scenario. Because the environments could vary within 10^8 yr due to the active galactic nucleus (AGN) duty cycle and/or the galactic rotation timescale, the merger time should be shorter than 10^8 yr. Besides, the merger time is almost inversely proportional to the gas density (Section 3.2.1). From these conditions, the gas number density should be higher than 10^5 cm^{-3}. Therefore, galactic nuclear regions and dense interstellar cloud cores are favorable sites for the merger from non-binary isolated BHs in GW150914.

In the non-binary BH merger scenario, the mass accretion by gas is important to explain the GW150914 event. Although the detailed mechanism is not revealed, there is a possibility that such mass accretion is relevant to the high energy emission during merger (Connaughton et al., 2016).

Here, we discuss the validation of the initial condition. It is not obvious that BHs are virialized in interstellar clouds. The virialization of the BHs is required that the velocity dispersion of BHs are smaller than the escape velocity of interstellar clouds. For Pop I/II stars, young stars have the velocity dispersion of about 20-30 km/s (Nordstrom et al., 2004). Then, the velocity dispersion of Pop I/II BHs are presumably smaller than the velocity dispersion of young Pop I/II stars because of the effects of the equipartition (Binney & Tremaine, 2008) and the dynamical friction. However, to decide whether Pop I/II BHs are virialized in interstellar clouds, another simulation is required.

For Pop III BHs, the virialization in interstellar clouds is supposed to be difficult.

From the numerical simulation of Ishiyama et al. (2016), most of light Pop III stars exist in the halo and the bulge regions. However, Ishiyama et al. (2016) did not consider the effects of the dynamical friction by gas in gas-rich primordial galaxies, and the dynamical friction by stars in dense bulge regions that is important for the Pop III BHs in center regions within 100 pc. Hence, the distribution of the Pop III BHs also remains uncertain. In the future, we would like to investigate the distribution of Pop I/II/III BHs realistically.

4.2 Event rates

We roughly estimate the event rates based on the non-binary BH merger scenario for the first observing run of LIGO advanced detectors. First, we estimate the event rate for the mergers of population I/II remnant BHs (Pop I/II BHs) in dense interstellar cloud cores. Roughly, there are 10^8 Pop I/II BHs in each Milky Way (MW)-sized galaxy (Remillard & McClintock, 2006). Here, the volume of the MW Galaxy is about $10\ \mathrm{kpc} \times 10\ \mathrm{kpc} \times 1\ \mathrm{kpc} = 100\ \mathrm{kpc}^3$, and the total volume of all giant molecular clouds (GMCs), whose number is supposed to be about 1000 in the MW Galaxy, is about $10\ \mathrm{pc} \times 10\ \mathrm{pc} \times 10\ \mathrm{pc} \times 1000 = 10^{-3}\ \mathrm{kpc}^3$. Thus, the expected number of BHs that exist in GMCs is roughly $10^8 \times (10^{-3}\ \mathrm{kpc}^3/100\ \mathrm{kpc}^3) = 1000$. If we consider the Poisson distributions, about 100 GMCs are likely to possess multiple BHs. Since the merger time in GMCs is about 20 Myr (Tagawa et al., 2015), the merger rate in a MW-sized galaxy is $100/20\ \mathrm{Myr} = 5\ \mathrm{Myr}^{-1}$. For the binary with total mass of 65 $M_\odot$, we adopt a horizon distance of $D_h \approx 3$ Gpc($z \approx 0.3$) for the first advanced LIGO observation run (Belczynski et al., 2016), corresponding to a comoving volume $V_c \approx 50\ \mathrm{Gpc}^3$. By assuming the number density of the MW-sized galaxies as about $2 \times 10^6\ \mathrm{Gpc}^{-3}$, the number of MW-sized galaxies involved in this volume is $50\ \mathrm{Gpc}^3 \times 2 \times 10^6\ \mathrm{Gpc}^{-3} = 1 \times 10^8$. We also assume that ratio of massive BHs to Pop I/II BHs is 0.1, and so the fraction of massive BH pairs to Pop I/II BH pairs is 0.01. From these assumptions, the event rate for the mergers of Pop I/II BHs in GMCs is estimated to be $5\ \mathrm{Myr}^{-1} \times 0.01 \times 1 \times 10^8 = 5\ \mathrm{yr}^{-1}$.

Second, we consider the event rate for the mergers of population III remnant BHs (Pop III BHs) in dense interstellar cloud cores. We assume that 10 Pop III BHs born in minihalo of $10^5 - 10^6\ M_\odot$. In this case, $\sim 10^6$ Pop III BHs exist in MW-sized galaxy (Ishiyama et al., 2016). We also assume that all Pop III BHs exist as a multiple system of four Pop III BHs since Pop III stars are likely to born as multiple stars (Susa et al., 2014). Then, 25 GMCs possess multiple Pop III BH systems on average. We suppose that the ratio of massive BHs to Pop III BHs is 0.5, and so the fraction of massive BH pairs to Pop III BHs is 0.25. From these conditions, we estimate that

the event rate for the mergers of Pop III BHs in GMCs is ~ 3 yr^{-1} by following the estimate of the event rate of Pop I/II BHs in GMCs.

Next, we estimate the event rates for the mergers of Pop I/II and Pop III BHs in galactic nuclear regions (GNRs). In the MW Galaxy, about 3×10^6 stars exist within 1 pc from the supermassive BH (Alexander, 2005). By assuming that about one Pop I/II BH exists per 1000 stars, we can suppose that $\sim 3 \times 10^3$ Pop I/II BHs exist in GNRs. Also, if ratio of Pop III BHs to Pop I/II BHs is constant in the whole galaxy including GNRs, $\sim 3 \times 10^1$ Pop III BHs possibly exist in GNRs in MW-sized galaxy. Based on our simulations, we envisage that all stellar-mass BHs in GNRs can merge with each other in the AGN phase (~ 100 Myr) because of the high density of GNRs in the AGN phase. Besides, we assume that all MW-sized galaxies experience one AGN phase during the cosmic time. From these assumptions, we calculate that the event rate for the mergers of Pop I/II BHs in GNRs is ~ 0.3 yr^{-1} and that of Pop III BHs is ~ 0.1 yr^{-1} by following the estimate of the event rates in GMCs.

Combining the event rates of Pop I/II BHs and Pop III BHs, we estimate that the event rates are about ~ 8 yr^{-1} for the mergers in GMCs and ~ 0.4 yr^{-1} for the mergers in GNRs. We find that these estimated event rates are broadly consistent with the observed frequency of previous GW events. Note that these estimated events rates are thought to be accompanied by the uncertainties of $\sim 1 - 2$ order of magnitude, which are mainly come from the uncertainties of the spatial and kinematic BH and gas distribution. Especially the spatial and kinematic distributions of Pop III stars have large uncertainties. Although Ishiyama et al. (2016) calculate the Pop III star distribution using the N-body simulation, their study does not consider the effects of the dynamical friction by gas due to the abundant gas in high-redshift galaxies, and the dynamical friction by stars due to the high density in bulge regions. To estimate the BH merger rate using more realistic BH and gas distributions, cosmological hydrodynamic simulations are required.

Furthermore, the non-binary BH merger scenario prefers late-type galaxies as host galaxies of GW events, because gas rich environments are required. To confirm the scenario, additional GW observations are desired.

Chapter 5

Application to several issues

5.1 Origin of r-process elements by neutron star mergers

We explore the possibility of mergers in a system composed of multiple NSs as well as BHs assuming the environments of first-generation objects. In this section, we present the results of post Newtonian N-body simulations, incorporating the gas dynamical friction, the gas accretion, and the GW emission including the recoil kick.

Figure 5.1 shows the timescale of NSMs in our simulations for the no accretion cases ($\epsilon = 0$). In this thesis, we suppose that NS-NS or NS-BH ($m_{\rm BH} < 68\ M_\odot$) mergers are accompanied by the r-process elements ejection. From Figure 5.1, the r-process elements ejection events occur in 84 systems across our 144 models for $\epsilon = 0$. In Figure 5.1, open and filled plots represent that NSMs occur first and second or more mergers, respectively. Therefore, from this figure, the occurrence of the BH-BH mergers is almost earlier than that of the NS-BH or NS-NS mergers. This is because massive BHs are easy to be a closest binary due to the effects of the dynamical friction and the equipartition (Binney & Tremaine, 2008). After first merger of massive BHs, the merged heavy BH is mostly flied by the recoil kick due to the anisotropy of GW radiation. Thereafter, the probability of NS-BH mergers that satisfy the condition for the mass ejection of r-process elements at realistic spin magnitude is greatly increased. This is because NSs and light BHs are mostly left in the system. Thus, the conditions required to eject the r-process elements are easy to be satisfied due to the effect of the recoil kick.

The timescale of NSMs is almost inversely proportional to the gas density. On the other hand, the dependence of the timescale of NSMs on the BH density appears around $r_{\rm typ} \gtrsim 0.1$ pc. As seen in Figure 5.1, the NSMs within 10 Myr need the gas density of $n_{\rm gas} \gtrsim 10^7$ cm^{-3} and the BH density of $r_{\rm typ} \lesssim 0.3$ pc. These conditions for the NSMs within 10 Myr are likely to be satisfied in first-generation objects (Susa et al., 2014).

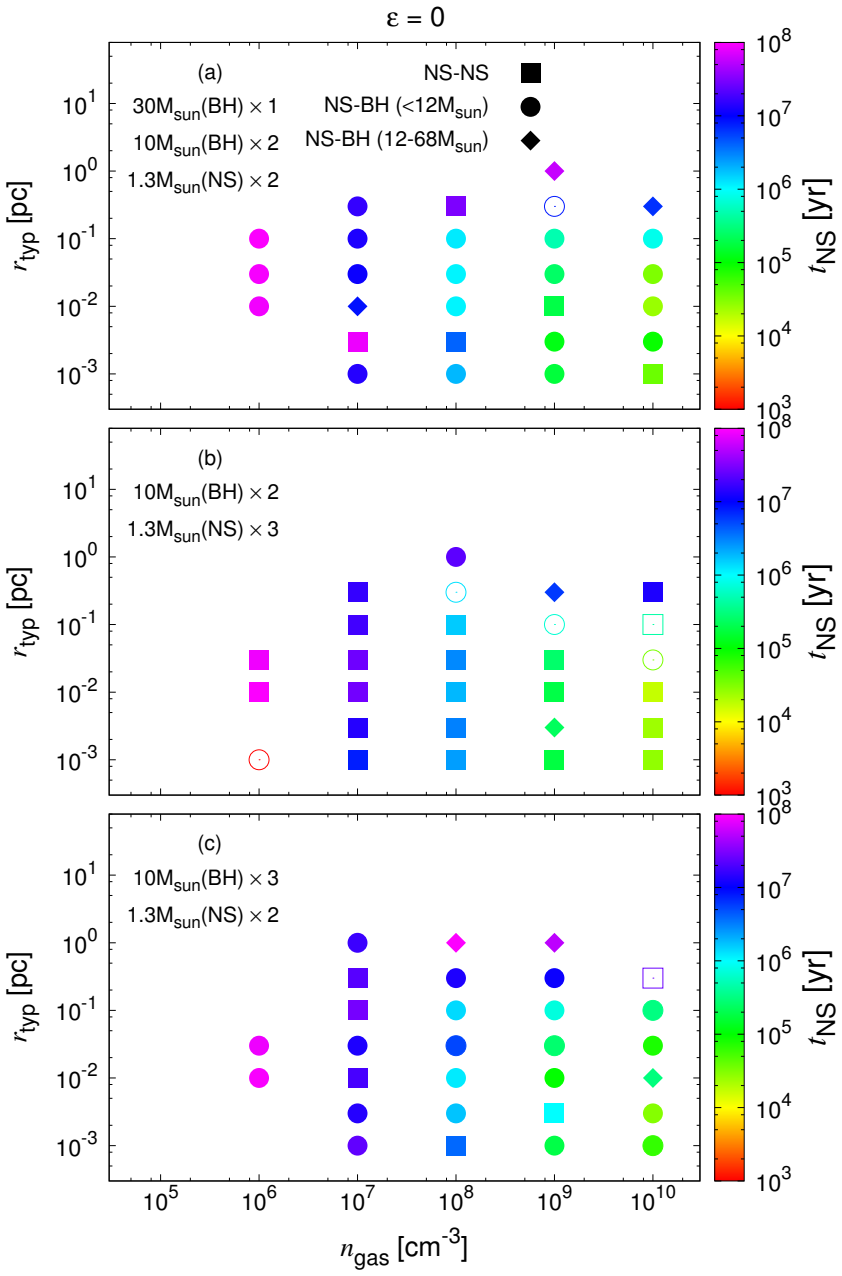

Fig. 5.1 The color of each symbol depicts the merger time of first NSM as functions of the gas density ($n_{\rm gas}$) and the initial typical extension of BH spatial distributions ($r_{\rm typ}$). These runs not incorporate the effects of the gas accretion. The initial compact star distribution is (a) BH ($30\ M_\odot$) $\times 1$, BH ($10\ M_\odot$) $\times 2$ and NB ($1.3\ M_\odot$) $\times 2$, (b) BH ($10\ M_\odot$) $\times 2$ and NB ($1.3\ M_\odot$) $\times 3$ and (c) BH ($10\ M_\odot$) $\times 3$ and NB ($1.3\ M_\odot$) $\times\ 2$. Square, circle and diamond plots represent NS-NS, NS-BH ($M_{\rm BH} < 12\ M_\odot$) and NS-BH ($12\ M_\odot \leq M_{\rm BH} \leq 68\ M_\odot$), respectively. Open and filled plots represent that NSMs occur first and second or more mergers, respectively. 12 and 68 $M_\odot$ are correspond to the mass shedding conditions for the BH spins of $\alpha = 0.75$ and 1, respectively.

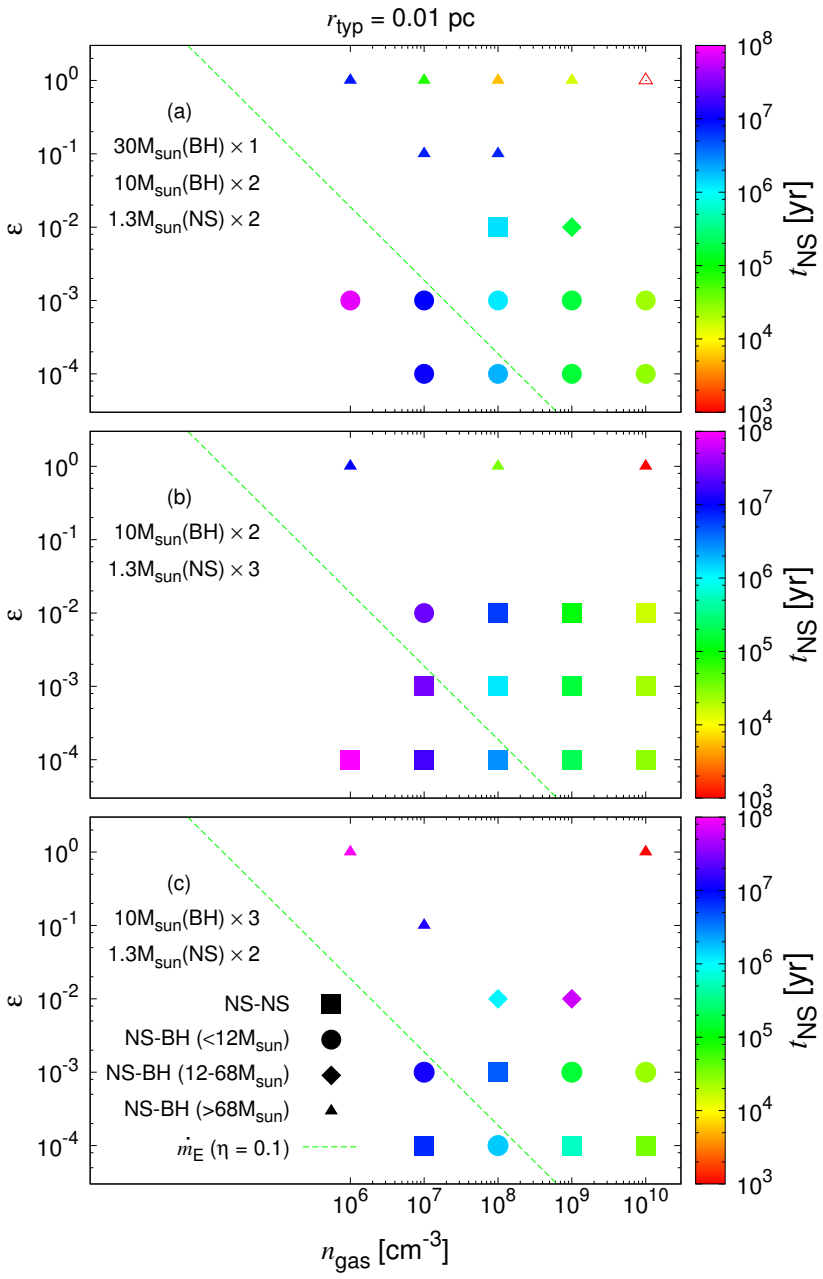

Fig. 5.2 The color of each symbol depicts the merger time of NSMs as functions of the accretion rate (ϵ) and the gas density (10^6 cm^{-3} $\leq n_{\rm gas} \leq 10^{10}$ cm^{-3}) for $r_{\rm type} = 0.01$ pc. The initial compact star distribution is (a) BH (30 $M_\odot$) × 1, BH (10 $M_\odot$)×2 and NB (1.3 $M_\odot$)×2, (b) BH (10 $M_\odot$)×2 and NB (1.3 $M_\odot$)×3 and (c) BH (10 $M_\odot$) × 3 and NB (1.3 $M_\odot$) × 2. Square, circle, diamond and triangle plots represent NS-NS, NS-BH ($M_{\rm BH} < 12\ M_\odot$), NS-BH ($12\ M_\odot \leq M_{\rm BH} \leq 68\ M_\odot$) and NS-BH ($M_{\rm BH} > 68\ M_\odot$), respectively. Open and filled plots represent first and second or more mergers, respectively. The green dashed line represents the Eddington accretion rate $\dot{m}_{\rm E}$ for the BH of 10 $M_\odot$.

The types of the first NSMs (NS-NS or NS-BH) are strongly influenced by the initial compact star distribution. The types are related to whether the initial number of BHs is odd or even. Actually, in the cases (a) and (c) whose BH number is odd, first NSMs are almost NS-BH mergers. On the other hand, in the cases (b) whose BH number is even, first NSMs are almost NS-NS mergers. Also, the timescale of NSMs hardly depend on initial compact star distribution.

Next, we investigate the conditions on the accretion efficiency for the ejection of r-process elements. In Figure 5.2, we show the merger time of NSMs as functions of the gas density and the accretion efficiency for $r_{\rm typ} = 0.01$ pc. In the high accretion efficiency of $\epsilon \gtrsim 0.1$, there are no cases that NSMs with the mass ejection of r-process elements occur. This is because BHs grow over 68 $M_\odot$ or NSs grow over 1.4 $M_\odot$ before NS-BH or NS-NS mergers occur. Hence, the NSMs with the mass ejection of r-process elements occur in the cases of the low accretion efficiency of $\epsilon < 0.1$.

5.2 Event rates for short gamma-ray bursts

In this section, we roughly estimate the event rates of short GRBs in the non-binary merger scenario. Here, the contribution of the NS-NS mergers to short GRBs is considered. The NS-NS merger rates are calculated in the same manner as the estimate in Section 4.2. In Milky Way Galaxy, about 100 million NSs exist (Camenzind, 2007). By assuming the situations as the event rates for the mergers of Pop I/II BHs, the merger rates of NSs in GMCs are ~ 2 yr^{-1}Gpc^{-3}, and that in GNRs are ~ 0.6yr^{-1}Gpc^{-3}. Therefore, the merger rates of NSs in the non-binary merger scenario is ~ 3 yr^{-1}Gpc^{-3}.

On the other hand, from the observation of short GRBs, estimated event rate is ~ 4yr^{-1}Gpc^{-3} (Wanderman & Piran, 2015). Intrinsic event rate is higher than observed event rate by $(1 - \cos\theta_{\rm j})^{-1}$ because of the collimation of a jet, where $\theta_{\rm j}$ is the opening angle of a jet. From the observed opening angle distribution of short GRBs of $3-15^\circ$ (Berger, 2014; Fong et al., 2015), the intrinsic event rate is calculated to be $\sim 100 - 1000$ yr^{-1}Gpc^{-3}. This rate is almost consistent with the merger rate of NS-NS binaries of $\sim 200 - 3000$ yr^{-1}Gpc^{-3} estimated from the binary pulsars in Milky Way Galaxy (Kalogera et al., 2004; Naker et al., 2006). Besides, the NS-NS merger rates estimated from the population synthesis study are $\sim 60-160$ yr^{-1}Gpc^{-3} (Dominik et al., 2015). Thus, the merger rate in the non-binary merger scenario is much smaller than that in the binary evolution model. The results are consistent with the observations that short GRBs occur in low circumburst densities (Berger, 2014) if the origin of short GRBs is the NS merger. This is because the non-binary merger scenario requires high gas density environments for the mergers. Hence, in

regard to the NS mergers at low redshifts, the non-binary merger scenario is likely to be a minor evolutional path.

5.3 Formation processes of supermassive black holes

It remains poorly understood how SMBHs with the mass higher than $10^9 M_\odot$ formed and grew at high redshifts $z > 6$. For the growth of SMBHs, there are two major competitive scenarios, that is, the mass accretion and the merger of BHs (or stars). If the accretion rate is limited by the Eddington accretion rate, massive BHs of about $10^4 M_\odot$ are required to exist in the redshift of about 10. According to the results of Section 3.2.1, we find that non-binary stellar-mass BHs can merge with each other within short timescale of about 10 Myr if dense gas of about $10^7 \mathrm{cm}^{-3}$ exists (Tagawa et al. 2015).

In first generation objects, the density of BH remnants of about $10^7\ M_\odot \mathrm{pc}^{-3}$ and the gas density of about $10^7 \mathrm{cm}^{-3}$ can be expected (Susa et al., 2014). Therefore, from our numerical results in Section 3.2.1, all the multiple BHs formed as first star remnants are likely to merge into one BH via type B or C mergers if gas accretion and recoil kick due to the anisotropy of GW radiation are inefficient. On the other hand, the escape velocity of first generation objects ($\lesssim 50$km/s) is lower than typical recoil velocities due to the anisotropic GW radiation, although the kick velocities have large uncertainties because of the uncertainties of the BH spin directions as mentioned in Section 3.4. Thus, most of merged BHs are likely to escape from the systems. Here, there is a possibility that escaped BHs are again captured by the other systems. However, the growth of BHs by mergers in first generation objects is expected to be not efficient.

In primordial galaxies of $M_{\mathrm{halo}} \sim 10^9 M_\odot$ at $z \sim 15$, the escape velocities of the galactic center regions (several hundreds km/s) can be higher than the typical recoil velocities. Besides, the dense gas can be expected in galactic center regions within 1 pc especially during active galactic nucleus phase. Furthermore, about 3×10^3 BHs are likely to exist in the galactic center regions within 1 pc of Milky Way Galaxy (Alexander, 2005). If such a large number of BHs exist and merge into one massive BH in center regions of primordial galaxies, massive BHs of $10^4 M_\odot$ can be formed at high redshifts. Therefore, the center regions of primordial galaxies are promising environments where BHs grow via BH-BH mergers. To investigate this growth process of massive BHs using realistic BH and gas distribution, the cosmological hydrodynamic simulation is a superior tool. I will investigate how early BH growth proceeds by BH mergers by performing the cosmological hydrodynamic simulation in the future.

Chapter 6

Summary and conclusions

In this thesis, we have newly proposed the mergers from multiple non-binary BHs in gas rich environments, and investigated the merger processes of this evolutional channel. Furthermore, we applied the merger processes to the several issues, an evolutional path for the GW150914 event, the origin of r-process elements, the event rates of short gamma-ray bursts, and the formation processes of supermassive BHs.

6.1 Merger processes of multiple black holes

In Section 3, to unveil how BHs grow, and how BH mergers proceed, we investigate the merger of multiple BHs under gas-rich environments. Here, we focus on the mergers of multiple BHs in primordial gas at early cosmic epochs. For the purpose, we have performed highly accurate post-Newtonian numerical simulations, incorporating the effects of the gas dynamical friction, gas accretion, and gravitational wave (GW) emission. Besides, the three-body interaction is solved precisely, and so the merger processes of multiple BHs with effects of gas is investigated for the first time. Parameters in these simulations are the initial typical extention of BH spatial distribution ($r_{\rm typ}$), the gas number density ($n_{\rm gas}$), the accretion efficiency (ϵ), and the initial BH mass (m_0). We consider two cases of the BH mass: one is 30 $M_\odot$ BHs as first star remnants, which are born in a first-generation object, and other is 10^4 $M_\odot$ BHs resulting from supermassive stars, which are incorporated into a primordial galaxy. As an initial condition, we assume that ten BHs are randomly distributed, and have the random and circular velocities to be virialized at $\sim r_{\rm typ}$ in gas cloud of 10^5 $M_\odot$.

Consequently, we have found the followings.

1. The merger mechanisms are classified into a gas drag-driven merger (type A), an interplay-driven merger (type B), a three body-driven merger (type C), or an accretion-driven merger (type D). The merger mechanisms are classified by the manner of orbit decay just before the GW emission drives the merger. In

type A, the separation of BHs monotonically shrinks due to the gas dynamical friction before the GW works. In both of types B and C, there are the discontinuous changes of the orbit during the first merger. In type B, there are both type of mergers that are prompted by the gas dynamical friction and the three-body interaction just before the GW works. In type C, the strong disturbance of the orbit by the three-body interactions continues until the final merger. There are no merger that is prompted mainly by the gas dynamical friction just before the GW works in type C. In type D, significant accretion takes place before the first merger.
In a type A, B, or C merger, successive mergers occur, while the BH merger precedes the gas accretion. However, in a type D, the merger of all BHs into one BH is hard to occur, leaving several BHs around a primary BH.

2. Multiple BHs are able to merge into one BH within 100 Myr in a wide range of parameters when the gas accretion can be ignored. Commonly, if the gas density is higher than $n_{\rm gas} = 5 \times 10^5$ cm^{-3}, the BH merger occurs once at least in 100 Myr. There is no dependence of the merger time and the merger mechanisms on the mass of gas cloud in the range of $M_{\rm gas} \geq 10^5\ M_\odot$, and the accretion efficiency (ϵ) if the merger type is A, B, or C.

3. Based on the argument of merger timescales, type A or B merger occurs if $n_{\rm gas}\rho_{\rm BH}^{-1}r_{\rm typ}^{-1}$ is higher or lower than 8×10^4 cm^{-3}pc$^2/M_\odot$, respectively.

4. The dominant mechanisms for the growth of BHs vary according to the gas accretion rate $\dot{m}$, the BH density $\rho_{\rm BH}$, and the gas number density $n_{\rm gas}$. We have derived the critical accretion rate $\dot{m}_{\rm c}$, below which the BH growth is predominantly promoted by mergers. The $\dot{m}_{\rm c}$ is fitted as

$$\frac{\dot{m}_{\rm c}}{\dot{m}_{\rm HL}} = \begin{cases} 6 \times 10^{-3} \\ \qquad \text{for } n_{\rm gas} \lesssim 10^8\ \text{cm}^{-3} \\ 2 \times 10^{-3} \left(\frac{n_{\rm gas}}{10^8\ \text{cm}^{-3}}\right)^{-1.0} \left(\frac{\rho_{\rm BH}}{10^6\ M_\odot \text{pc}^{-3}}\right)^{0.74} \\ \qquad \text{for } n_{\rm gas} \gtrsim 10^8\ \text{cm}^{-3}. \end{cases} \tag{6.1}$$

Note that the effect of the recoil kick may reduce the critical accretion rate by about one order of magnitude for high gas density regions.

5. The recoil kick due to the anisotropic emission of GW radiation is important to consider the growth of BHs via BH mergers. We have estimated that roughly ninety percent of merged BHs can escape from a first-generation object, if the

directions and magnitudes of BH spins are completely random. The escape probability is reduced, if BH spins and the orbital angular momentum are aligned with each other.

These results suggest that the BH merger can contribute significantly to the formation of SMBHs at high-redshift epochs. In these studies, we do not consider the dynamics of the gas. However, the effect of the gas dynamics may affect the merger or accretion mechanism. We will investigate the influence of the effect of the gas dynamics on the BH merger processes in the future.

6.2 Non-binary black hole merger in GW150914

In Section 4, we propose a novel path of the merger stemming from non-binary isolated stars. Here, we focus on the mergers of multiple Pop I/II or III BHs incorporated in gas-rich environments, such as galactic nuclear regions, dense interstellar cloud cores, and interstellar clouds, in low-z galaxies. Then, we elucidate the conditions of the BH mergers in the GW150914 event from non-binary isolated BHs with the effects of gas. For the purpose, we have performed highly accurate post-Newtonian numerical simulations, incorporating dynamical friction and gas accretion. Parameters in these simulations are the initial typical extention of BH spatial distribution ($r_{\rm typ}$), the gas number density ($n_{\rm gas}$), the accretion efficiency (ϵ), and the initial BH mass (m_0). As an initial condition for the simulations, we consider the situation that five BHs are virialized at $\sim r_{\rm typ}$ in gas cloud of $10^5\ M_\odot$. Besides, we roughly estimate the event rate by the aLIGO first run. Consequently, we have found the followings.

1. We have found that the multiple non-binary BHs can account for the merger in the GW150914 event.

2. As required conditions for the non-binary merger scenario, the initial extension of the BH spatial distribution ($r_{\rm typ}$) ought to be lower than 1 pc, the gas density is higher than 10^5 cm^{-3}, and the merger timescale is shorter than 10^8 yr. The merger in GW150914 is likely to be driven by the three-body driven merger or interplay driven merger. From these conditions, favorable sites for the non-binary merger scenario are galactic nuclear regions and dense interstellar cloud cores. If seed BH masses are smaller than the masses of GW150914, the accretion rate should be around 0.01 Hoyle-Lyttleton accretion rate, and initial seed mass is likely to be higher than 25 $M_\odot$. Also, the non-binary merger scenario prefers late-type galaxies as host galaxies of GW events, because gas

rich environments are required.

3. We have estimated the event rates of BH mergers similar to GW150914 in the non-binary merger scenario by the first advanced LIGO observation run. We consider the mergers of multiple Pop III BHs which are formed as multiple systems, and the mergers of multiple Pop I/II BHs which are formed through the galactic evolution. We suppose that possible environments for the BH mergers from non-binary BHs are galactic nuclear regions and/or dense interstellar cloud cores. For the estimate, we assume the Pop I/II/III BH number, the ratio of massive BHs, the distribution of BHs and gas, and the merger timescale. As a result, the event rates are ~ 0.4 yr^{-1} in galactic nuclear regions and ~ 8 yr^{-1} in dense interstellar cloud cores. The main uncertainties of event rates are supposed to come from the spatial and kinematic BH and gas distribution, which may give uncertainties of $\sim 1-2$ order of magnitude.

We suggest that mergers of multiple BHs in gas-rich environments can explain the GW150914 events. In the future, to estimate the merger rate using more realistic BH and gas distributions, I would like to perform cosmological hydrodynamic simulations.

6.3 Application to several issues

6.3.1 Origin of r-process elements by neutron star mergers

In Section 5.1, to solve the problem for the confliction of the NS merger timescale, we propose the rapid merger processes in gas-rich first-generation objects in a high redshift epoch. To clarify the conditions of the NS mergers (NSMs) in gas-rich first-generation objects, we have performed highly accurate post-Newtonian numerical simulations, incorporating the gas dynamical friction, the gas accretion, and the recoil kick due to the anisotropy of the GW radiation. Parameters in these simulations are the initial typical extention of BH spatial distribution ($r_{\rm typ}$), the gas number density ($n_{\rm gas}$), the accretion efficiency (ϵ), and the compact star distribution. We consider the situation that a few BHs and a few NSs are virialized in gas-rich first-generation objects of 10^5 $M_\odot$. Consequently, we have found the followings.

1. The NSMs within 10 Myr require the gas density of $n_{\rm gas} \gtrsim 10^7$ cm^{-3} and the initial extension of the compact star spatial distribution of $r_{\rm typ} \lesssim 0.3$ pc.

2. The effect of the recoil kick due to the anisotropic GW radiation at mergers increases the probability of NS-NS mergers or light BH-NS mergers. Furthermore, the accretion rate need to be lower than 0.1 Hoyle-Lyttleton accretion

rate for NSMs that satisfy the conditions of the ejection of r-process elements.

3. NS-NS or NS-BH mergers as the first NSMs are likely to occur when the initial number of BHs is even or odd, respectively.

These results imply that the mergers in early cosmic epochs may reconcile the conflict on the timescale of NS mergers. However, in first-generation objects, it should be investigated more realistically how gas is distributed. I would like to investigate the mergers in first-generation objects using realistic gas distribution by performing cosmological hydrodynamical simulations in the future.

6.3.2 Event rates for short gamma-ray bursts

In Section 5.2, we have roughly estimated the event rates of short GRBs by the NS-NS mergers evolved from non-binary stars. We consider the mergers of multiple NSs in galactic nuclear regions and/or dense interstellar cloud cores. For the estimate, we assume the number of NSs, the distribution of NSs and gas, and the merger timescale.

As a result, the NS-NS merger rates are $\sim 0.6\ \mathrm{yr}^{-1}\mathrm{Gpc}^{-3}$ in galactic nuclear regions and $\sim 2\ \mathrm{yr}^{-1}\mathrm{Gpc}^{-3}$ in dense interstellar cloud cores. Since the intrinsic event rate of short GRBs is calculated to be $\sim 100 - 1000\ \mathrm{yr}^{-1}\mathrm{Gpc}^{-3}$, the contributed ratio of the event rate for NS mergers evolved from non-binary stars to the event rate for short GRBs is $\sim 1\%$. Hence, we find that the non-binary star merger is likely to be a minor path of short GRBs.

6.3.3 Formation processes of supermassive black holes

In Section 5.3, we consider the possibility of the growth of BHs via BH-BH mergers at high-redshift epochs. The efficient growth of BHs via BH-BH mergers requires high gas density, high BH density, and high escape velocity. Then, we suppose that the center regions of primordial galaxies can be promising environments for the efficient growth of BHs via BH-BH mergers. To investigate this growth processes more realistically, cosmological hydrodynamic simulations are required.

AppendixA

A.1 Merger mechanisms without gas accretion

To scrutinize the merger mechanism of non-binary isolated BHs, we here classify the merger mechanism in the cases that gas accretion is not incorporated and gas is

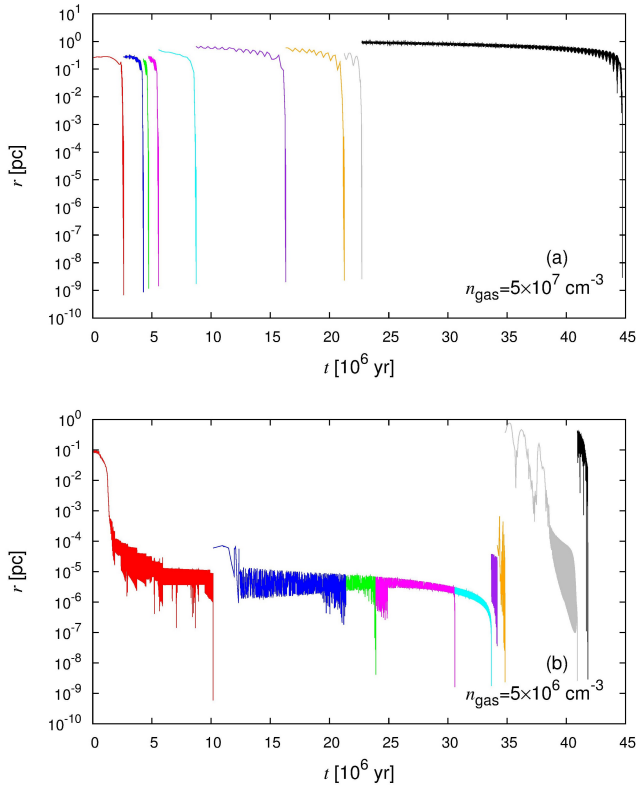

Fig. A.1 The separation of the closest pair within all BHs as a function of time. The initial BH mass is $M_{\rm BH} = 30\ M_\odot$, the initial typical extension of the BH spatial distribution is $r_{\rm typ} = 1.0$ pc, and the gas density is $n_{\rm gas} = 5 \times 10^7$ (top) or 5×10^6 (bottom) cm^{-3}. Taken from figure 1 of Tagawa et al. (2015).

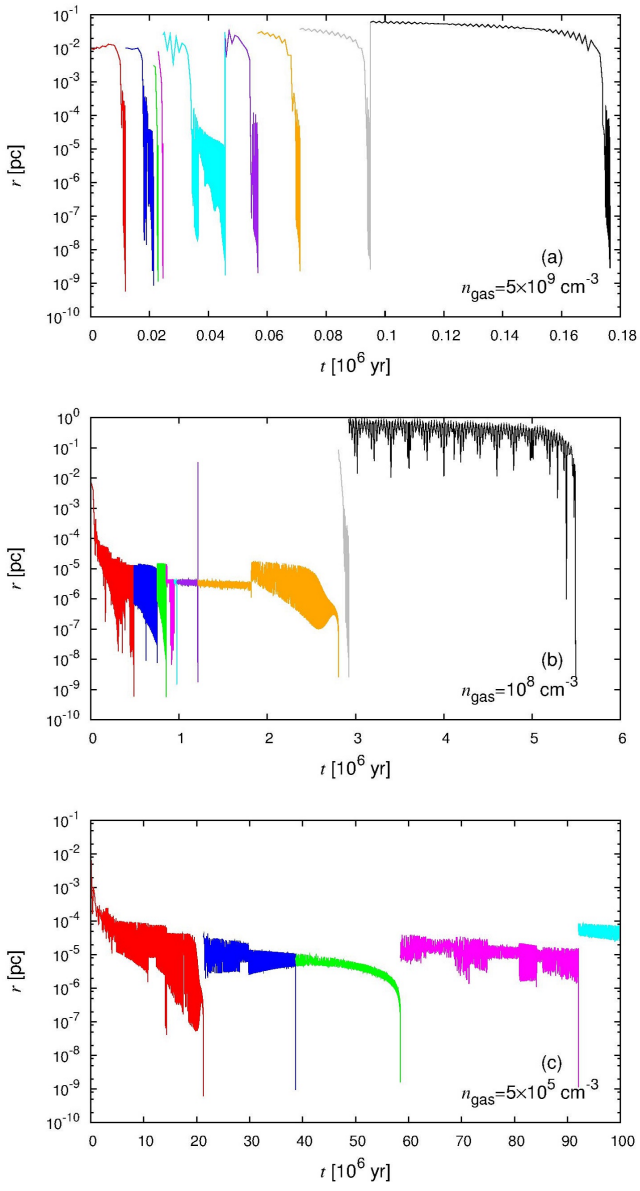

Fig. A.2 Same as Figure A.1, but for $r_{\rm typ} = 0.1$pc, and $n_{\rm gas} = 5 \times 10^9$ (top), 10^8 (middle), or 5×10^5 (bottom) cm^{-3}. Taken from figure 2 of Tagawa et al. (2015).

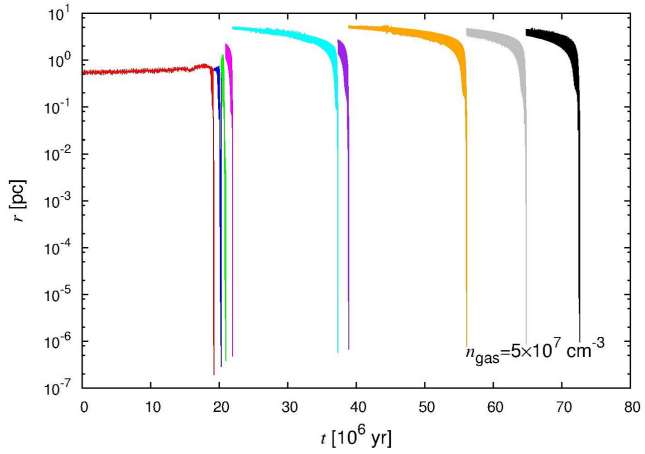

Fig. A.3 Same as Figure A.1, but for $M_{\rm BH} = 10^4\ M_\odot, r_{\rm typ} = 10.0$ pc, and $n_{\rm gas} = 5 \times 10^7\ {\rm cm}^{-3}$. Taken from figure 3 of Tagawa et al. (2015).

infinitely distributed. When a BH merger is induced by the gas dynamical friction, the separation of the same pair of BHs smoothly shrinks. On the other hand, the three-body interaction between a close BH binary and an intruding BH often replaces one BH in the binary by the intruder and therefore the separation of the closest pair changes violently. In Figs. A.1-A.5, we show the time evolution of the separation of the closest pair within all BHs, where the colors of lines change at every event of the BH merger.

Fig. A.1 shows the case of stellar-mass BHs ($M_{\rm BH} = 30\ M_\odot$). The initial extension of the BH spatial distribution is $r_{\rm typ} = 1.0$ pc. The upper and lower panels correspond to higher and lower gas density, respectively. As seen in the upper panel, the apocenter and pericenter distances of the closest pair decay smoothly. Such smooth decay indicates that the dynamical friction by gas induces the merger. On the hand, in the lower panel of Fig. A.1, the orbit is highly eccentric, because the apocenter and pericenter distances are largely different. The distances sometimes oscillate discontinuously. Such strong variance is caused by the three-body interaction. After the apocenter decays to less than $\sim 10^{-8}$ pc, the pair separation decreases rapidly due to the effect of the GW emission, and eventually the BH binary merges.

We classify the merger mechanism for the cases with no gas accretion according to the manner of decay just before the GW drives the merger as that with gas accretion in Section 3.1. Here, we have categorized the merger mechanism into three types: gas-drag-driven merger (type A), three-body-driven merger (type C), and interplay-driven merger (type B). In type A, the gas dynamical friction effectively decays the

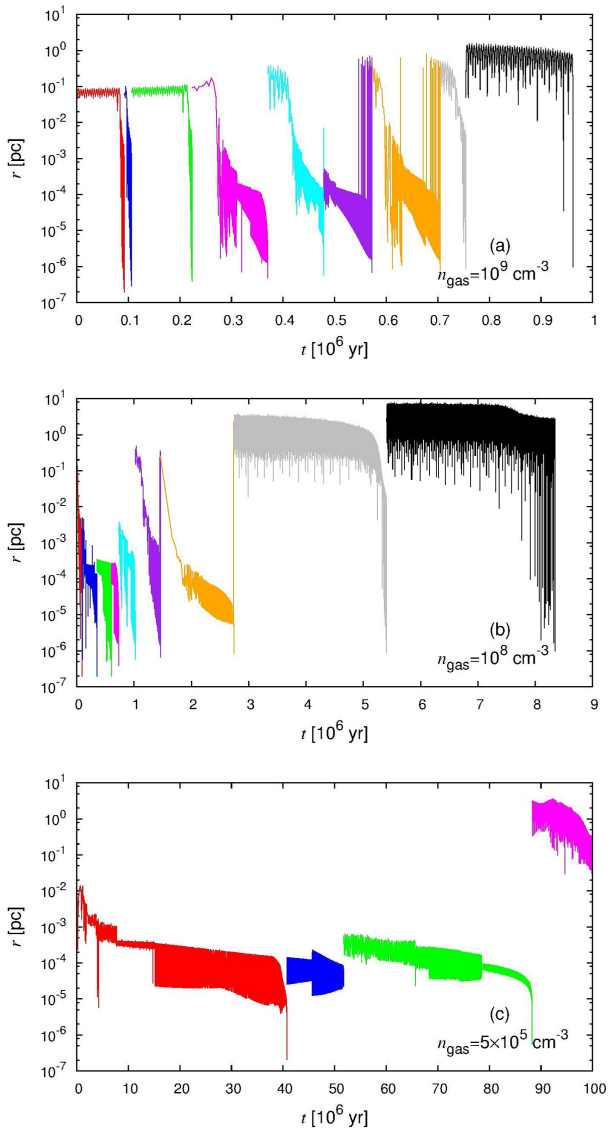

Fig. A.4 Same as Figure A.1, but for $M_{\rm BH} = 10^4\ M_\odot, r_{\rm typ} = 1.0$ pc, and $n_{\rm gas} = 10^9$ (top), 10^8 (middle), or 5×10^5 (bottom) cm^{-3}. Taken from figure 4 of Tagawa et al. (2015).

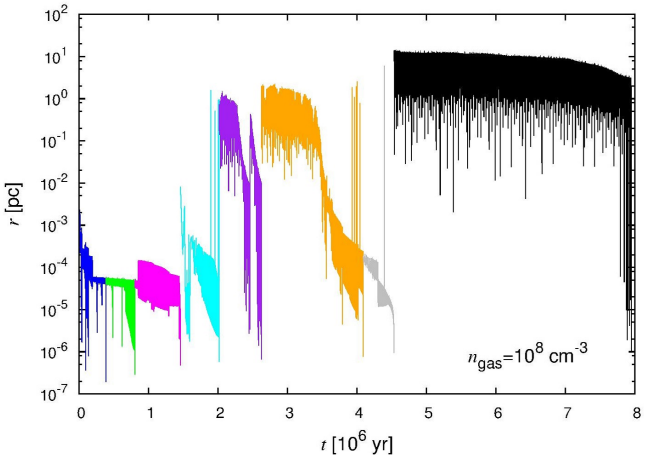

Fig. A.5 Same as Figure A.1, but for $M_{\rm BH} = 10^4\ M_\odot, r_{\rm typ} = 0.1$ pc, and $n_{\rm gas} = 10^8\ {\rm cm}^{-3}$. Taken from figure 5 of Tagawa et al. (2015).

orbit and then the GW drives the merger. The type A is seen in the cases with lower BH density and higher gas density. The examples of type A are seen in the top panels of Figs. A.1, A.2 and A.4, and Fig. A.3. In both types B and C, the strong disturbance of the orbit is prompted by the three-body interaction during the first merger. But in type B, after the first few mergers are prompted by three-body interaction, the orbit decays slowly for a long time through the gas dynamical friction. The examples of type B are shown in the middle panels of Figs. A.2 and A.4, and Fig. A.5. In these results, after the mergers are prompted by three-body interaction, the orbital evolution starts from a larger separation than initial typical separation ($r_{\rm typ}$). Such increase of separation is induced by the slingshot mechanism when an intruder interacts with the binary. This mechanism causes a negative effect on the merger timescale. In other words, the three-body interaction play a positive and negative role for the merger. In type C, the strong disturbance of the orbit is seen until the final merger. The three-body interaction of BHs solely transfers the angular momentum, eventually causing the merger via the GW radiation. Type C is seen in the cases of low gas density and high BH density. The examples of type C are seen in the bottom panels of Figs. A.2 and A.4.

References

Aasi J., et al., 2013, Phys. Rev. D., 87, 022002

Abbott B., et al., 2006, Phys. Rev. D., 73, 062001

Abbott B., et al., 2016, Phys. Rev. Lett., 116, 061102

Abbott B., et al., 2016, arXiv: 1602.03847

Abbott B., et al., 2016, Phys. Rev. Lett., 116, 241103

Abel T., Bryan G. L.,Norman M. L., 2000, ApJ, 540, 39

Abramowicz M. A., Czerny B., Lasota J. P., Szuszkiewicz E., 1988, ApJ, 332, 646

Alexander T., 2005, Physics Reports, 419, 65

Alvarez M. A., Wise J. H., Abel T., 2009, ApJ, 701, L133

Argast D., Samland M., Thielemann F.-K., Qian Y.-Z., 2004, A & A, 416, 997

Aso Y., Michimura Y., Somiya K., Ando M., Miyakawa O., Sekiguchi T., Tatsumi D., Yamamoto H., 2013, PhRvD, 88, 043007

Bate M. R., 2000, MNRAS, 314, 33

Bauswein A., Pulpillo R. A., Janka H.-T., Goriely S., 2014, ApJL, 795, L9

Begelman M. C., Blandford R. D., Rees M. J., 1980, Nature, 287, 307

Belczynski K., Dominik M., Bulik T., O'Shaughnessy R., Fryer C., Holz D. E., 2010, ApJ, 715, L138

Belczynski K., Daniel E. H., Bulik T., O'Shaughnessy R., 2016, Nature, 534, 512

Berger E., 2014, ARA&A, 52, 43

Bergin E. A., Snell R. L., Goldsmith P. F., 1996, ApJ, 460, 343

Barnard R., Garcia M. R., Primini F. Murray S. S., 2014, ApJ, 791, 33

Berti E., Cardoso V., Will C. M., 2006, Phys. Rev. D., 73, 064030

Binney J., Tremaine S., 2008, Galactic Dynamics: Second Eddition. Princeton univ. Press, Princeton, NJ

Bondi H., Hoyle F., 1944, MNRAS, 104, 273

Boss A. P., 1986, ApJS, 62, 519

Bramante J., Linden T., 2016, arXiv: 1601.06784

Bromm V., Coppi P. S.,Larson R. B., 2002, ApJ, 564, 23

Bromm V., Loeb A., 2003, ApJ, 596, 34

Camenzind M., 2007, Compact Objects in Astrophysics: White Dwarfs, Neutron Stars and Black Holes (Berlin: Springer)

Campanelli M., Lousto C. O., Zlochower Y., Merritt D., 2007, PhRvL, 98, 1102

Campanelli M., Lousto C. O., Zlochower Y., Merritt D., 2007, ApJL, 659, L5

Cescutti G., Romano D., Matteucci F., Chiappini C., Hirschi R., 2015, A & A, 577, 139

Choi D.-I., Kelly B. J., Boggs W. D., Baker J. G., Centrella J., van Meter J., 2007, Phys. Rev. D, 76, 104026

Connaughton V., et al., 2016, arXiv, arXiv:1602.03920

Costa E., et al., 1997, Nature, 387, 783

Clark P. C., Glover S. C. O., Klessen R. S., Bromm V., 2011, ApJ, 727, 110

del Valle L., Escala A., 2014, ApJ, 780, 84

Dominik M., Belczynski K., Fryer C., Holz D. E., Berti E., Bulik T., Mandel I., O'Shughnessy R., 2012, ApJ, 759, 52

Dominik M., et al. 2015, ApJ, 806, 263

D'Orazio D. J., Haiman Z., MacFadyen A., 2013, MNRAS, 436, 2997

Djorgovski S. G., Courbin F., Meylan G., Sluse D., Thompson D., Mahabal A., Glikman E., 2007, ApJ, 662, L1

Escala A., Larson R., Coppi P., Mardones D., 2004, ApJ, 507, 765

Escala A., Larson R., Coppi P., Mardones D., 2005, ApJ, 630, 152

Fan X. et al., 2001, AJ, 122, 2833

Farina E. P., Montuori C., Decarli R., Fumagalli M., 2013, MNRAS, 431, 1019

Farris B. D., Duffell P., MacFadyen A. I., Haiman Z., 2015, MNRAS, 447, L80

Fiacconi D., Mayer L., Roskar R., Colpi M., 2013, 777, L14

Fong, W., Berger E., Margutti R., Zauderer B. A., 2015, ApJ, 815, 102

Foucart F., Deaton M. B., Duez M. D., O'Connor E., Ott C. D., Haas R., Kidder L. E., Pfeiffer H. P., Scheel M. A., Szilagyi B., 2014, Phys. Rev. D, 90, 024026

Frail D. A., et al. 2001, ApJL, 562, L55

Freiburghaus C., Rosswog S., Thielemann F.-K., 1999, ApJL, 525, L121

Fruchter A. S., et al., 2006, Nature, 441, 463

Fukushige T., Ebisuzaki T., Makino J., 1992, PASJ, 44, 281

Greif T. H., Springel V., White S. D. M., Glover S. C. O., Clark P. C., Smith R. J., Klessen R. S., Bromm V., 2011, ApJ, 737, 75

Greene J. E., 2012, NatureCommunications, 3, 1304

Haiman Z., 2013, in Wiklind T., Mobasher B., Bromm V., eds, Astrophysics and Space Science Library, Vol. 396, The First Galaxies. Springer-Verlag, Berlin, p. 293

Hanamoto K., Ioroi M., Fukue J., 2001, PASJ, 53, 105

Heger A., Woosley S. E., 2002, ApJ, 567, 532

Heger A., Fryer C. L., Woosley S. E., Langer N., Hartmann D. H., 2003, ApJ, 591, 288

Hirano S., Hosokawa T., Yoshida N., Umeda H., Omukai K., Chiaki G., Yorke H. W., 2014, ApJ, 781, 60

Hjorth J., Bloom J. S., 2012, in Kourveliotou C., Wijers R. A. M. J., Woosley S., eds, Cambridge Astrophysics Series 51: Gamma-Ray Bursts. Cambridge Univ. Press, Cambridge, p. 169

Hollenbach D., McKee C. F. 1989, ApJ, 342, 306

Hoyle F., Lyttleton R. A., 1939, Proc. Camb. Phil. Soc., 35, 405

Lorimer D. R., 2008, LRR, 11, 8

Lück H., et al., 2006, CQGra, 23, S71

Inayoshi K., Omukai K., 2012, MNRAS, 422, 2539

Ishiyama T., Sudo K., Yokoi S., Hasegawa K., Tominaga N., Susa H., 2016, ApJ, 826, 9

Iwasawa M., Funato Y., Makino J., 2006, ApJ, 651, 1059

Ji A. P., Frebel A., Chiti A., Simon J. D., 2015, arXiv: 1512.01558

Jiang L., et al., 2007, ApJ, 134, 1150

Just O., Bauswein A., Ardevol Pulpillo R., Goriely S., Janka H.-T., 2015, MNRAS, 448, 541

Kalogera V., et al., 2004, ApJ, 601, L179

Khan F. M., Just A., Merritt D., 2011, ApJ, 732, 89

Khan F. M., Preto M., Berczik P., Berentzen I., Just A., Spurzem R., 2012, ApJ, 749, 147

Khan F. M., Holley-Bockelmann K., Berczik P., Just A., 2013, ApJ, 773, 100

Kim W.-T., El-Zant A., Kamionkowski M., 2005, ApJ 632, 157

Kinugawa T., Inayoshi K., Hotokezaka K., Nakauchi D., Nakamura T., 2014, MNRAS, 442, 2963

Komiya Y., Yamada S., Suda T., Fujimoto M. Y., 2014, ApJ, 783, 132

Kormendy J., Ho L. C., 2013, ARA&A, 51, 511

Korobkin O., Rosswog S., Arcones A., Winteler C., 2012, MNRAS, 426, 1940

Kupi G., Amaro-Seoane P., Spurzem R., 2006, MNRAS, 371,45

Kurk J. D., et al., 2007, ApJ, 669, 32

LIGO Scientific Collaboration et al. 2015, Classical and Quantum Gravity, 32, 074001

Liu X., Shen Y.,Strauss M. A., 2011, ApJ, 736, L7

Lützgendorf N., Gebhardt K., Baumgardt H., Noyola E., Neumayer N., Kissler-Patig Markus., de Zeeuw T., 2015, A&A, 581, 8

Maccarone T. J., Kundu A., Zepf S. E., Rhode K. L., 2007, Nature, 445, 183

MacFadyen A. I., Milosavljevic M., 2008, ApJ, 672, 83

Makino J. Aarseth S., 1992, PASJ, 44, 141

Matsubayashi T., Makino J., Ebisuzaki T., 2007, ApJ, 656, 879

Martínez-Pinedo G., Fischer T., Lohs A., Huther L., 2012, PhRvL, 109, 251104

Matteucci F., Romano D., Arcones A., Korobkin O., Rosswog S., 2014, MNRAS, 438, 2177

Merritt D., Poon M. Y., 2004, ApJ, 606, 788

Meszaros P., 2002, Annu. Rev. Astron. Astrophys., 40, 137

Milosavljevic M., Couch S. M., Bromm V., 2009, ApJ, 696, 146

Mortlock D. J., et al., 2011, Nature, 474, 616

Nakamura F., Umemura M., 2001, ApJ, 548, 19

Nakamura T. et al., arXiv: 1607.00897

Naker E., Gal-Yam A., Fox D. B., 2006, ApJ, 650, 281

Namekata D., Umemura M., 2016, MNRAS, 460, 980

Narayan R., Paczynski B., Piran T., 1992, ApJ, 395, L83

Natarajan P., Pringele J. E., 1998, ApJ, 506, L97

Noble S. C., et al., 2012, ApJ, 755, 51

Nordstrom B., et al. 2004, A& A, 418, 989

Omukai K., 2000, ApJ, 534, 809

Ostriker E. C., 1999, ApJ, 513, 252

Palla F., Salpeter E. E., Stahler S. W., 1983, ApJ, 271, 632

Paciesas W. S., et al., 1999, ApJS, 122, 465

Panaitescu A., Kumar P., Narayan R., 2001, ApJL, 561, L171

Perna R., Belczynski K., 2002, ApJ, 570, 252

Portegies Zwart S. F., Yungelson L. R., 1998, A & A, 332, 173

Rees M. J., Meszaros P., 1992, MNRAS, 258, 41

Reddy S., Prakash M., Lattimer J. M., 1998, PhRvD, 58, 013009

Remillard R. A., McClintock J. E., 2006, ARA&A, 44, 49

Roedig C., Dotti M., Sesana A., Cuadra J., Colpi M., 2011, MNRAS, 415, 3033

Roedig C., Sesana A., Dotti M., Cuadra J., Amaro-Seoane P., Haardt F., 2012, A&A, 545, A127

Rodriguez C. L., Haster C.-J., Chatterjee S., Kalogera V., Rasio F. A., 2016, ApJL, 824, L8

Salvaterra R., et al., 2008, MNRAS, 388, L6

Sana H., Gosset E., Naze Y., Rauw G., Linder N., 2008, MNRAS, 386, 447

Schawinski K.,Urry M., Treister E., Simmons B., Natarajan P., Glikman E., 2011, ApJ, 743, L37

Sesana A., Haardt F., Madau P., Volonteri M., 2005, ApJ, 623, 23

Shi J.-M., Krolik J. H., Lubow S. H., Hawley J. F., 2012, ApJ, 749, 118

Shibata M., Shapiro S., 2002, ApJ, 572, L39

Shibata M., Taniguchi K., 2011, LRR, 14, 6

Silk J., Rees M. J., 1998, A&A, 331, L1

Sneden C., Cowan J. J., Gallino R., 2008, ARAA, 46, 241

Susa H., 2013, ApJ, 773, 185

Susa H., Hasegawa K., Tominaga N., 2014, ApJ, 792, 32

Susa H., Umemura M., 2004, ApJ, 600, 1

Tagawa H., Umemura M., Gouda N., Yano T., Yamai Y., 2015, MNRAS, 451, 2174

Tagawa H., Umemura M., Gouda N., 2016, MNRAS, in press

Tanaka T., Haiman Z., 2009, A & A, 696, 1798

Tanikawa A., Umemura M., 2011, MNRAS, 728, 31

Tanikawa A., Umemura M., 2014, MNRAS, 440, 652

Thompson T. A., Burrows A., Meyer B. S., 2001, ApJ, 562, 887

Thoul A. A., Weinberg D. H., 1995, ApJ, 442, 480

Tsujimoto T., Shigeyama T., 2014, A & A, 565, L5

Umemura M., Loeb A., Turner E. L., 1993, ApJ, 419, 459

Umemura M., Susa H., Hasegawa K., Suwa T., Semelin B., 2012, PTEP, 2012, 01A306

van de Voort F., Quataert E., Hopkins P. F., Kereš D., Faucher-Giguère C.-A., 2015, MNRAS, 447, 140

Vasiliev E., Antonini F., Merritt D., 2014, ApJ, 785, 163

Venemans B. P., et al., 2013, ApJ, 779, 24

Venemans B. P., et al., 2015, ApJL, 801, L11

Volonteri M., Rees M. J., 2005, ApJ, 633, 624

Volonteri M., Sikora M., Lasota J.-P., 2007, ApJ, 667, 704

Volonteri M., Lodato G., Natarajan P., 2008, MNRAS, 383, 1079

Volonteri M., Bellovary J., 2012, Rep. Prog. Phys., 75, 124901

Wanajo S., Janka H.-T., Müller B., 2011, ApJL, 716, L15

Wanajo S., Janka H.-T., 2012, ApJ, 746, 180

Wanajo S., 2013, ApJL, 770, L22

Wanajo S., Sekiguchi Y., Nishimura N., Kiuchi K., Kyoutoku K., Shibata M., 2014, ApJL, 789, L39

Wanderman D., Piran T., 2015, MNRAS, 448, 3026

Wang R., et al., 2010, ApJ, 714, 699

Watarai K., Fukue J., Takeuchi M., Mineshige S., 2000, PASJ, 52, 133

Woosley S. E., Bloom J. S., 2006, ARAA, 44, 507

Wu X.-B., et al., 2015, Nature, 518, 512

Wyithe J. S. B., Loeb A., 2003, ApJ, 590, 691

Yajima H., Li Y., Zhu Q., Abel T., 2015, ApJ, 801, 52

Yoshida N., Omukai k., Hernquist L., Abel T., 2006, ApJ, 652, 6

Yost S. A., Harrison F. A., Sari R., Frail D. A., 2003, ApJ, 597, 459